

Mapping The Spatio-Temporal Dynamics of Drought in Northeast Thailand

PHONGPHAT JAPHICHOM

A THESIS SUBMITTED IN PARTIAL FULFILLMENT OF
THE REQUIREMENTS FOR MASTER DEGREE OF SCIENCE
IN GEOINFORMATICS
FACULTY OF GEOINFORMATICS
BURAPHA UNIVERSITY
2025
COPYRIGHT OF BURAPHA UNIVERSITY



การวิเคราะห์และทำแผนที่พลวัตเชิงพื้นที่และเวลาของภัยแล้งในภาคตะวันออกเฉียงเหนือของ ประเทศไทย

พงศ์พัฒน์ จ่าพิชม

วิทยานิพนธ์นี้เป็นส่วนหนึ่งของการศึกษาตามหลักสูตรวิทยาศาสตรมหาบัณฑิต สาขาวิชาภูมิสารสนเทศศาสตร์ คณะภูมิสารสนเทศศาสตร์ มหาวิทยาลัยบูรพา 2568 ลิบสิทธิ์เป็นของมหาวิทยาลัยบูรพา



PHONGPHAT JAPHICHOM

A THESIS SUBMITTED IN PARTIAL FULFILLMENT OF THE REQUIREMENTS FOR MASTER DEGREE OF SCIENCE IN GEOINFORMATICS FACULTY OF GEOINFORMATICS **BURAPHA UNIVERSITY** 2025 COPYRIGHT OF BURAPHA UNIVERSITY



The Thesis of Phongphat Japhichom has been approved by the examining committee to be partial fulfillment of the requirements for the Master Degree of Science in Geoinformatics of Burapha University

Advisory Committee	Examining Committee
Principal advisor	
Zhenfeng Shao	Principal examiner
(Professor Dr. Zhenfeng Shao)	(Professor Dr. Wolfgang Kainz)
Co-advisor	Zhenfeng Shao Member (Professor Dr. Zhenfeng Shao) Member
(Assistant Professor Dr. Phattraporn	(Professor Dr. Timo Balz)
S. Ponali Hiwison	Zrongai In Member (Professor Dr. Zhangcai Yin) Dean of the Faculty of Humanities and
J	Dean of the Faculty of Humanities and Social Sciences
(Associate Professor Dr. Such 3 March, 2015	
be partial fulfillment of the requirements for Geoinformatics of Burapha University	Dean of Graduate School wat Jangiam)
3.000	

65910037: MAJOR: GEOINFORMATICS; M.Sc. (GEOINFORMATICS) KEYWORDS: drought, Machine learning, Random Forest (RF), Remote sensing PHONGPHAT JAPHICHOM: MAPPING THE SPATIO-TEMPORAL DYNAMICS OF DROUGHT IN NORTHEAST THAILAND. ADVISORY COMMITTEE: ZHENFENG SHAO, Ph.D. PHATTRAPORN SOYTONG, Ph.D. 2025.

Drought, a globally significant natural disaster, imposes considerable economic and environmental impacts, severely impacting agriculture and socioeconomic systems annually. The frequency of global drought occurrences can be attributed to the impacts of climate change and human activities. This study aims to investigate the spatiotemporal dynamics of drought in Northeast Thailand by integrating remote sensing (RS) and ground observations with machine learning models.

This study specifically focused on northeast Thailand. This area is situated within the tropical zone, characterized by mainly sandy soil that has a limited capacity to retain water. Therefore, effective water resource management and drought monitoring efforts are needed in northeast Thailand.

The main contents of this thesis include:

- 1) Investigation of spatio-temporal drought patterns (shorth term and long term) of the study area from 2014 to 2023 using ML modeling from Landsat 8 satellite and ground observation data.
- 2) Performance comparison of machine learning (ML) models for monitoring drought in Northeast Thailand.
- 3) Mapping spatial distribution of drought events in the Northeast of Thailand from 2014 to 2023.

This study leverages the fusion of RS and ground data to enhance drought monitoring. Ground indicators offer precision but have limited coverage, while RS indices cover larger areas with less accuracy. ML algorithms were used to combine these data sources, improving spatial resolution and accuracy. The study used five RS parameters such as The Vegetation Condition Index (VCI), The Enhanced Vegetation Index (EVI), The Temperature Condition Index (TCI), Topography, Precipitation,

combined with ground data as The Standardized Precipitation Evapotranspiration Index (SPEI). ML techniques, including XGBoost, Random Forest, and Extra Trees, assessed the relationship between variables. Additionally, cross-validation techniques were utilized to validate the model performance. The optimal model was used to generate a spatial distribution of drought, contributing to more effective drought management strategies, and enhancing drought dynamics in the region.

The results demonstrate that the Extra Trees model is outperform for accurate drought index prediction. For short-term, the results show an R² ranging from 65.26% to 94.28%, an RMSE between 1.58% to 33.28%, and an MAE ranging from 0.09% to 18.55%. Similarly, for long-term, the results show an R² ranging from 78.73% to 94.8%, an RMSE between 4.55% and 31.93%, and an MAE ranging from 0.45% to 18.14%. In particular, the variables contributing to model accuracy include precipitation (27%-67%), topography (19%-37%), and land surface temperature (6%-21%). The feature importance values of these variables enhance the model performance. The study examines both short-term and long-term precipitation patterns using the Standardized Precipitation Evapotranspiration Index (SPEI) to assess drought conditions. Short-term analysis identified significant drought occurrences in June 2015 and April 2016, with recurrent drought periods observed in late 2018 and 2019, as well as the beginning of 2020 and 2021. These findings underscore the cyclic nature of decreased precipitation and the associated risk of water scarcity within shorter time frames. Moreover, long-term precipitation trends analyzed through SPEI indicated sustained negative values from mid-2015 to 2016, indicating the onset of drought conditions. Particularly noteworthy was the persistent negativity of SPEI values from mid-2018 to 2020, indicating an extended drought period spanning multiple months. indicating the severity and duration of the drought.

The main initiatives of the thesis are as follows:

- 1) Developed method that fuses the drought index using remote sensing (RS) data from the Landsat 8 satellite and ground observations. This provides insights into drought-related environmental parameters and precise meteorological measurements.
 - 2) Compared the performance of three ML models to identify the most

effective method for drought monitoring in the study area.

3) Explored spatiotemporal trends in drought distribution to inform water management and mitigation strategies.

In conclusion, the study provides a framework for strategic planning in drought management by integrating RS and ground observation data. Future work could explore deep learning or neural networks to enhance drought monitoring and understanding of regional environmental implications.

ACKNOWLEDGEMENTS

During my master's degree studies, I am deeply grateful to my supervisor, Prof. Zhenfeng Shao, for his invaluable guidance, advice, expertise, and experience, which provided insight and direction for my dissertation work. Additionally, his words, "Trust yourself. I also believe you can do it well," have been a source of inspiration for me throughout my studies and future research.

I would like to thank the Thai Meteorological Department for providing ground observation data, which was essential for training the model used in my research. Special thanks to Flight Sergeant First Class Tiwakorn Sena, my colleague and classmate, for his assistance with the technical methods of this research.

I am also grateful to my seniors, Ms. Sunantha Ousaha and Flight Lieutenant Sitthisak Thotsaphon, both from SCGI#4, for their invaluable advice. Additionally, I want to thank my fellow SCGI#5 classmates, especially my compatriot, for their constant support and assistance over the past two years, making my studies enjoyable and fulfilling.

I extend my gratitude to the lecturers from the Faculty of Geo-Informatics at Burapha University, Thailand, and the State Key Information Engineering Laboratory for Surveying, Mapping, and Remote Sensing (LIESMARS) in China. I also appreciate the Geo-Informatics and Space Technology Development Agency of Thailand (GISTDA) for providing me with the opportunity to continue my studies.

I am thankful to the commander of the Royal Thai Air Force (RTAF) for allowing me this opportunity to enhance my experience. Finally, I would like to express my deepest gratitude to my parents for their unwavering encouragement and pure love, as well as to everyone behind the scenes. It would have been impossible for me to graduate without the help of these people.

Phongphat Japhichom

TABLE OF CONTENTS

Page
ABSTRACTD
ACKNOWLEDGEMENTSG
TABLE OF CONTENTS
LIST OF TABLESK
LIST OF FIGURESL
ABSTRACT1
CHAPTER 1 INTRODUCTION
1.1 Background4
1.2 Scientific Questions
1.3 Objectives5
1.4 Structure of Thesis
CHAPTER 2 LITERATURE REVIEW7
2.1 Background of This Study
2.1.1 The Seasons of Thailand
2.1.2 Temperature of Thailand
2.1.3 Rainfall in Thailand8
2.1.4 Drought in Thailand9
2.2 Geoinformatics Technology
2.2.1 Remote Sensing
2.2.2 Geographic Information System
2.2.3 Global Navigation Satellite System
2.3 Drought indices
2.3.1 The Vegetation Condition Index
2.3.2 The Enhanced Vegetation Index
2.3.3 The Temperature Condition Index

2.4 Topography	13
2.5 The Standardized Precipitation Evapotranspiration Index	13
2.6 Related Works	15
2.7 Machine Learning Models Algorithms	18
2.7.1 Extreme Gradient Boosting	18
2.7.2 Random Forest	19
2.7.3 Extra Trees Regression	20
2.8 Summary of this chapter	21
CHAPTER 3 MATERIALS AND METHODS	22
3.1 General Background of Study Area	22
3.2 Workflow of Research	23
3.3 Data Collections	24
3.3.1 Remote Sensing data	24
3.3.2 Ground Station Data	25
3.4 Preprocessing Data	25
3.4.1 The Vegetation Condition Index	26
3.4.2 The Enhance Vegetation Index	27
3.4.3 The Temperature Condition Index	27
3.4.4 Topographic Data	29
3.4.5 Climate Hazards Group InfraRed Precipitation with Station Data	29
3.4.6 The Standard Precipitation Evapotranspiration Index	30
3.5 Predictive Model	33
3.5.1 Extreme Gradient Boosting	33
3.5.2 Random Forest Regression.	34
3.5.3 Extra Trees Regression	35
3.5.4 Cross-validation.	36
3.6 Accuracy Assessment	37
3.7 Mapping the Spatial Distribution Drought	37
3.8 Summary of this chapter	38

CHAPTER 4 RESULTS AND VALIDATION	39
4.1 Analysis of Spatio-Temporal of drought	39
4.2 Comparing Performance of ML Models	42
4.2.1 Performances of Machine Learning Models	42
4.2.2 The Importance of Variables	46
4.3 Mapping The Spatial Distribution Drought	47
4.3.1 Short-Term Drought Occurrences	48
4.3.2 Long-Term Drought Trends	50
4.4 Summary of Experiment and Result	52
CHAPTER 5 CONCLUSION AND FUTURE WORK	53
5.1 Conclusion	53
5.2 Future work and Suggestions	54
REFERENCES	56
APPENDIX	63
APPENDIX A	64
APPENDIX B	65
APPENDIX C	68
APPENDIX D	71
DIOCDADIIV	74

LIST OF TABLES

		Page
Table	1 The area experienced drought	.10
Table	2 Summary of selected drought indices	.14
Table	3 Summary of related works	.17
Table	4 Summary of data collections	.25
Table	5 Summary formula remote sensing and ground observation data	.32
Table	6 SPEI classification	.32
Table	7 Summary parameter of Machine learning	.42
Table	8 Accuracy assessment of the Machine Learning	.43



LIST OF FIGURES

P	ag
Figure 1 Diagram Framework in This Study	.6
Figure 2 Diagram of Random Forest	20
Figure 3 Study area the northeast of Thailand	23
Figure 4 Methodology framework of this study2	23
Figure 5 The Vegetation Condition Index 2014 - 2023	26
Figure 6 The Enhance Vegetation Index 2014 - 20232	27
Figure 7 The Temperature Condition Index 2014 - 20232	28
Figure 8 Elevation (DEM)2	29
Figure 9 Climate Hazards Group InfraRed Precipitation with Station Data (CHIPRS) 2014 – 2023	_
Figure 10 Ground Observations (a) SPEI 3 and (b) SPEI 6 Month scale3	31
Figure 11 Average annual precipitation from TMD (2014-2023)3	39
Figure 12 The evolution of SPEI indicating the development of drought from (a) 3 months, (b) 6 months, (c) 9 months, (d) 12-month time scale in the northeast of Thailand from 2014 - 2023	‡ 1
Figure 13 Overall accuracy: (a) R ² , (b) RMSE, (c) MAE from SPEI 3 and (d) R ² , (e) RMSE, (f) MAE from SPEI 6	
Figure 14 The relative importance (%) of the drought factors for (a) XGBoost, (b) Random Forest, (c) Extra Trees from SPEI 3 and (d) XGBoost, (e) Random Forest, (for the Extra Threes from SPEI 6	
Figure 15 Short-term drought distribution map in the northeast Thailand from 2014 20234	
Figure 16 Area based on drought classes SPEI 3	19
Figure 17 Long-term drought trends distribution map in the northeast of Thailand from 2014 – 20235	51
Figure 18 Area based on drought classes SPEL6	7 1



ABSTRACT

Drought, a globally significant natural disaster, imposes considerable economic and environmental impacts, severely impacting agriculture and socio-economic systems annually. The frequency of global drought occurrences can be attributed to the impacts of climate change and human activities. This study aims to investigate the spatiotemporal dynamics of drought in Northeast Thailand by integrating remote sensing (RS) and ground observations with machine learning models.

This study specifically focused on northeast Thailand. This area is situated within the tropical zone, characterized by mainly sandy soil that has a limited capacity to retain water. Therefore, effective water resource management and drought monitoring efforts are needed in northeast Thailand.

The main contents of this thesis include:

- 1) Investigation of spatio-temporal drought patterns (shorth term and long term) of the study area from 2014 to 2023 using ML modeling from Landsat 8 satellite and ground observation data.
- 2) Performance comparison of machine learning (ML) models for monitoring drought in Northeast Thailand.
- 3) Mapping spatial distribution of drought events in the Northeast of Thailand from 2014 to 2023.

This study leverages the fusion of RS and ground data to enhance drought monitoring. Ground indicators offer precision but have limited coverage, while RS indices cover larger areas with less accuracy. ML algorithms were used to combine these data sources, improving spatial resolution and accuracy. The study used five RS parameters such as The Vegetation Condition Index (VCI), The Enhanced Vegetation Index (EVI), The Temperature Condition Index (TCI), Topography, Precipitation, combined with ground data as The Standardized Precipitation Evapotranspiration Index (SPEI). ML techniques, including XGBoost, Random Forest, and Extra Trees, assessed the relationship between variables. Additionally, cross-validation techniques were utilized to validate the model performance. The optimal model was used to



generate a spatial distribution of drought, contributing to more effective drought management strategies, and enhancing drought dynamics in the region.

The results demonstrate that the Extra Trees model is outperform for accurate drought index prediction. For short-term, the results show an R2 ranging from 65.26% to 94.28%, an RMSE between 1.58% to 33.28%, and an MAE ranging from 0.09% to 18.55%. Similarly, for long-term, the results show an R² ranging from 78.73% to 94.8%, an RMSE between 4.55% and 31.93%, and an MAE ranging from 0.45% to 18.14%. In particular, the variables contributing to model accuracy include precipitation (27%-67%), topography (19%-37%), and land surface temperature (6%-21%). The feature importance values of these variables enhance the model performance. The study examines both short-term and long-term precipitation patterns using the Standardized Precipitation Evapotranspiration Index (SPEI) to assess drought conditions. Short-term analysis identified significant drought occurrences in June 2015 and April 2016, with recurrent drought periods observed in late 2018 and 2019, as well as the beginning of 2020 and 2021. These findings underscore the cyclic nature of decreased precipitation and the associated risk of water scarcity within shorter time frames. Moreover, long-term precipitation trends analyzed through SPEI indicated sustained negative values from mid-2015 to 2016, indicating the onset of drought conditions. Particularly noteworthy was the persistent negativity of SPEI values from mid-2018 to 2020, indicating an extended drought period spanning multiple months. indicating the severity and duration of the drought.

The main initiatives of the thesis are as follows:

- 1) Developed method that fuses the drought index using remote sensing (RS) data from the Landsat 8 satellite and ground observations. This provides insights into drought-related environmental parameters and precise meteorological measurements.
- 2) Compared the performance of three ML models to identify the most effective method for drought monitoring in the study area.
- 3) Explored spatiotemporal trends in drought distribution to inform water management and mitigation strategies.

In conclusion, the study provides a framework for strategic planning in drought management by integrating RS and ground observation data. Future work could explore deep learning or neural networks to enhance drought monitoring and understanding of regional environmental implications.

Keywords: drought; remote sensing data; machine learning; Data fusion; XGBoost; Random Forest; Extra trees;

CHAPTER 1 INTRODUCTION

1.1 Background

Drought being a significant global natural calamity, incurs substantial costs and inflicts extensive damage on agriculture the environment and the socio-economic fabric annually (Bahta & Myeki, 2022). The monitoring and forecast of drought can assist policymakers in their response to drought situations (Fu et al., 2022). The occurrence of drought has become more frequent on a global scale due to the combined impacts of climate change and human activity. Typically, droughts occur both in a sequential and concurrent manner (X. Li, Jia, & Wang, 2023). The main factors contributing to drought include uneven and insufficient precipitation, along with insufficient rainfall distribution in specific areas (Carrillo et al., 2023). the primary impact of drought in Thailand is predominantly on the agricultural sector (Marks, 2011).

Thailand located in Asia is very susceptible to fluctuations and shifts in climatic patterns (Sedtha, Pramanik, Szabo, Wilson, & Park, 2023; Shrestha, Chaweewan, & Arunyawat, 2017), as well as extreme weather events such as droughts and floods. The region of Northeast Thailand is situated within the tropical zone, characterized by predominantly sandy soil that has a limited capacity to retain water (Fujii et al., 2017; Suzuki, Noble, Ruaysoongnern, & Chinabut, 2007). The frequency and severity of droughts have increased, causing significant damage to the agricultural and economic sectors, resulting in reduced crop yields and hardships for farmers (Arpakorn & Chen, 2021; Suwanlee, Homtong, & Som-ard, 2023). The northeast of Thailand has 5 provinces, which cover an area of about 63,554 square kilometers, or one-third of the whole country. On the Korat plateau (Saruda, Jinda, & Apiwat, 2021), droughts usually occur when there is a lack of rain for a long period of time, especially in the northeastern region, when there will be a decrease in the amount of rain (Saruda et al., 2021). As a result, the amount of water stored in reservoirs and dams is much less than before. This causes agricultural areas to lack water.

This research uses machine learning XGBoost (XGB), Random Forest (RF) and Extra Trees Regressor (ETR) to integrate remote sensing and ground observation data from

the Thai Meteorological Department to calculate drought indices. The study focuses on leveraging Landsat 8 satellite data from 2014 to 2023 to analyze drought conditions using the Google Earth Engine and scikit-learn and analyzing the spectral indices The Vegetation Condition Index (VCI), The Enhanced Vegetation Index, The Temperature Condition Index (TCI), A Digital Elevation Model (DEM), Climate Hazards Group InfraRed Precipitation (CHIPRS) and The Standardized Precipitation Evapotranspiration Index (SPEI) and using accuracy and the R², RMSE and MAE for the assessment performance of machine learning models (XGB, RF, ETR) and drought mapping in the northeast region of Thailand.

1.2 Scientific Questions

- What are the spatiotemporal patterns of drought occurrences in the Northeast region of Thailand from 2014 to 2023, as observed through Landsat 8 satellite data?
- How does the performance of machine learning models, specifically XGBoost (XGB), Random Forest (RF), and Extra Trees (ETR), compare in accurately calculating drought monitoring in Northeast Thailand?
- What is the spatial distribution of drought events in the Northeast of Thailand from 2014 to 2023?

1.3 Objectives

- To analyze and investigate the spatio-temporal patterns of drought occurrences in the Northeast region of Thailand from 2014 to 2023 using Landsat 8 satellite data.
- To assess and compare the performance of machine learning models between specifically XGBoost (XGB), Random Forest (RF), and Extra Trees (ETR) for the accurate calculation of drought monitoring in Northeast Thailand.
- To map the spatial distribution of drought events in the Northeast of Thailand from 2014 to 2023.

1.4 Structure of Thesis

This research aims to analyze drought within the Northeast of Thailand for the period from 2014 to 2023 using Landsat 8 and ground station data for The Vegetation Condition Index (VCI), The Enhanced Vegetation Index, The Temperature Condition Index(TCI), A Digital Elevation Model (DEM), Climate Hazards Group InfraRed Precipitation (CHIPRS) analysis in Python and The Standardized Precipitation Evapotranspiration Index (SPEI) analysis in R Studio for training and validation. using machine learning models, XGBoost (XGB), Random Forest (RF), and Extra Trees (ETR) to find the best model to assess and compare the performance of the model by R², RMSE, and MAE within the Northeast region of Thailand. The scope of the study is the entire Northeast of Thailand, which is characterized by predominantly sandy soil with limited water retention capacity (Fujii et al., 2017; Suzuki et al., 2007).

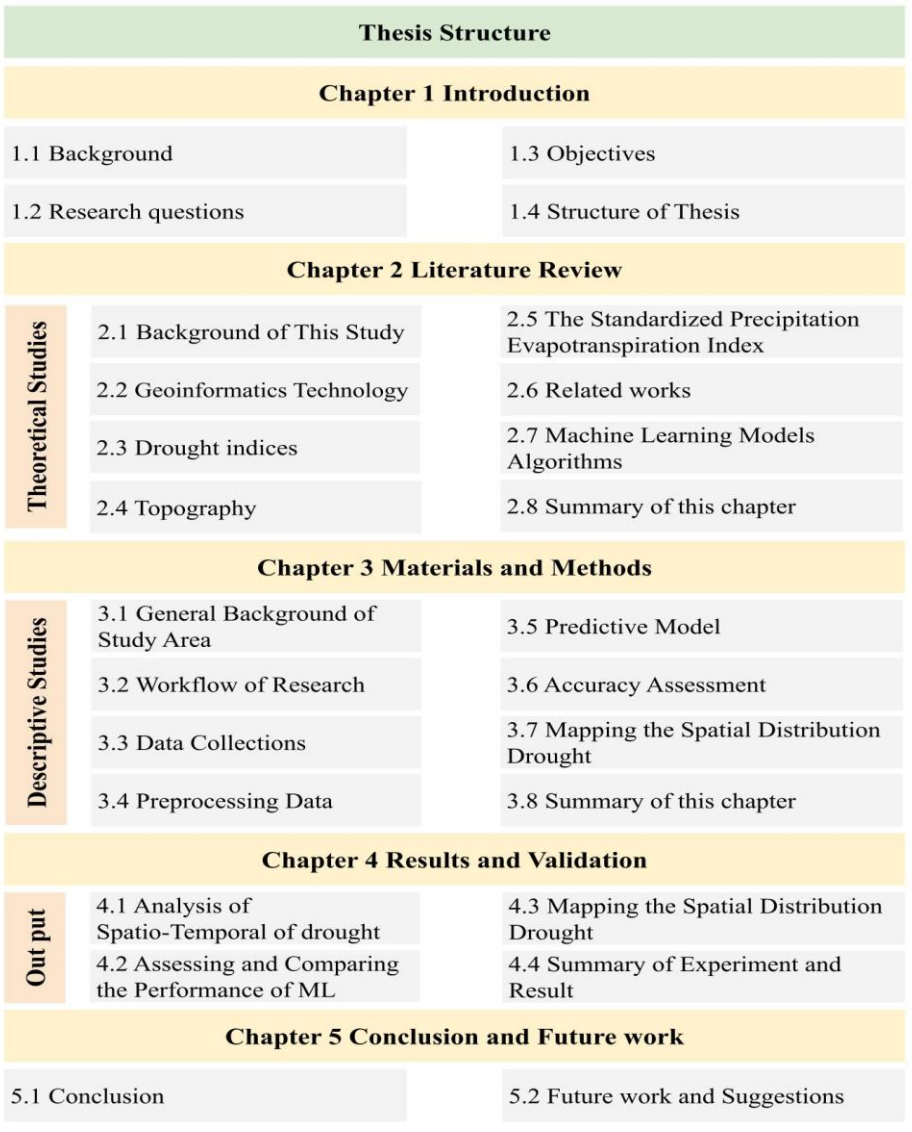


Figure 1 Diagram Framework in This Study

CHAPTER 2 LITERATURE REVIEW

2.1 Background of This Study

2.1.1 The Seasons of Thailand

Thailand generally can be divided into 3 seasons as follows (Thai Meteorological Department) Summer season starts around the middle of February until the middle of May, this is when things will change from the northeast monsoon. It is a storm in the southwest and is how far away the North Pole is from the sun. As a result, the weather is usually hot and stuffy, especially in April. These days, it's mostly hot and dry, but sometimes a cold air mass from China will come through. spread down to cover the top of Thailand.

The rainy season starts around the middle of May until the end of June as the southwest monsoon blows over Thailand, a low-pressure trough will cross the country, causing a lot of rain. It will then move through the southern China area. Thailand has been getting less rain for a while, and it's called rain. This could last for a week or two, a year, or even longer, and it could get worse. and it didn't rain for months.

Winter season starts around mid-October to mid-February. When the northeast monsoon It has blanketed Thailand. In mid-October for 1-2 weeks, the season changes from the rainy season to the winter season. The weather is unstable. It may start to get cold. Or there may still be thunderstorms. Especially in the lower central region. and the eastern region down there will stop raining and the weather will begin to cool later than the northern and northeastern regions (Thai Meteorological Department).

2.1.2 Temperature of Thailand

Thailand is in the tropics. The general weather conditions are therefore hot and humid most of the year. The average year-round temperature in Thailand is approximately 27 °C. However, temperatures vary in each area and season. The area is deep inland from the central region. The upper eastern region up to the northern region will have very different temperatures between summer and winter and between day and night in summer, the highest temperature is in the afternoon. It usually reaches nearly 40 °C or more from March to May. Especially April will be the hottest month of the year. In

winter, the lowest temperature in the early morning drops to a range of cold to very cold. Especially December to January is the coldest period of the year. During this period, temperatures can drop below freezing in the northern region. and the northeastern region, areas that are mountain ranges or high mountain peaks for areas next to the sea, including the lower eastern region, and the southern region, temperature variations across days and seasons are less. The summers are not as hot, and the winters are not as cold as in areas deeper inland (Thai Meteorological Department).

2.1.3 Rainfall in Thailand

Many Thailand has good rainfall. Most areas receive 1,200-1,600 millimeters of rainfall per year. The average annual total rainfall throughout the country is approximately 1,587.7 millimeters. The amount of rainfall in each area varies according to topographical features. In addition to seasonal variations Upper Thailand is normally dry and has little rain in winter. When entering summer, the amount of rain It will increase somewhat along with thunderstorms. And when the rainy season enters, the amount of rain will greatly increase.

The highest amount of rain will occur in August or September. Areas with a lot of rain Most are in front of the mountain range. or the side receiving the southwest monsoon winds, including areas on the western side of the country and the eastern region. Most of the areas with little rain are behind the mountains. Including the central areas of the northern and central regions. and the western area of the northeastern region for the southern region, there is a lot of rain throughout the year except during the summer.

Area in the southern west coast which is the side receiving the southwest monsoon winds There will be more rainfall than the southern region on the eastern coast during the rainy season. With the highest amount of rain in September. During the winter in the southern and eastern areas which is the side receiving the northeast monsoon winds There will be more rainfall than the southern west coast. With the highest amount of rain in November (Thai Meteorological Department).

2.1.4 Drought in Thailand

In Current global climate change It causes the rainy season to become shorter, which means that the dry season will be longer. as a result, the amount of water in dams and reservoirs throughout the country is insufficient for consumption. especially in agricultural areas in addition, the prosperity of the community Economic expansion such as the industrial sector Service business sector and the number of the population has continued to increase at the same time as a result, the demand for water use in various activities in every sector has increased. Therefore, it is one of the factors that cause the problem of water shortage.

Thailand has drought problems quite frequently. Most droughts in Thailand are caused by abnormally long periods of rain during the rainy season. or caused by natural phenomena such as El Niño. Almost every region in Thailand has experienced drought problems. Droughts have occurred since the past until the present. The most recent drought in Thailand was of 2019 - 2020, which may have been quite severe. Due to the amount of demand for water increasing every day, but the lack of rain and El Niño, there is very little water in various reservoirs and dams within Thailand. Droughts in Thailand mostly occur in two periods.

- 1) The winter period continues into the summer. Starting from the second half of October onwards. The upper Thailand area (Northern, Northeastern, central and eastern regions) will have a progressive decrease in rainfall until entering the rainy season in mid-May of next year. This type of drought occurs every year.
- 2) In the middle of the rainy season Around the end of June to July There will be some rain. This kind of drought occurs only in certain localities or areas. Sometimes it may cover a wide area almost all over the country (Thai Meteorological Department).

The area most affected by drought is the northeast region. Because it is an area where the influence of the southwest monsoon cannot reach. And if in any year there is no tropical cyclone moving through this line, it will cause danger. The drought is more severe. In addition to the areas mentioned above, there are other areas that frequently experience drought—problems as shown in the Table 1.

	=
-	
V	
_	=
Ν.	=
$\overline{}$	
v	=
⊃	
٥	=
~	=
2	
D	
	=
	=
	=
	ш

T 1 1	-1	701			•	1		1 1 .
Inhia		Tho.	0400	O 371	0 0 111	2222	_	lrought
Tane		1110	агеа	- x				

Month	North	Novella a set	Control	East -	South	
Month	North	Northeast	Central		east	west
Jan						Drought
Feb		Drought	Drought			Drought
Mar	Drought	Drought	Drought	Drought	Drought	Drought
Apr	Drought	Drought	Drought	Drought		Drought
May						Drought
Jun	Lack of Rain	Lack of Rain	Lack of Rain	Lack of Rain		
Jul	Lack of Rain	Lack of Rain	Lack of Rain	Lack of Rain		

2.2 Geoinformatics Technology

Geo-information technology includes of Remote Sensing technology, Geographic Information System and Global Positioning System. For application in various fields of work. Details of these technologies are as follows:

2.2.1 Remote Sensing

RS refers to the science and art of acquiring information about objects, areas, or phenomena from data recording devices without touching the target object. It relies on the properties of electromagnetic waves as a medium for acquiring information in 3 ways. Characteristics include wavelength (Spectral), morphology of objects on the earth's surface (Spatial), and changes over time (Temporal) (Abdulraheem et al., 2023). If weather observation station data are not covered enough, remote sensing data can make up for it with their wide coverage, high spatial resolution, and strong timeliness.

2.2.2 Geographic Information System

Geographic information system means an information system that brings information to be collected, stored, and analyzed in a systematic way (Ershad & Ali, 2020). Data can be searched and updated, including data obtained from analysis to help make decisions in various matters. The data collected and stored in the system can be used to manage and analyze spatial data. The spatial data is also linked with Attribute data that is used to describe in detail the phenomena and characteristics of that area. This will make the use of data more accurate and accurate.

2.2.3 Global Navigation Satellite System

Global Navigation Satellite System is a satellite navigation system. Using electronic equipment as a receiver to process the positional information at the point where the receiving device is located. This technology is becoming very popular in surveying and research applications. Currently, many satellite navigation systems have been developed, such as BeiDou (China), GPS (USA), GLONASS (Russia), Galileo (Europe), QZSS (Japan), SBAS (Ashour, El-Tokhey, Mogahed, & Ragheb, 2022).

There are many remote sensing drought indices that have been proposed and used to track droughts on a global or regional level. These indices are based on new denoising algorithms and atmospheric correction algorithms. The effects of drought on plant growth and development can be seen on remote sensing images as changing spectral features. Lack of water can change plants' biochemical and physiological features, which can then cause changes in their spectral properties. So, most remote sensing drought indices figure out what a drought is by checking the condition of the plants on the ground. Now, RS provides data about rainfall, temperature, groundwater storage, evaporation, plant response, and plant functions. Such information can be used to characterize drought from both temporal and spatial perspectives.

2.3 Drought indices

2.3.1 The Vegetation Condition Index

In The Vegetation Condition Index (VCI) useful for identifying and tracking droughts and colors to show how healthy the plants are. NDVI data is modified and used to create vegetation conditions (Kogan, 1995). The Normalized Difference Vegetation Index (NDVI), calculated from the ratio of red and near-infrared in the electromagnetic spectrum [11].

$$NDVI = \frac{(NIR - red)}{(NIR + red)}$$

NDVI has become the primary way to describe crops. Area covered around the world Vegetation classification and dynamics and the life cycle of plants (Kogan, 1995). The NDVI measures the amount of green vegetation by considering that during photosynthesis, plants absorb visible light and strongly reflect near-infrared light, which is not used for photosynthesis. NDVI values relate to green biomass, green leaf

area index (LAI) (Caruso, Palai, Tozzini, D'Onofrio, & Gucci, 2023), and the percentage of vegetation cover (SalİK & Karacabey, 2019).

it shows the health of the plants and helps with more accurate labeling. The lowest to highest monthly NDVI values were looked at to see how different they were each year, VCI shows how the weather affects vegetation (Ejaz, Bahrawi, Alghamdi, Rahman, & Shang, 2023). so, the following equations were used.

$$VCI = \frac{(NDVI - NDVImin)}{(NDVImax - NDVImin)} \times 100$$

VCI value is higher, which means that the plants are very healthy. In other words, a high VCI number means that drought problems are less likely to happen (Arpakorn & Chen, 2021).

2.3.2 The Enhanced Vegetation Index

The Enhanced Vegetation Index is often used to measure the health of vegetation (Diodato & Bellocchi, 2008). EVI looks like the Normalized Difference Vegetation Index (NDVI). EVI can be saturation or the influence of aerosols and soil background on vegetation indices (Xiao et al., 2003). By considering the differential scattering of aerosols in blue and red bands, EVI mitigates the effects of aerosols on the red band, enhancing the accuracy of vegetation monitoring. Unlike NDVI, EVI exhibits a more significant linear relationship with actual vegetation coverage and provides better sensitivity to vegetation changes across different landscapes and densities (B. Li, Tang, & Chen, 2009), so the following equations were used.

$$EVI = \frac{(NIR - Red)}{(NIR + 6 x Red - 7.5 x Blue + 1)}$$

2.3.3 The Temperature Condition Index

The Temperature Condition Index (TCI) derived thermal infrared bands. It is related to the response of vegetation to temperature calculated with The Land Surface Temperature (LST) and provides important information about the health of vegetation (Kogan, 1995). surface evapotranspiration by LST variations and assessing evapotranspiration, vegetation water stress (Karnieli et al., 2010), and drought occurrence by soil moisture content changes (X. Li et al., 2023), and is defined as:

$$TCI = \frac{(LST - LSTmin)}{(LSTmax - LSTmin)} \times 100$$

where LST is actual, LSTmin and LSTmax are the multi-year minimum and maximum LST values for each pixel, respectively, calculated from multiyear time series data. Higher TCI values indicate higher temperatures compared to the multi-year range, suggesting drought conditions or stress on vegetation (Kocaaslan, Musaoglu, Türkeş, & Tanik, 2017), while lower TCI values suggest lower temperatures relative to the multi-year range, which may indicate healthier vegetation or more favorable conditions (Singh, Roy, & Kogan, 2003).

2.4 Topography

Drought is related to topography (Xu et al., 2023). This study also considered information from topography and geographic locations, topography at high elevations in the mountains exhibited a higher sensitivity to drought. Despite having low climatic water deficits, high-elevation forests face constraints such as shallow, rocky soils and steep slopes that limit soil water storage and tree root development leading to vulnerability during drought events (Cartwright, Littlefield, Michalak, Lawler, & Dobrowski, 2020).

2.5 The Standardized Precipitation Evapotranspiration Index

The Standardized Precipitation Evapotranspiration Index (SPEI) serves as a comprehensive tool for monitoring both wet and dry conditions, with potential evapotranspiration (PET) playing a crucial role in the frequency, severity, and intensity of drought occurrences (Vicente-Serrano & Beguería, 2015). PET estimation methods, such as Thornthwaite, Hargreaves, and Penman-Monteith, are instrumental in SPEI calculations (Lin & Shelton, 2020). The Thornthwaite and Hargreaves methods rely on maximum and minimum temperatures for PET computation, with Hargreaves additionally utilizing the latitude of the station to estimate extraterrestrial radiation (Pan et al., 2015). In contrast, the Penman-Monteith method integrates humidity and wind speed, necessitating more extensive meteorological data. The choice among these methods depends on the availability of meteorological data (Páscoa, Gouveia, Russo, & Trigo, 2017).

The SPEI index reflects the accumulated water content, both above and below ground, throughout the season and year, making it sensitive to precipitation and atmospheric evaporative demand (Vicente-Serrano & Beguería, 2015). Calculated over various timescales, the SPEI provides insights into different temporal patterns of wetness or dryness. The SPEI 1-month scale is particularly useful for monitoring rapid changes in drought conditions and their immediate impacts on ecosystems, agriculture, and water resources. Meanwhile, the SPEI 3-month scale proves valuable for assessing drought effects on seasonal vegetation growth, water availability, (Tomas-Burguera et al., 2020) and agricultural productivity. For agricultural planning, the SPEI 6-month scale is significant as it covers a substantial portion of the growing season (Potopová et al., 2018), aiding in the evaluation of drought stress on crops and natural vegetation. Finally, the SPEI 12-month scale facilitates the understanding of cumulative drought effects over an entire year, including impacts on water resources, ecosystems, and long-term agricultural sustainability (Nwayor & Robeson, 2024; Saruda et al., 2021).

Table 2 Summary of selected drought indices

Drought indices	Usage	Reference
Normalized difference vegetation index (NDVI)	It is used for measuring agricultural drought and monitoring the health of vegetation.	(SalİK & Karacabey, 2019),(Kogan, 1995),(Qin et al., 2021)
The Land Surface Temperature (LST)	High LST values over agricultural areas can indicate insufficient soil moisture for crop growth.	(Kogan, 1995),(Karnieli et al., 2010),(X. Li et al., 2023),(Holzman, Rivas, & Piccolo, 2014)
The Vegetation Condition Index (VCI)	Assesses the health of vegetation from the impact of drought. low VCI values can be indicative of vegetation stress due to inadequate water availability.	(Arpakorn & Chen, 2021),(Ejaz et al., 2023),(Kogan, 1995),(Rousta et al., 2020)
The Enhanced Vegetation Index (EVI)	EVI provides better sensitivity to vegetation changes across different landscapes and densities	(Diodato & Bellocchi, 2008),(B. Li et al., 2009)

Drought indices	Usage	Reference
The Temperature Condition Index (TCI)	TCI values indicate higher temperatures, suggesting drought conditions or stress on vegetation, TCI values suggest lower temperatures, suggesting healthier vegetation	(Kogan, 1995),(Karnieli et al., 2010),(X. Li et al., 2023),(Kocaaslan
		et al., 2017)
The Standardized Precipitation Evapotranspiration Index (SPEI)	Uses monthly rainfall to calculate the evapotranspiration potential, which indicates the amount of accumulated water both above ground and underground.	(Pan et al., 2015),(Vicente- Serrano & Beguería, 2015)

2.6 Related Works

Xiehui Li (2023) investigated drought monitoring in southwest China from 2010 to 2019, focusing on comparing land surface temperature (LST) using remote sensing with meteorological station measurements from 144 weather stations across southwest China from 1980 to 2019. They employed remote sensing data and machine learning techniques, specifically Random Forest (RF) and eXtreme Gradient Boosting (XGBoost). Their model's effectiveness was validated against historical drought records and various drought indices, including the Standardized Precipitation Evapotranspiration Index (SPEI) and the Meteorological Drought Composite Index (MCI). The model demonstrated exceptional accuracy and performance, achieving an average score of 0.955 for RF and 0.931 for XGBoost in 5-fold cross-validation (X. Li et al., 2023).

Yangyang Zhao (2022) used machine learning to investigate the relationships between independent and dependent factors to replicate the Standard Precipitation Evapotranspiration Index (SPEI) for Shandong province, China. They utilized seven drought effect factors from the Moderate Resolution Imaging Spectroradiometer (MODIS) satellite sensor, the Global Precipitation Measurement Mission (GPM), and the Global Land Data Assimilation System (GLDAS). The study also incorporated ground-based SPEI derived from monthly temperature and precipitation data from various weather sites. The Bias-Corrected Random Forest (BRF) model outperformed eXtreme Gradient Boosting (XGBoost) and Support Vector Machines (SVM), accurately predicting SPEI distribution and tracking drought conditions in areas lacking ground-based observations (Zhao et al., 2022).

Shahana Sultana (2021) assessed the northwestern regions of Bangladesh by comparing multiple drought indices (VCI, TCI, VHI, TVDI, VSDI) from 1990 to 2018. Their study revealed vegetation reduction (NDVI) and land surface temperature (LST) increased between 2014 and 2002, leading to drought in 2018, particularly affecting water-deficient and unfarmed lands. Emphasizing the importance of satellite-based drought measurement, the study highlights the necessity of better understanding and managing droughts in northwest Bangladesh's agricultural landscape (Sultana, Gazi, & Mia, 2021).

Savittri Ratanopad Suwanlee (2023) utilized Earth observation (EO) satellites and MODIS NDVI data to monitor drought in Northeast Thailand from 2001 to 2019. Employing the Savitzky-Golay method for noise reduction, the study identified distinctive drought patterns using optimal indicators like the Vegetation Condition Index (VCI). Severe and frequent droughts in 2005, 2004, 2007, and 2001 significantly impacted northern and central regions. The VCI demonstrated high accuracy (R2=0.85), offering a reliable tool for drought monitoring in the region and effectively displaying the spatial distribution of long-term drought regions (Suwanlee et al., 2023).

Nuaman Ejaz (2023) focused on drought monitoring in the hyper-arid region of the Kingdom of Saudi Arabia using remote sensing to analyze the Standardized Precipitation Evapotranspiration Index (SPEI) and Remote Sensing Retrieved Drought Indices (RSDIs) from 2001 to 2020. Utilizing multi-temporal Landsat sensors and the Google Earth Engine platform, they identified the Vegetation Condition Index (VCI), Temperature Condition Index (TCI), and Vegetation Health Index (VHI) as key drought indicators. The study found stronger agreement between VHI and SPEI compared to TCI and VCI, indicating their suitability for drought measurement, especially in data-limited hyper-arid regions of Saudi Arabia (Ejaz et al., 2023).

Junyong Zhang (2023) employed machine learning for drought estimation in the semi-arid zone of northern China. Using multiple linear regression and bias-corrected Random Forest algorithms, they analyzed spectral aridity index, VSDI, VCI, TCI, VHI, GVMI, VSWI, NDWI, RVI, MSAVI, PDI, SPSI, and NMDI from 2001 to 2019,

along with ground-based climate datasets. They calculated Standard Precipitation Index (SPI), Standardized Precipitation Evapotranspiration Index (SPEI), and Palmer Drought Index (PDSI) for various time scales. The bias-corrected RF model demonstrated superior accuracy, establishing it as an effective tool for monitoring drought at multiple time scales (J. Zhang et al., 2023).

N. Zaabar (2022) utilized a Convolutional Neural Network (CNN) with Object-Based Image Analysis (OBIA) to analyze spectral index combinations from Sentinel-2 imagery in northern Algeria. NDVI, NDBI, and NDWI were key indices. The CNN-OBIA approach demonstrated strong accuracy, with Overall accuracy and Kappa Index reaching 93.1% and 0.91, respectively, outperforming RF-based OBIA (Narimane, Niculescu, & Mihoubi, 2021).

Foyez Ahmed Prodhan (2021) employed deep forward neural network (DFNN) to monitor agriculture in South Asia from 2001 to 2016. DFNN outperformed distributed Random Forest (DRF) and gradient boosting machine (GBM), exhibiting stability in cross-validated training data and accurately estimating Soil Moisture Deficit Index (SMDI) across phenology stages. DFNN-estimated SMDI closely matched in-situ SPEI, suggesting its potential for consistent drought monitoring over a wide area (Prodhan et al., 2021).

Table 3 Summary of related works

Study area	ML	Dataset used	Indices	Ref.
	algorithm			
Southwest	RF,	MODIS,	NDVI, EVI,	(X. Li et
China	XGBoost	TRMM3B43	TRMM-SPI, VCI,	al., 2023)
			TCI, VTCINDVI,	
			VTCIEVI,	
			TVDINDVI,	
			TVDIEVI,	
			VSWINDVI,	
			VSWIEVI, SPEI,	
			MCI	
Shandong	BRF,	MODIS,	VCI, TCI, PCI,	(Zhao et
province, China.	XGBoost,	GLDAS2.1,	SMCI, EVI, ET,	al., 2022)
	SVM	GPM	PET	

Study area	ML	Dataset used	Indices	Ref.
	algorithm			
The	-	Landsat TM,	VCI, TCI, VHI,	(Sultana et
Northwestern		Landsat ETM+,	TVDI, VSDI	al., 2021)
regions of		Landsat		
Bangladesh.		OLI/TIRS		
The Northeast	-	MODIS	NDVI, VCI, SVI	(Suwanlee
Thailand.				et al.,
				2023)
The hyper-arid	-	Landsat 7 and 8	SPEI, VCI, TCI,	(Ejaz et al.,
region of the			VHI	2023)
Kingdom of				
Saudi Arabia.				
The semi-arid	MLR, RF	MODIS,	VSDI, VCI, TCI,	(J. Zhang
zone of northern		GLDAS2.1,	VHI, GVMI, VSWI,	et al.,
China.		GPM	NDWI, RVI,	2023)
			MSAVI, PDI, SPSI,	
			NMDI	
The North-	CNN,	Sentinel 2	NDVI, NDWI,	(Narimane
western region	OBIA		NDBI	et al.,
Algeria	(SVM, RF)			2021)
The South Asia	DFNN	MODIS,	TCI, VHI, VCI,	(Prodhan et
		MERIS,	EDI, SPEI, SPI,	al., 2021)
		GLDAS,	PAI, PCI	
		CHIRPS,		
		GIMMS,		
		Station Data		

2.7 Machine Learning Models Algorithms

This study further employed the Logistic Regression (LR), XGBoost (XG), Random Forest (RF), and Extra Trees (ETR) models as baseline models against which to benchmark the predictive performance. The baseline models chosen to possess the ability to allow a robust assessment of the model against various degrees of complexity. The model was further used to benchmark the explainability of the drought in northeast Thailand.

2.7.1 Extreme Gradient Boosting

The XGBoost algorithm, developed by Chen and Guestrin (Chen & Guestrin, 2016). Which is a machine learning technique for regression and classification problems which produces a prediction model in the form of an ensemble of weak prediction models (R. Zhang, Chen, Xu, & Ou, 2019). The XGBoost algorithm represents a

significant improvement in computational efficiency within research (B. Zhang et al., 2023). Its robust architecture not only enhances reliability but also facilitates the attainment of more dependable results. This algorithm has garnered preference in research due to its adeptness in handling vast datasets through parallel processing and distributed computing capabilities, thereby amplifying its efficacy in addressing complex scientific inquiries is a unique way to apply both Gradient Boosting Machine and Regression Trees (CART) (Ekmekcioğlu, 2023). It tries to avoid overfitting while making the best use of computing resources by combining predictive and regularization terms in simplified objective functions. XGBoost also does parallel math automatically while the training is going on (Gul, Staiou, Safari, & Vaheddoost, 2023). XGBoost starts with a single leaf and adds more branches to the tree repeatedly until the best split is found. With XGboost, you can't train multiple trees at the same time, but you can make separate tree nodes at the same time. XGBoost has a distributed weighted quantile sketch method that helps you find the best split points and work with weighted datasets (Ali, Abduljabbar, Tahir, Sallow, & Almufti, 2023; Chen & Guestrin, 2016). The weights of individual trees can be scaled down by a constant, thus reducing the impact of a single tree on the final score (Mehraein, Mohanavelu, Naganna, Kulls, & Kisi, 2022).

2.7.2 Random Forest

The Random Forest algorithm, developed by Breiman (Breiman, 2001). RF is a combination classification or regression method based on statistical learning theory. The resampling bootstrap method is used to get several samples in an RF, and regression trees are built for each bootstrap sample (J. Li et al., 2021). Most of the time, RF use bootstrapping to make random groups from a starting dataset while keeping the population size the same. A decision tree is built for each of these groups. In regression tasks, the final output of an RF model is simply the average of the predictions made by each tree. In classification tasks, on the other hand, the outcome that appears most often is picked as the final output of the RF model (Niazkar et al., 2024). The random forest method is famous for being able to handle a lot of data, find complex relationships between factors, and make correct predictions. As part of this regression method, we used estimators that consider the number of trees, the

maximum depth set as the tree's highest level, and other factors (Aziz, Camana, Garcia, Hwang, & Koo, 2023). algorithm shown in figure 2.

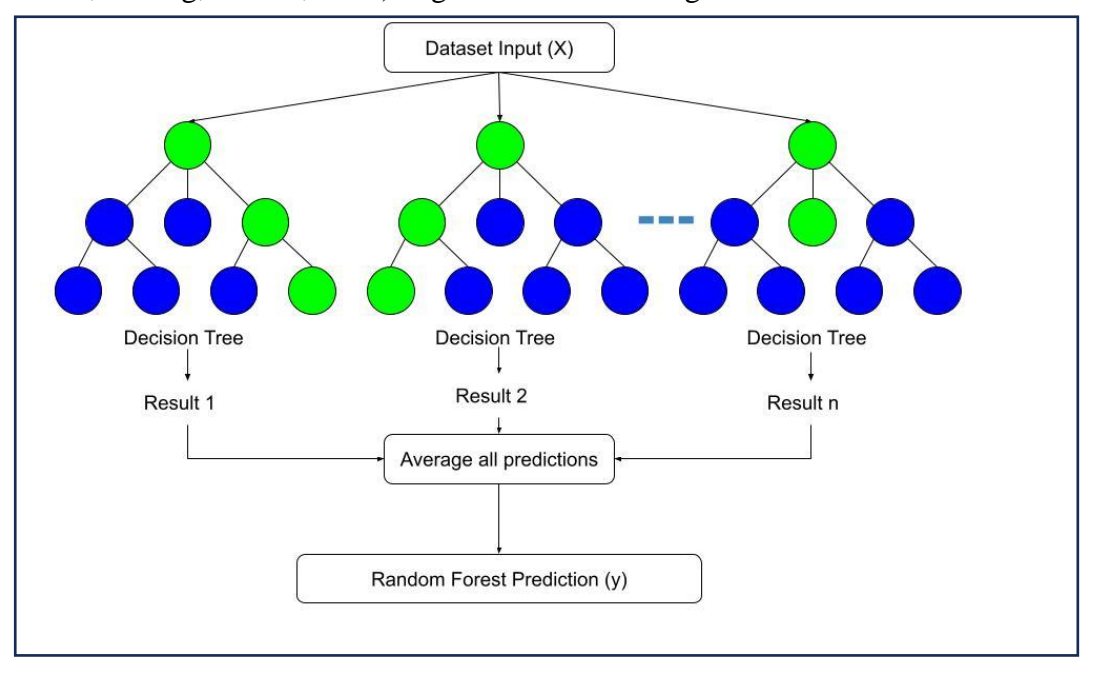


Figure 2 Diagram of Random Forest

2.7.3 Extra Trees Regression

The Extra Tree Regression (ETR) algorithm was created by building on the Random Forest (RF) model and developed by Geurts et al (Geurts, Ernst, & Wehenkel, 2006). The distinction between Extra Trees and Random Forest lies in their approach to selecting cut points for node splitting (John, Liu, Guo, Mita, & Kidono, 2016). Random Forest selects the optimal split, while ETR chooses it randomly. Consequently, in terms of computational efficiency, the ETR algorithm is faster as it randomly selects the split point without calculating the optimal one. (Lou et al., 2022) The ETR is a supervised learning algorithm that needs to be trained on a labelled dataset that has input features and goal values that go with them. Like the Random Forest algorithm, ETR algorithm makes a lot of decision trees, but each tree's samples are chosen at random and are not replaced. This makes a set of datasets with unique samples for each tree. Each tree also gets a random set of a certain number of features from the whole set of features. In particular, the ETR algorithm predicts a continuous target variable by looking at the properties of the input. This algorithm proves particularly valuable when dealing with complex regression problems (Aziz et al., 2023).

2.8 Summary of this chapter The In conclusion, the literatus

The In conclusion, the literature review provides various factors influencing weather patterns, particularly focusing on Thailand. Thailand's seasonal variations, including summer, rainy season, and winter, and the meteorological conditions during each period. the temperature and rainfall patterns across Thailand, the variations in different regions and seasons. Additionally, it discusses the prevalent issue of drought in Thailand, attributing it to factors such as climate change, population growth, and increased water demand. The chapter also outlines the geographic and topographic factors influencing drought susceptibility, particularly noting the sensitivity of high-elevation regions.

Moreover, the theories of geoinformatics technologies such as remote sensing, geographic information systems (GIS), and global navigation satellite systems (GNSS), emphasize their significance in monitoring and analyzing weather-related phenomena. these technologies aid in drought assessment and mitigation efforts through the analysis of various indices such as the Vegetation Condition Index (VCI), Enhanced Vegetation Index (EVI), Temperature Condition Index (TCI), and the Standardized Precipitation Evapotranspiration Index (SPEI).

Furthermore, the chapter introduces machine learning models, including Logistic Regression, XGBoost, Random Forest, and Extra Trees, which are utilized for predictive analysis and understanding the complexities of drought in northeast Thailand. It provides the algorithm's functions through data analysis and prediction.

CHAPTER 3 MATERIALS AND METHODS

The methodology of this study contains XGBoost, Random Forest and Extra Trees models using remote sensing data from Landsat 8 and ground observation data from the Thai Meteorological Department for the calculation of drought indices. This chapter includes data collection, data preprocessing, machine learning drought period 2014 - 2023 and model accuracy comparison. All steps will be detailed in the following.

3.1 General Background of Study Area

The purpose of this research is to investigate the effects of drought in the northeast of Thailand. It's between the latitudes of 14° and 16° N and the longitudes of 101° and the 106° East (Mongkolsawat et al., 2001). The terrain is on the Korat plateau because most of it is a plateau show in figure 3. Slopes from west to east. The edge of the area is a high mountain. Most of the area is covered with rocks. The plain area is a large basin of land. The Korat Basin covers three-quarters of the entire northeastern region. It is considered the widest plain in Thailand, with an average height of 120–170 meters above mean sea level. The area in the middle of the basin is a low plain. The Mun River is the main river that drains water from the plain edge of the basin. It is the most important tributary of the Mekong River. Its origin is in Nakhon Ratchasima Province.

It is the longest river in this region, 641 kilometers long, with a basin area of approximately 70,100 sq. km., lying parallel to the Phanom Dong Rak mountain range. The Mun River is a river. The slope is very slight, meaning that the entire length of the river will decrease by an average of 52 meters, or 16 centimeters per kilometer, causing the plains in the Mun River area to be flooded every year. This is because the water cannot be drained out in time with the water capacity. The Mun River flows through Nakhon Ratchasima, Buriram, Surin, Sisaket and Ubon Ratchathani provinces. and the Mun River flows into the Mekong River in Khong Chiam District. Ubon Ratchathani Province (Arts and Culture Center Khon Kaen University). showed in Figure 3.

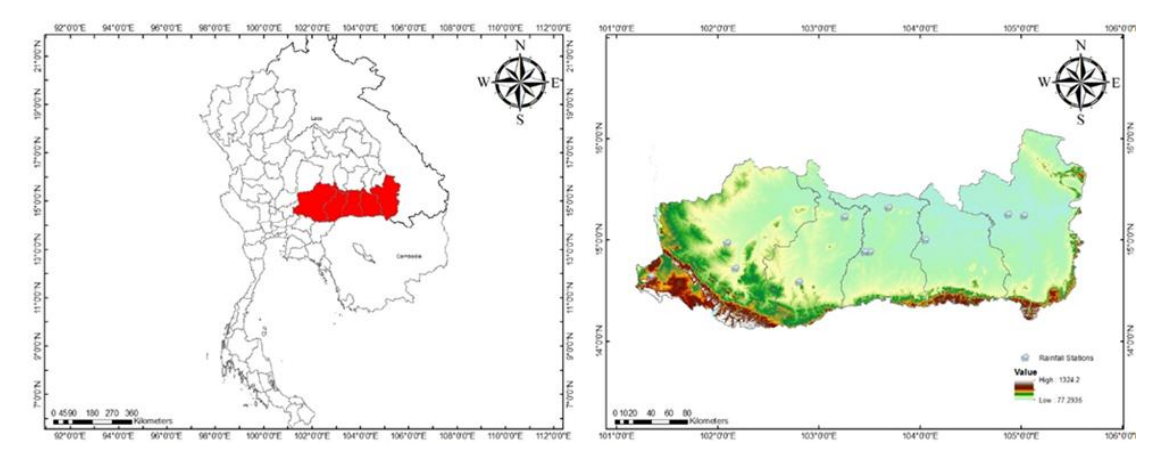


Figure 3 Study area the northeast of Thailand

3.2 Workflow of Research

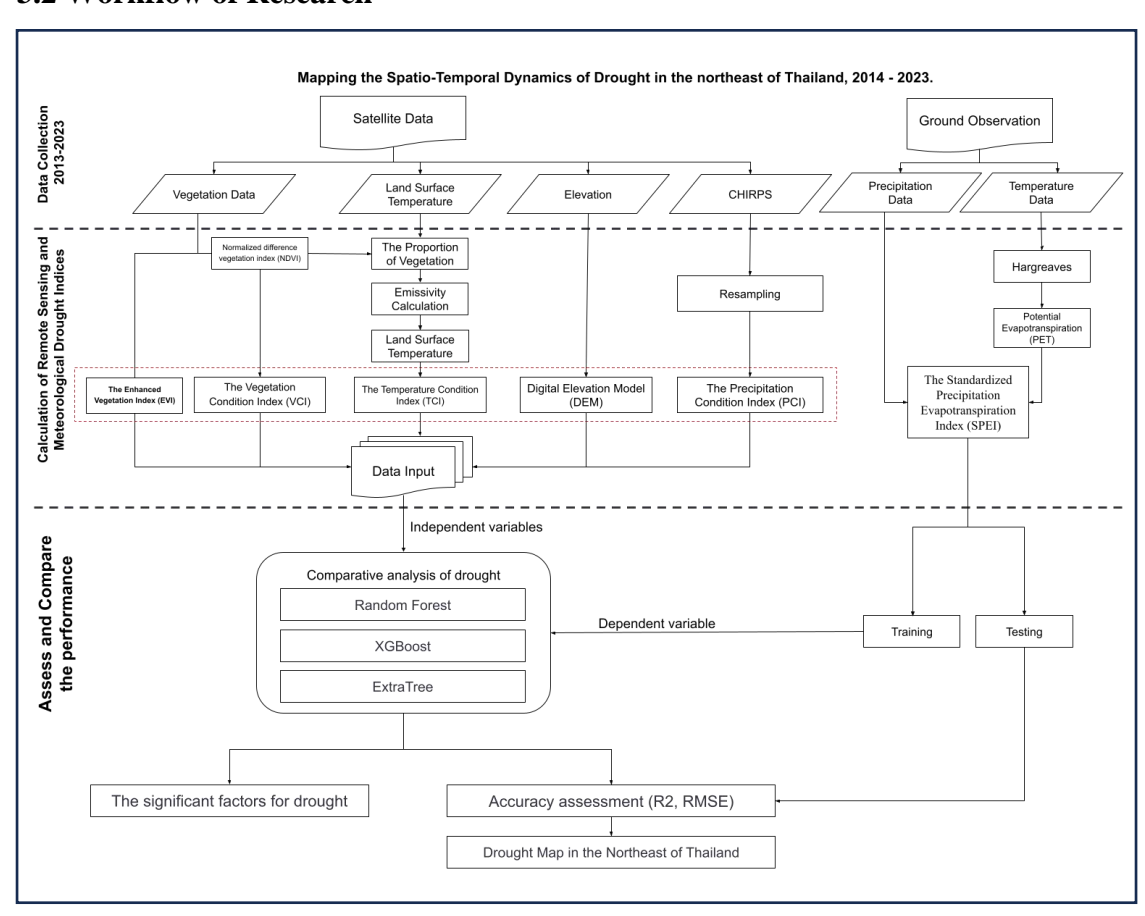


Figure 4 Methodology framework of this study

This workflow explains from beginning to completion, the methods for conducting this investigation. Figure 4 displays all data variables and sources, including data preprocessing and remote sensing data such as vegetation, temperature, topography, and precipitation. While ground observation was calculated according to SPEI, the data were processed, and the data were also converted from vector to raster formats. For the model prediction. Three machine learning algorithms were used to estimate the drought in the study area and identify the most effective model with the most important feature variables. Finally, the spatial distribution of the drought area was computed using the Zonal statistic from the best model output.

3.3 Data Collections

This study combines remote sensing techniques and ground observations to calculate the drought area. Remote sensing data sourced from Google Earth Engine, a cloud-based geospatial data analysis platform, enables the access and analysis of vast quantities of satellite imagery, climate data, and other pertinent geospatial information. Additionally, meteorological data obtained from the Thai Meteorological Department contributed to the comprehensive dataset utilized in this calculation of the drought area.

3.3.1 Remote Sensing data

The remote sensing data used The Landsat 8 has a 30-meter spatial resolution. This dataset contains atmospherically corrected surface reflectance and land surface temperature derived from the data produced by the Landsat 8 OLI/TIRS ("LANDSAT/LC08/C02/T1_L2") sensors (Holden & Woodcock, 2016; Orusa, Viani, Cammareri, & Borgogno Mondino, 2023; Perez & Vitale, 2023). using Band 2 (blue), Band 4 (red), Band 5 (near infrared), and Band 10 (surface temperature). This data covered a period of 10 years, from 2014 to 2023. This data was used to analyze the drought indices VCI, EVI, TCI and topography this study use DEM from Copernicus ("COPERNICUS/DEM/GLO30") (Guth et al., 2021; Im, 2023; T. Li et al., 2023; Yuzugullu, Fajraoui, Don, & Liebisch, 2024) DEM is a Digital Surface Model (DSM) that represents the surface of the Earth including buildings, infrastructure and vegetation. This DEM is derived from an edited DSM named WorldDEM&trade and Precipitation from Climate Hazards Group InfraRed Precipitation ("UCSB-

CHG/CHIRPS/DAILY") with Station Data (CHIRPS) is a quasi-global rainfall dataset (Du et al., 2023; Gwatida et al., 2023). CHIRPS incorporates 0.05° resolution satellite imagery with in-situ station data to create gridded rainfall time series for trend analysis and seasonal drought monitoring by Google Earth Engine.

3.3.2 Ground Station Data

These ground observations cover a period of 11 years from 2013 to 2023 because SPEI 12 requires data from the previous year to calculate the period to ensure accurate and comprehensive assessments of drought severity over a full year. The meteorological data, including precipitation and temperature data, is collected monthly from 11 weather stations (showing station data in Appendix A) across the northeast of Thailand. The data comes from the Thai Meteorological Department. And prepare the data from the table in pdf to csv format using the Microsoft Excel program to prepare the data (showing precipitation and temperature data in the appendix B, C, D) from the original format into the SPEI package format before calculating in the R program.

Table 4 Summary of data collections

Type Sources	Dataset	Index	Spatial	Period	Source
			resolution		
Remote sensing Data		VCI			HCCC
	Landsat 8	EVI	20 m		USGS
		TCI	30 m	2014- 2023	
	GLO-30	DEM			Copernicus
	CHIPRS	PCI			USGS/
	CHIFKS	rcı			CHC
Ground station	Precipitation	SPEI	11 -4-4:	2013 - 2023	TMD
Data	Temperature		11 stations		TMD

3.4 Preprocessing Data

The workflow includes several key steps. It begins with data loading, followed by index computation. During the index calculation phase, each index is processed individually, and subsequently merged into a singular image using the addBands function in Google Earth Engine. This combine image is later exported as a GeoTiff file, resulting in the generation of multiple images. After that, exporting image data will receive multiple images because of the large area. Subsequently, the integration of these image merges using the GDAL library in Python 3.11 within the Jupyter Notebook environment. Each year, the summary formula for preprocessing is shown in Table 5.

3.4.1 The Vegetation Condition Index

The Vegetation Condition Index (VCI) is derived from the Normalized Difference Vegetation Index (NDVI), computed utilizing Landsat 8 bands 4 (red) and 5 (near infrared). The NDVI is a metric widely employed for assessing vegetation health (Gessner, Reinermann, Asam, & Kuenzer, 2023). Utilizing Google Earth Engine, NDVI values are processed to generate the VCI, which provides insights into the vegetation's condition at a spatial resolution of 30 meters. After that, computation, the resulting VCI values undergo a normalization process to standardize their scale to a range of 0 to 1. The methodology is iterated each year, covering the period from 2014 to 2023. The entire process, ranging from the calculation of the Normalized Difference Vegetation Index (NDVI) to the normalization of the Vegetation Condition Index (VCI), The formula for this process summary is in Table 5. showed VCI in Figure 5.

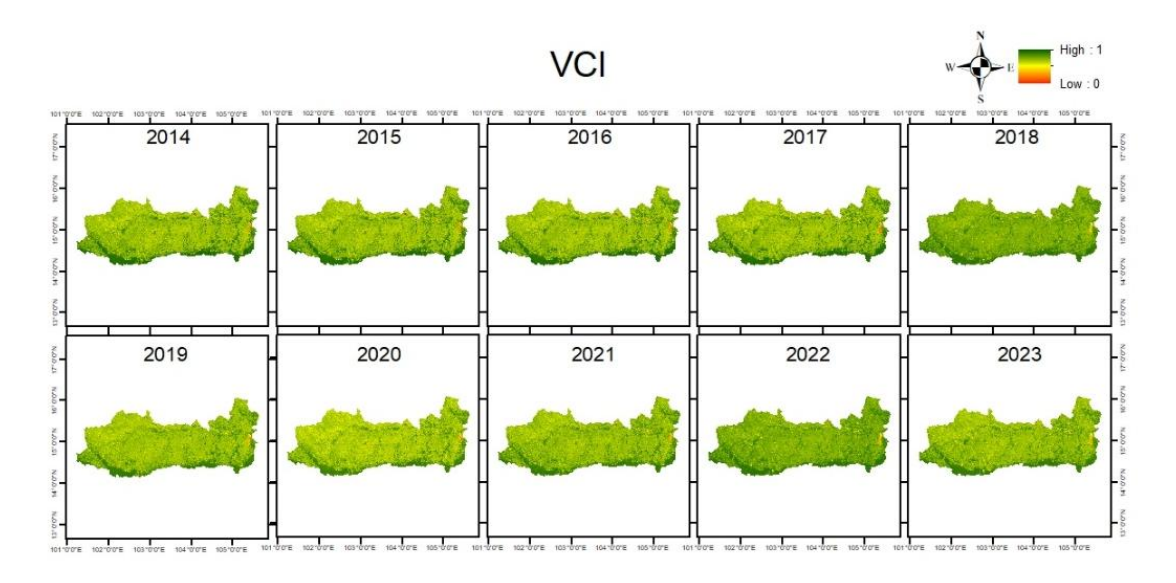


Figure 5 The Vegetation Condition Index 2014 - 2023



3.4.2 The Enhance Vegetation Index

The Enhanced Vegetation Index (EVI) exhibits heightened sensitivity in regions characterized by dense vegetation and can effectively discern stress and alterations attributed to drought conditions. (Yang, Xu, Stovall, Chen, & Lee, 2021) Its calculation involves the utilization of Landsat 8 bands 2 (blue), 4 (red), and 5 (near-infrared). The formula for EVI computation is detailed in Table 5. Following computation, the resultant EVI values undergo a normalization process, scale is standardized within the range of 0 to 1. This methodology is recurrently applied annually throughout the timeframe spanning from 2014 to 2023. showed in Figure 6.

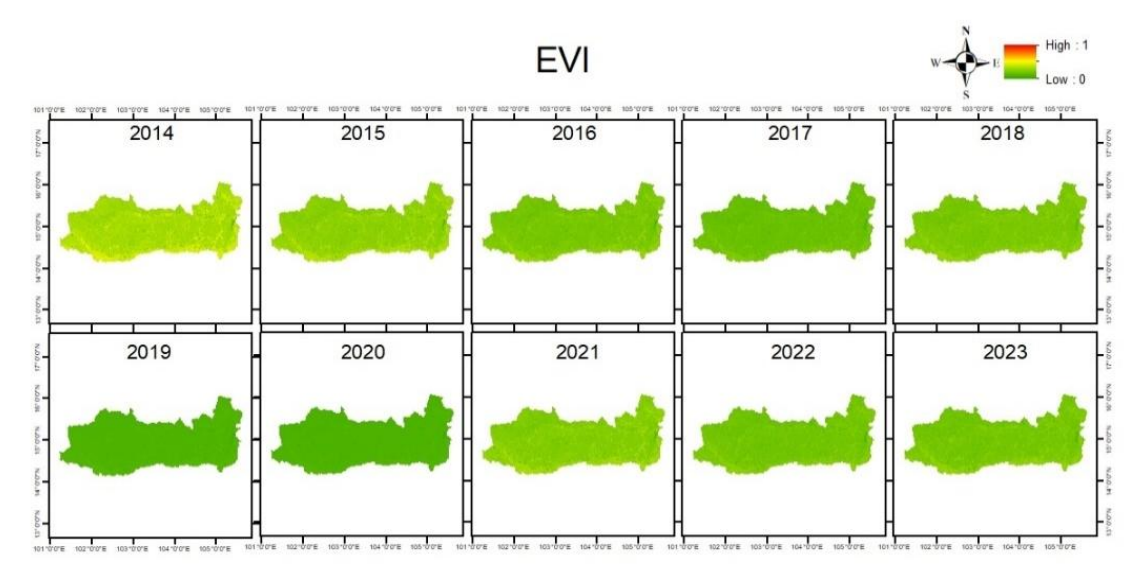


Figure 6 The Enhance Vegetation Index 2014 - 2023

3.4.3 The Temperature Condition Index

The Temperature Condition Index (TCI) extracted from satellite imagery data stands as a pivotal metric elucidating the thermal characteristics of the land surface. Stemming from the computed Proportion of Vegetation cover (PV), TCI acts as a comprehensive indicator of vegetative abundance, exerting a profound influence on surface temperature dynamics. This influence stems from vegetative processes such as transpiration, altering surface energy balance, and thermal conductivity, modulating heat exchange with the atmosphere. Leveraging the Normalized Difference Vegetation Index (NDVI) facilitates precise quantification of vegetation density and health, enriching the accuracy of TCI assessments (Spadoni, Cavalli, Congedo, & Munafò, 2020).

Concurrently, the variable emissivity is a fundamental parameter dictating the surface's emissive properties. Emissivity exhibits variability across surface types, contingent upon factors such as moisture content, surface roughness, and material composition. Integrating "PV" into the calculation of "EM" enhances the estimation of land surface temperature (LST), a pivotal metric reflecting the thermodynamic state of the Earth's surface.

Subsequently, the computation of LST employs thermal band data from Landsat 8, incorporating emissivity values derived from NDVI. Emissivity, indicative of a surface's ability to emit thermal radiation, plays a crucial role in refining LST estimates, facilitating robust assessments of surface thermal conditions.

Upon deriving LST values, the Temperature Condition Index (TCI) is computed, the thermal state of the land surface. TCI serves as a vital tool for discerning ecological processes, agricultural productivity, and broader climate dynamics. The normalization of TCI values to a standardized scale of 0 to 1. Summary formula indices showed in Table 5. showed TCI in Figure 7.

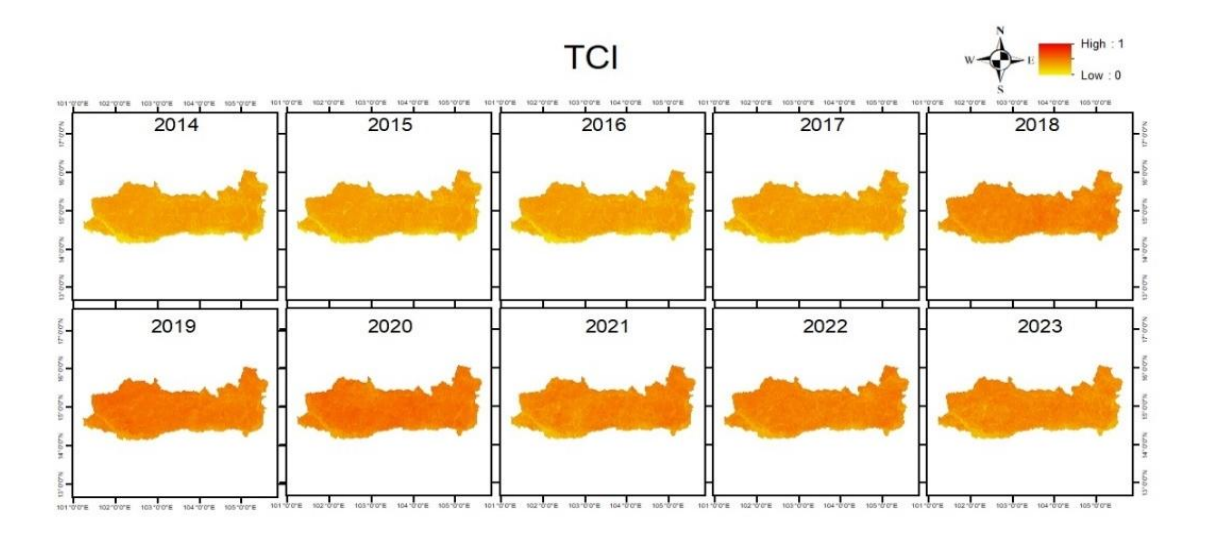


Figure 7 The Temperature Condition Index 2014 - 2023



3.4.4 Topographic Data

Drought is related to topography and local climate conditions, therefore. This study also considered information from topography and geographic locations. The Digital Elevation Model (DEM), influence on hydrology, vegetation, and climate is therefore crucial for this study (Wilson, 2012). the slope from the elevation data can provide significant topographic input data. after that normalization scale range of values to a standardized scale of 0 to 1. showed in Figure 8.

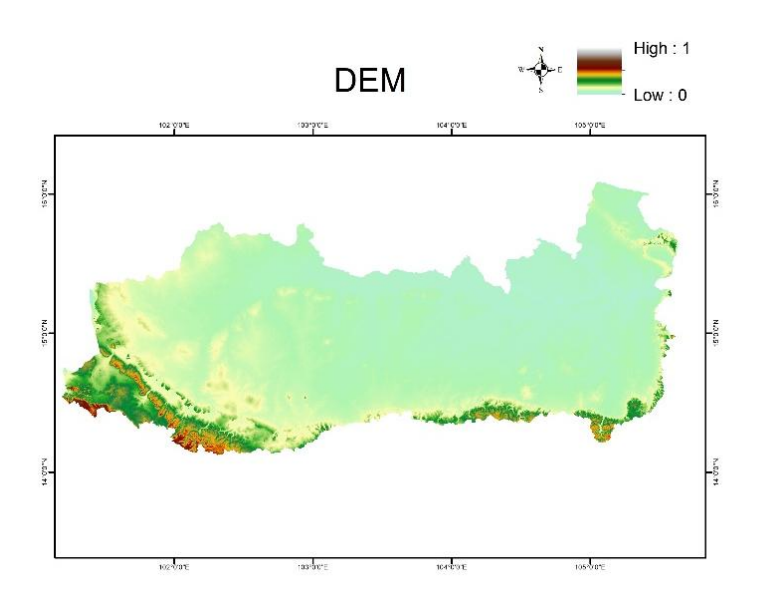


Figure 8 Elevation (DEM)

3.4.5 Climate Hazards Group InfraRed Precipitation with Station Data

This study using precipitation products. The precipitate on datasets for this study were obtained from the Climate Hazards Group InfraRed Precipitation with Station Data (CHIRPS), covering over past 10 years. The CHIRPS is a satellite-estimated product blended with gauge observation from GHCN (Global Historical Climate Network) and GSOD (Global Summary of the Data set) data sources. can be extracted yearly. (Prodhan et al., 2021) using the 'bilinear resampling technique'. after that normalization scale range of values to a standardized scale of 0 to 1. Showed in Figure 9.

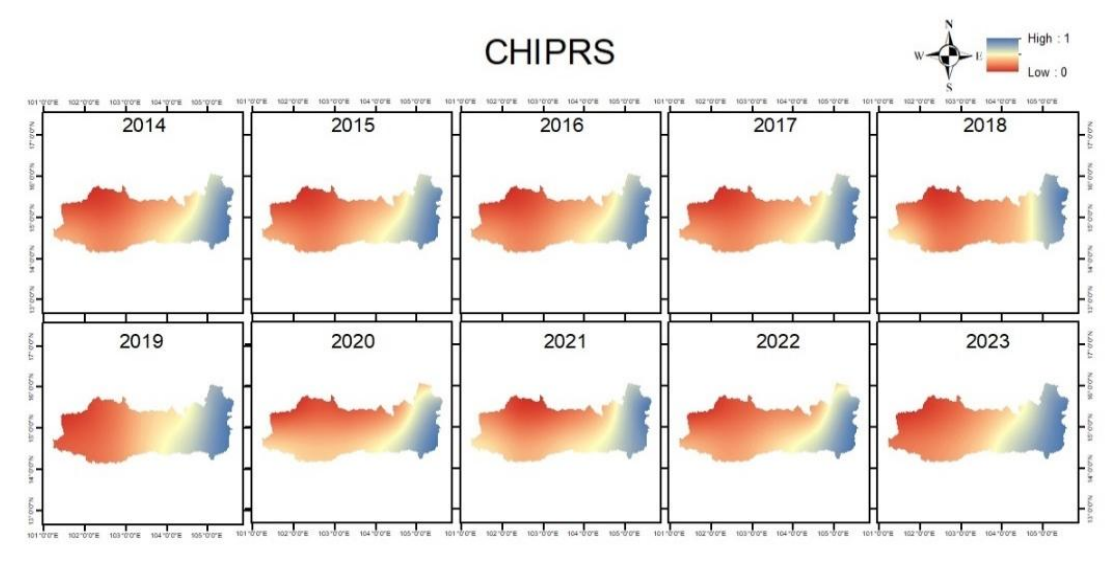


Figure 9 Climate Hazards Group InfraRed Precipitation with Station Data (CHIPRS) 2014-2023

3.4.6 The Standard Precipitation Evapotranspiration Index

The ground station data for the preprocessing of the Standard Precipitation Evapotranspiration Index (SPEI) for drought assessment, comprising monthly precipitation and temperature data collected from Thai Meteorological Department during 2013-2023. The analysis is conducted at each station, involving the calculation of the SPEI using R packages in R Studio (Montes-Vega, Guardiola-Albert, & Rodríguez-Rodríguez, 2023). SPEI and its estimation at different time scales (3, 6, 9, and 12 months) (Zhang, Wang, Chen, & Bai, 2020).

The first step is to calculate potential evapotranspiration (PET) using the Hargreaves method and minimum, maximum temperatures and the station's latitude are parameters (Slavková, Gera, Nikolova, & Siman, 2023). Subsequently, the climatic water balance (CWB) is derived by subtracting PET from precipitation data (Bandoc & Prăvălie, 2015). This equation, precipitation minus PET, quantifies the interplay between precipitation supply and evapotranspiration demand. SPEI is computed across various time scales, including 3, 6, 9, and 12 months. The SPEI values are then exported to a CSV file and combined for all stations into a single CSV file.

Afterward, using ArcMap, a feature class is created from latitude and longitude coordinates extracted from the CSV file, displaying the point stations. Subsequently, spatial interpolation is performed using Inverse Distance Weighting (IDW) (Liu, Yang,

Yang, & Wang, 2021) within ArcGIS to interpolate data points and generate spatially continuous surfaces. Following interpolation, the data is reclassified according to predefined criteria outlined in Table 6. After that, the Create Fishnet Tool is creating a grid of points covering the study area, which is then clipped to the desired extent. Subsequently, the Extract Values to Points tool within the Spatial Analyst toolbox is utilized to extract raster values to the point locations with raster information.

Finally, the data is converted from a feature class to a shapefile format and processed using GeoTile Python library within the Jupyter Notebook environment program to convert it into raster format through rasterization. each year 2014 – 2023, with SPEI3 and SPEI6 This was selected. Showed in Figure 10.

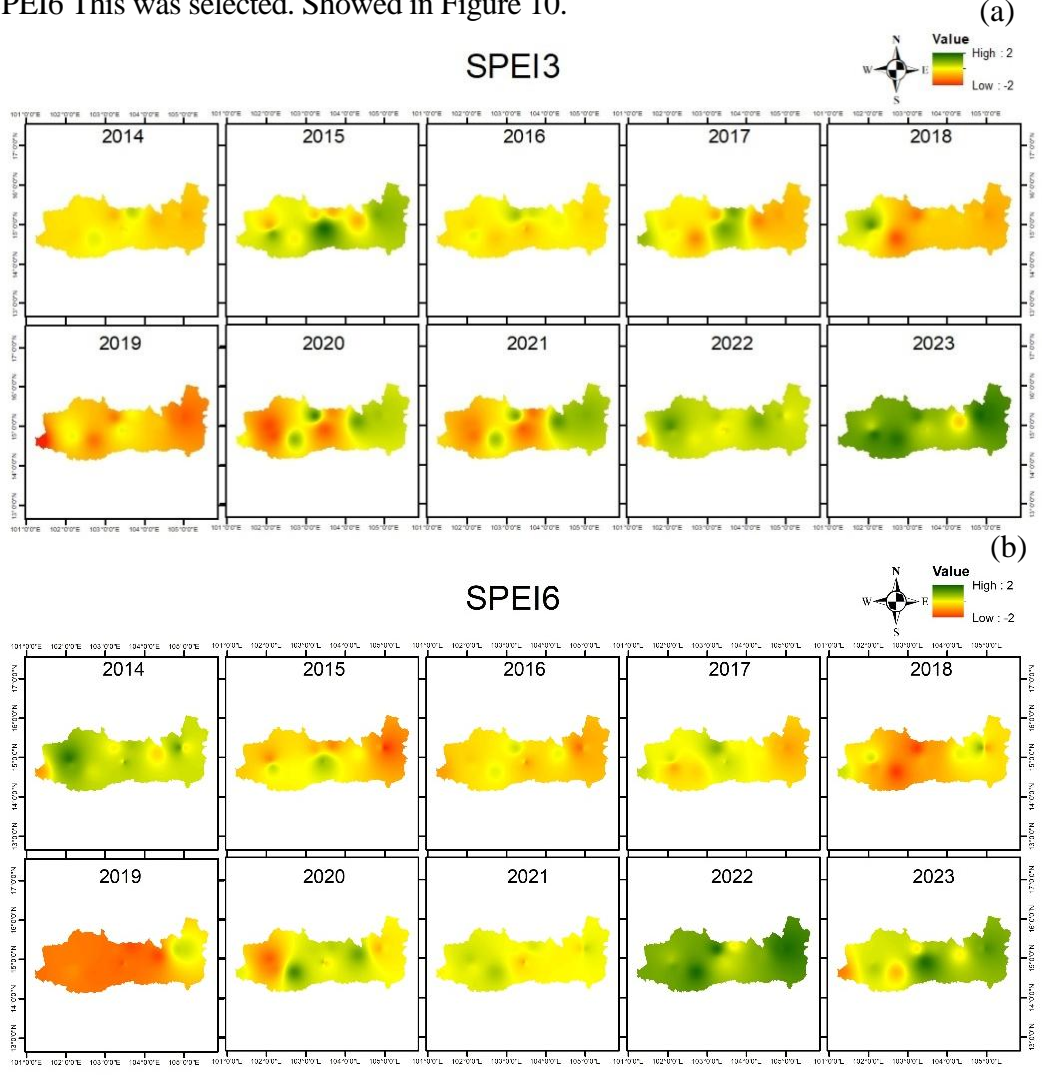


Figure 10 Ground Observations (a) SPEI 3 and (b) SPEI 6 Month scale

Table 5 Summary formula remote sensing and ground observation data

Indices	Formula	Note	Reference
NDVI	$NDVI = \frac{(NIR - red)}{(NIR + red)}$	-	(Qin et al., 2021)
LST	1. Digital Numbers to Spectral Radiance. $L\lambda = ML \times Qcal + AL$ 2. Spectral Radiance to Brightness Temperature. $BT = \frac{K2}{\ln\left(\frac{K1}{L\lambda} + 1\right)} - 273.15$ 3. Proportion of Vegetation. $PV = \left[\frac{(NDVI - NDVImin)}{(NDVImax - NDVImin)}\right]^2 \times 100$ 4. Land Surface Emissivity. $EM = 0.004 * PV + 0.986$ 5. Land Surface Temperature. $LST = \left(\frac{BT}{1}\right) + W \times \left(\frac{BT}{14380}\right) \times \ln(EM)$	•	(Sobrino, Jimenez, & Paolini, 2004),(Periasamy, Palanisamy, Ravichandran, & Jothiramalingam, 2021),(Chander, Markham, & Helder, 2009)
EVI	$EVI = \frac{(NIR - Red)}{(NIR + 6 \times Red - 7.5 \times Blue + 1)}$		
VCI	$VCI = \frac{(NDVI - NDVImin)}{(NDVImax - NDVImin)} \times 100$	NDVImin and NDVImax are the minimum and maximum values of the NDVI, respectively; the The smaller the VCI, the more likely a drought will occur. (X. Li et al., 2023)	(Qin et al., 2021)
TCI	$TCI = \frac{(LST - LSTmin)}{(LSTmax - LSTmin)} \times 100$	-	
scaleVCI	$scaleVCI = \frac{(VCI - VCImin)}{(VCImax - VCImin)}$	-	
scaleEVI	$scaleVCI = \frac{(VCI - VCImin)}{(VCImax - VCImin)}$ $scaleEVI = \frac{(EVI - EVImin)}{(EVImax - EVImin)}$	-	
scaleTCI	$scaleTCI = \frac{(TCI - TCImin)}{(TCImax - TCImin)}$	-	
scaleDEM	$scaleTCI = \frac{(TCI - TCImin)}{(TCImax - TCImin)}$ $scaleDEM = \frac{(DEM - DEMmin)}{(DEMmax - DEMmin)}$	-	
scalePCI	$scalePCI = \frac{(Precipitation - Precipitationmin)}{(Precipitationmax - Precipitationmin)}$	-	
SPEI	1. Potential Evapotranspiration. $PET = 0.0023 \cdot (Tmean - 17.8) \cdot Tmax - Tmin \cdot Ra$ 2. SPEI calculation. $D_i = P_i - PET_i$	Calculated according to the Hargreaves method	(Zhao et al., 2022),(Breiman, 2001) ,(Vicente-Serrano & Beguería, 2015)

Table 6 SPEI classification

Grade	Type	SPEI Value
1	No drought	-0.5 < SPEI
2	Light drought	$-1.0 \le \text{SPEI} \le -0.5$
3	Moderate drought	$-1.5 \le \text{SPEI} \le -1.0$
4	Severe drought	$-2.0 < \text{SPEI} \le -1.5$
5	Extreme drought	$SPEI \le -2.0$

3.5 Predictive Model

The machine learning models are Extreme Gradient Boosting (XGBoost), Random Forest (RF) and Extra Tree Regression (ETR), which are established in Python 3.11 through the integration of libraries such as GDAL, Numpy, Matplotlib, Scikit-learn, and the XGB Python Library within the Jupyter Notebook environment. which choose to predict and estimate drought, which can obtain effective results and calculate feature importance from each model using the machine learning method permutation importance calculation to rank each variable relevance.

3.5.1 Extreme Gradient Boosting

Extreme gradient boosting, or XGBoost, is a gradient boosting algorithm that is commonly used in regression problems. XGBoost makes model learning more effective by using parallel computing and an additive decision tree training technique to turn many weak learners into strong learners. XGBoost can do error assignments with this method. The XGBoost algorithm was implemented using the xgboost.xgb library. the model follows the below steps.

In the first step, the GDAL library is using to ingest both image X and image y, with the subsequent creation of an array whose dimensions are dynamically adjusted based on the raster dataset's characteristics, ensuring uniformity across identical band numbers. Following this, an iterative process ensues, systematically traversing each band of the image to populate a NumPy array with the pixel values of each band from the raster dataset.

next step, the NumPy library is used to stack arrays horizontally, the features (X) and labels (y) into a unified 2-D array denoted as DataX. This operation combines the respective elements from both X and y. Subsequently, the train_test_split function from scikit-learn is employed to partition the dataset, randomly dividing it into training and testing subsets, with 30% of the data allocated for testing and the remaining 70% for training.

In the subsequent step, an XGBoost regressor model is instantiated, with the scoring metrics for cross-validation being explicitly defined. The model is trained on the training dataset using the fit method, following which an evaluation is conducted and the results are recorded in a text file.

The subsequent step assessing the importance of each feature predictor variable within the model, aimed at identifying the most influential features crucial for accurate predictions. This information serves as a for feature selection, elucidating data relationships, and potentially enhancing model performance by prioritizing critical features.

Finally, the process culminates in the prediction and exportation of raster data. Utilizing a trained model, class labels for a raster dataset are predicted, subsequently exported into a new raster file.

3.5.2 Random Forest Regression

The Random Forest and several decision trees are put together in parallel, without interacting with each other. This means that the predicted values are not sensitive to or based on the trained data that was used, and the method does not over-fit. Random Forest approach is to combine some separate and parallel decision trees to get to the result. To sum up the step of random forest regression, the model follows the below steps (Zarei, Mahmoudi, & Moghimi, 2023).

In the first step, the GDAL library is using to ingest both image X and image y, with the subsequent creation of an array whose dimensions are dynamically adjusted based on the raster dataset's characteristics, ensuring uniformity across identical band numbers. Following this, an iterative process ensues, systematically traversing each band of the image to populate a NumPy array with the pixel values of each band from the raster dataset.

next step, the NumPy library is used to stack arrays horizontally, the features (X) and labels (y) into a unified 2-D array denoted as DataX. This operation combines the respective elements from both X and y. Subsequently, the train_test_split function from scikit-learn is employed to partition the dataset, randomly dividing it into training and testing subsets, with 30% of the data allocated for testing and the remaining 70% for training.



In the subsequent step, a Random Forest model is instantiated, with the scoring metrics for cross-validation being explicitly defined. The model is trained on the training dataset using the fit method, following which an evaluation is conducted and the results are recorded in a text file.

The subsequent step assessing the importance of each feature predictor variable within the model, aimed at identifying the most influential features crucial for accurate predictions. This information serves as a for feature selection, elucidating data relationships, and potentially enhancing model performance by prioritizing critical features.

Finally, the process culminates in the prediction and exportation of raster data. Utilizing a trained model, class labels for a raster dataset are predicted, subsequently exported into a new raster file.

3.5.3 Extra Trees Regression

Extra Trees construct multiple trees like RF algorithms during training time over the entire dataset. During training, the ETR will construct trees over every observation in the dataset but with different subsets of features (Baykal, Terzi, Yıldırım, & Taylan, 2023). that although bootstrapping is not implemented in ETR original structure, it can add it in some implementations. Furthermore, when constructing each decision tree, the ET algorithm splits nodes randomly (Adnan, 2022). The main advantage of Extra Trees is the reduction in bias (Zafari, Zurita-Milla, & Izquierdo-Verdiguier, 2019). This is in terms of sampling from the entire dataset during the construction of the trees. Different subsets of the data may introduce different biases in the results obtained, hence, Extra Trees prevents this by sampling the entire dataset. Extra Trees reduce variance. This is a result of the randomized splitting of nodes within the decision trees hance the algorithm is not heavily influenced by certain features or patterns in the dataset.

In the first step, the GDAL library is using to ingest both image X and image y, with the subsequent creation of an array whose dimensions are dynamically adjusted based on the raster dataset's characteristics, ensuring uniformity across identical band numbers. Following this, an iterative process ensues, systematically traversing each band of the image to populate a NumPy array with the pixel values of each band from the raster dataset.

Next step, the NumPy library is used to stack arrays horizontally, the features (X) and labels (y) into a unified 2-D array denoted as DataX. This operation combines the respective elements from both X and y. Subsequently, the train_test_split function from scikit-learn is employed to partition the dataset, randomly dividing it into training and testing subsets, with 30% of the data allocated for testing and the remaining 70% for training.

In the subsequent step, an Extra Trees model is instantiated, with the scoring metrics for cross-validation being explicitly defined. The model is trained on the training dataset using the fit method, following which an evaluation is conducted and the results are recorded in a text file.

The subsequent step assessing the importance of each feature predictor variable within the model, aimed at identifying the most influential features crucial for accurate predictions. This information serves as a for feature selection, elucidating data relationships, and potentially enhancing model performance by prioritizing critical features.

Finally, the process culminates in the prediction and exportation of raster data. Utilizing a trained model, class labels for a raster dataset are predicted, subsequently exported into a new raster file.

3.5.4 Cross-validation

A cross-validation was the choice to assessment of prediction model. A way to test prediction models is with K-fold cross-validation. There are k subsets, or folds, in the collection. It is trained and tested k times, with a different fold used as the validation set each time. To get an idea of how well the model generalizes, performance measures from each fold are averaged. This way helps with evaluating, choosing, and tuning hyperparameters, giving a more accurate picture of how well a model works. Then XGB, RF and ETR are separate data training and testing with 70% and 30% of dataset. To verify the validation and stability of the model for predicting SPEI, we used the 5-fold cross-validation (CV) method. Briefly, data is randomly divided into 5



groups by serial number or time. Four of the groups are used to build a model, which is called a training dataset, and the remaining group, called a test dataset, is used to validate the model. This process is repeated 5 times, and the average CV R2 (coefficient of determination), CV RMSE (root mean square error) and CV MAE (mean absolute error) are then obtained. During this whole process, the training and testing would be done exactly once in each set (fold). It helps to avoid overfitting (Santos, Soares, Abreu, Araujo, & Santos, 2018).

3.6 Accuracy Assessment

The estimation of drought XGB, RF, ETR models was constructed by machine learning methods. The model set 70% for drought training and validated the remaining 30% of the data. in this study, using the assessment comparison between the regression models was evaluated in terms of the difference between the actual values and the predicted statistical. R-squared (R2) and Root Mean Square Error (RMSE) and Mean Absolute Error (MAE) were commonly used metrics, R2 helps understand the proportion of variance explained by the model (Gond, Gupta, Patel, & Dikshit, 2023), while RMSE indicates the average magnitude of the residuals or errors made by the model. When comparing models, higher R-squared values and lower RMSE values generally indicate better model performance. using equations. These are defined as follows.

$$MAE = \frac{1}{n} \sum_{i=1}^{n} |P_i - O_i|$$

$$RMSE = \sqrt{\frac{1}{n}} \sum_{i=1}^{n} (P_i - O_i)^2$$

$$R^2 = \frac{\sum_{i=1}^{n} (P_i - \bar{O}_i)^2}{\sum_{i=1}^{n} (P_i - \bar{O}_i)^2}$$

3.7 Mapping the Spatial Distribution Drought

After training the drought models and obtaining suitable models and significant factors, their accuracy was evaluated using R2, Root Mean Square Error (RMSE), and Mean Absolute Error (MAE) for the study area. The model was then used to calculate drought values for each pixel each year, and then, to further analyze the spatial

distribution of drought, the zonal statistical technique within the QGIS geographic information system (GIS) platform was employed.

This technique facilitated the delineation of subdistrict areas within northeast Thailand and the calculation of their respective drought severity indices. Specifically, the average drought values within each subdistrict were computed, providing insights into the localized impact of drought, and allowing us to visualize the prediction of drought. The final method is mapping the spatial distribution of drought in northeast Thailand over a period from 2014 to 2023. ArcMap displays this method.

3.8 Summary of this chapter

In conclusion, Chapter 3 provides the methodology utilized for drought dynamics in northeast Thailand, primarily based on machine learning models and integrating remote sensing and ground observation data. The research area, characterized by the Korat Basin and the Mun River, is thoroughly described to provide context for the study's scope. The workflow encompasses data collection, preprocessing, and model training and evaluation. Remote sensing data from Landsat 8, including vegetation indices and topographic information, are combined with ground observation data from the Thai Meteorological Department to compute various drought indices.

The preprocessing phase involves steps such as data loading, index computation, and image merging using the GDAL library. Essential indices like the Vegetation Condition Index (VCI), Enhanced Vegetation Index (EVI), Temperature Condition Index (TCI), and precipitation products from the Climate Hazards Group InfraRed Precipitation with Station Data (CHIRPS). After that, the datasets are calculated and normalized across datasets.

Subsequently, the predictive modeling section details the implementation of machine learning algorithms, including XGB, RF, and ETR for drought estimation. Each model training and evaluation with cross-validation employed to assess prediction performance and ensure model robustness. Accuracy assessment metrics such as R-squared (R2), Root Mean Square Error (RMSE), and Mean Absolute Error (MAE) are utilized to evaluate model performance, providing insights into the spatial distribution and severity of drought across northeast Thailand.

CHAPTER 4 RESULTS AND VALIDATION

This chapter presents the experiment and the result of machine learning to evaluate the spatio temporal of drought described in Chapter 3 over northeast of Thailand. The results are the following.

4.1 Analysis of Spatio-Temporal of drought

The Precipitation data analysis Precipitation data collected from 11 stations of the Thai Meteorological Department which had data for 10 years from 2014 to 2023. The average annual precipitation is in the range of 1,100-1,800 mm per year, with the highest average in 2022 at 1,848 mm. and the lowest mean value in 2018 at 1,175 mm. showed in Figure 11

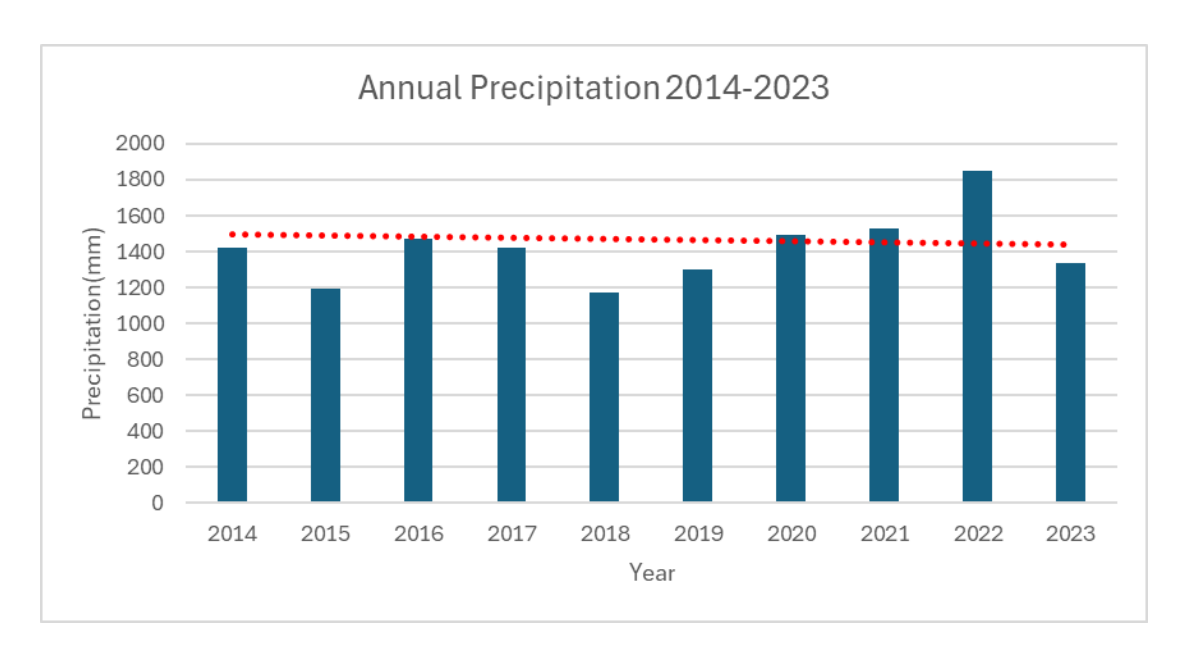


Figure 11 Average annual precipitation from TMD (2014-2023)

The results of the Standardized Precipitation Evapotranspiration Index (SPEI) across diverse temporal scales, ranging from 3, 6, 9, and 12 months, are presented. Figure 12 illustrates the temporal evolution of drought patterns aggregated monthly from 2014 to 2023 at the Northeast Thailand station. Over shorter durations, the SPEI index exhibits rapid fluctuations, whereas its variability diminishes with increasing temporal spans, resulting in protracted periods of calculated drought conditions. This phenomenon is attributed to the utilization of longer periods of rainfall data in the



computation process. Consequently, the selection of the temporal scale for rainfall data computation hinges on the specific objective of the analysis, whether it pertains to short-term drought monitoring or a broader overview across extended periods.

The short-term reflects cumulative precipitation patterns over cumulative with SPEI 3 scale precipitation patterns. Specifically, the investigation identified instances of drought, as indicated by the SPEI values. Notably, drought conditions were observed in June 2015, signifying a period of reduced precipitation and potential water scarcity. Subsequently, drought was again identified in April 2016, suggesting a persistence of reduced precipitation levels. Furthermore, the end of 2018 and 2019 marked drought conditions, emphasizing the severity of precipitation. Additionally, the onset of drought at the beginning of 2020 and 2021 signifies a period of reduced precipitation and potential water scarcity.

The long-term reflects cumulative precipitation patterns over with SPEI 12. This investigation discerned negative SPEI values from mid-year 2015 to 2016, indicative of incipient drought conditions. Subsequently, during mid-year 2018 to 2020, the persistence of negative values underscores prolonged drought conditions across various months. showed in Figure 12.

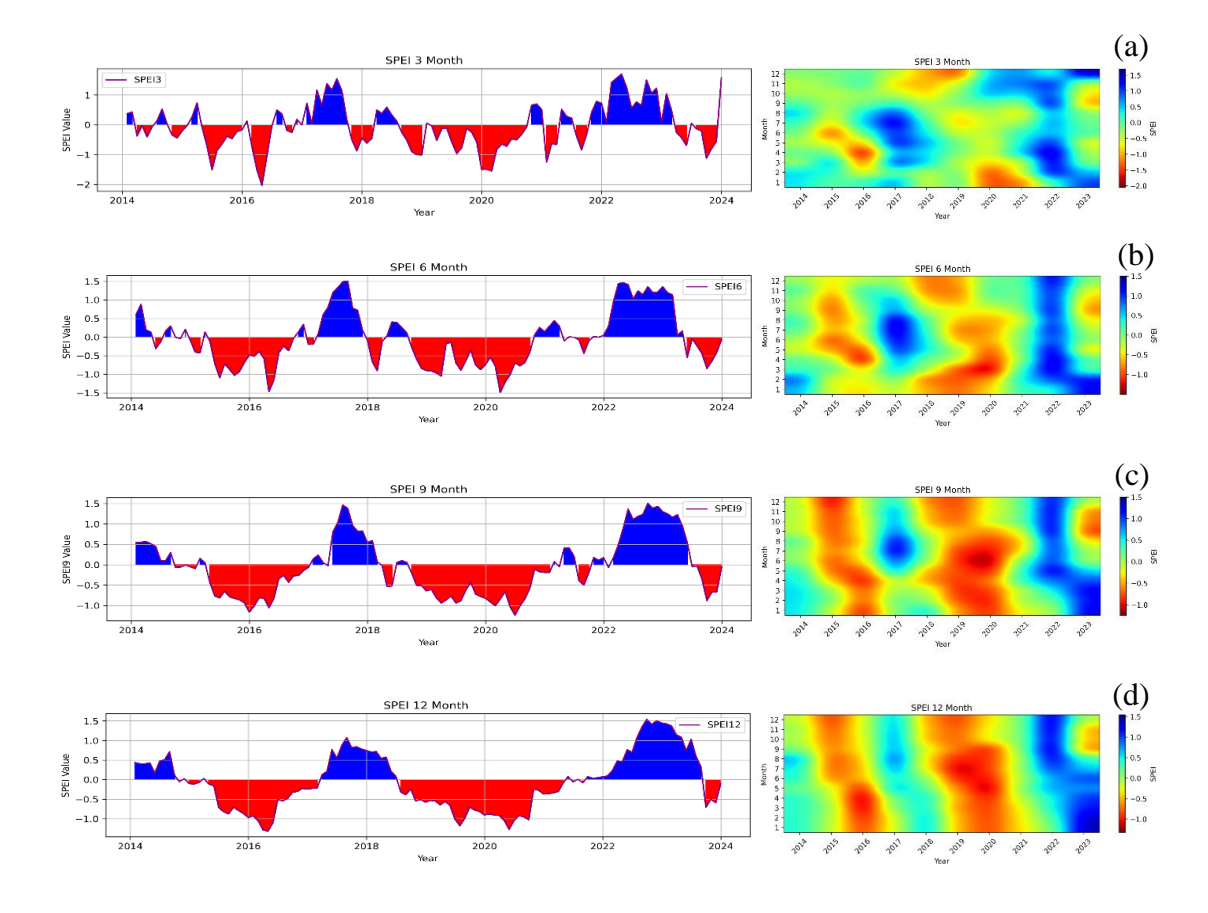


Figure 12 The evolution of SPEI indicating the development of drought from (a) 3 months, (b) 6 months, (c) 9 months, (d) 12-month time scale in the northeast of Thailand from 2014 - 2023

4.2 Comparing Performance of ML Models

4.2.1 Performances of Machine Learning Models

Traditional methods are often constrained by various factors and can incur high costs. In contrast, machine learning (ML) models leverage with RS and the capability to analyze extensive geographic areas, providing global coverage with accuracy. This section compares the performance of three machine learning models: XGB, RF, and ETR, in predicting drought indices based on remote sensing as independent variables (X) and ground observation data as the dependent variable (y). The evaluation employs metrics such as R2 and RMSE to assess the accuracy and reliability of the models in capturing the intricate relationships between spectral indices and drought conditions in the northeast region of Thailand.

The models were implemented in a Jupyter Notebook environment. A training set was created by randomly selecting 70% of the samples from the dataset, while the remaining 30% comprised the test set. Model parameters were fine-tuned using the 5fold cross-validation (CV) method. In this process, the training set of the RF model was divided into five partitions, with four partitions utilized for training and one for validation. The CV score for each fold was averaged to ensure a comprehensive assessment of model reliability and accuracy.

Table 7 Summary parameter of Machine learning

Characteristics	Descriptions
Model	XGBoost, Random Forest, Extra trees
Parameter	n_estimators = 200, K_fold = 5
Dependent variable	SPEI3, SPEI6
Independent variables	VCI, EVI, TCI, DEM, CHIPRS

Different models produced different outcomes. when integrated with data from remote sensing and environmental variables. The study compared the performance of different machine learning models, including XGB, RF, and ETR, in predicting drought indices (SPEI 3 and SPEI 6) using remote sensing and environmental variables in Northeast Thailand. The results showed that all three models exhibited varying levels of precision across different metrics and datasets. shown accuracy assessment of the machine learning in Table 8.



Table 8 Accuracy assessment of the Machine Learning

SPEI	ML	Accuracy	2014	2015	2016	2017	2018	2019	2020	2021	2022	2023
SPEI3	XGBoost	MAE	6.12	2.24	0.8	8.75	14.5	14.7	19.9	16.3	0.9	0.07
		RMSE	14.1	8.3	5.05	17.6	25.9	24.4	34.1	28.2	5.67	1.35
		R2	88.6	72.1	63.2	87.5	81.4	92.4	83.0	82.4	75.1	66.1
	RF	MAE	5.07	1.63	0.55	5.95	11.0	10.6	16.7	13.4	1.03	0.12
		RMSE	13.8	7.83	4.56	16.1	24.3	21.9	32.9	26.2	6.27	2.23
		R2	89.1	75.2	69.7	89.4	83.5	93.9	84.2	84.8	71.1	69.3
	ET	MAE	5.04	2.19	0.75	6.55	11.5	11.6	18.5	15.6	1.2	0.09
		RMSE	12.2	8.27	4.97	14.8	22.5	21.3	33.2	28.0	6.08	1.58
		R2	91.4	72.1	65.2	91.1	85.9	94.2	83.9	82.6	73.1	69.7
SPEI6	XGBoost	MAE	2.07	20.2	11.6	10.1	19.2	8.93	9.61	0.29	0.5	2.4
		RMSE	12.1	35.4	27.1	25.0	35.9	20.7	20.4	4.29	3.52	10.7
		R2	79.2	83.7	91.5	89.7	85.8	91.0	90.2	80.9	90.5	87.9
	RF	MAE	2.36	15.7	9.09	7.52	14.8	5.04	6.38	0.33	0.52	2.16
		RMSE	13.5	32.6	25.8	24.0	32.9	17.2	18.6	4.91	3.97	12.1
		R2	74.1	86.1	92.3	90.6	88.1	93.8	91.8	77.9	88.1	84.8
	ET	MAE	2.36	18.1	9.45	8.31	15.4	5.46	7.55	0.45	0.76	2.82
		RMSE	11.7	31.9	22.9	22.1	31.4	15.8	18.5	4.92	4.55	12.0
		R2	80.3	86.7	94.0	92.0	89.2	94.8	91.9	78.7	84.8	85.0

For SPEI 3, the XGBoost model demonstrated an overall precision with R2 ranging from 63.24% to 92.47%, RMSE spanning from 1.35% to 34.11%, and MAE fluctuating between 0.07% and 19.9%. Similarly, the Random Forest model exhibited R2 ranges of 69.38% to 93.98%, RMSE varying between 2.23% and 32.93%, and MAE spanning from 0.12% to 16.7%. Moreover, the Extra trees model showcased R2 ranges from 65.26% to 94.28%, RMSE spanning 1.58% to 33.28%, and MAE fluctuating between 0.09% and 18.55%.

For SPEI 6, the XGBoost model demonstrated an overall precision with R2 ranging from 79.23% to 91.59%, RMSE spanning from 3.52% to 35.97%, and MAE varying between 0.29% and 20.27%. Likewise, the Random Forest model displayed R2 ranges from 74.19% to 91.59%, RMSE fluctuating between 3.97% and 32.95%, and MAE spanning from 0.33% to 15.79%. Additionally, the Extra Trees model showcased R2 ranges from 78.73% to 94.8%, RMSE ranging from 4.55% to 31.93%, and MAE varying between 0.45% and 18.14%. showed overall accuracy in Figure 13.

In conclusion, the Extra Trees model emerges as the most promising candidate for drought index prediction in the Northeast region of Thailand, demonstrating competitive performance across various metrics and datasets. The analysis, aimed at assessing the congruence between predicted and observed values, consistently performed across various metrics. For both SPEI3 and SPEI6, the correlation coefficients (R values) ranged from 65.26% to 94.28% and 78.73% to 94.8%, respectively, indicating the model's ability to capture the nuances of drought dynamics. This proficiency not only elucidates the model's discernment of the relative significance of pertinent drought variables but also indicates its reliability in forecasting. The Root Mean Squared Error (RMSE), serving as an indicator of predictive capability, exhibited low values spanning from 1.58% to 33.28% and 4.55% to 31.93% for SPEI3 and SPEI6, respectively. Such minimal RMSE values signify a close relationship between predicted and observed values, meaning that prediction errors were comparatively low. Likewise, Mean Absolute Error (MAE) ranges of 0.09% to 18.55% and 0.45% to 18.14% for SPEI3 and SPEI6, respectively, further indicate the model's accuracy, with lower MAE values indicating performance in predicted and observed values. Moreover, this study uses cross-validation for a model assessment approach that effectively mitigates the risk of overfitting the training data, the ETR model used to generate drought distribution maps in the Northeast region of Thailand. Its performance and accuracy make it a compelling choice for further research and practical applications in drought assessment and monitoring.

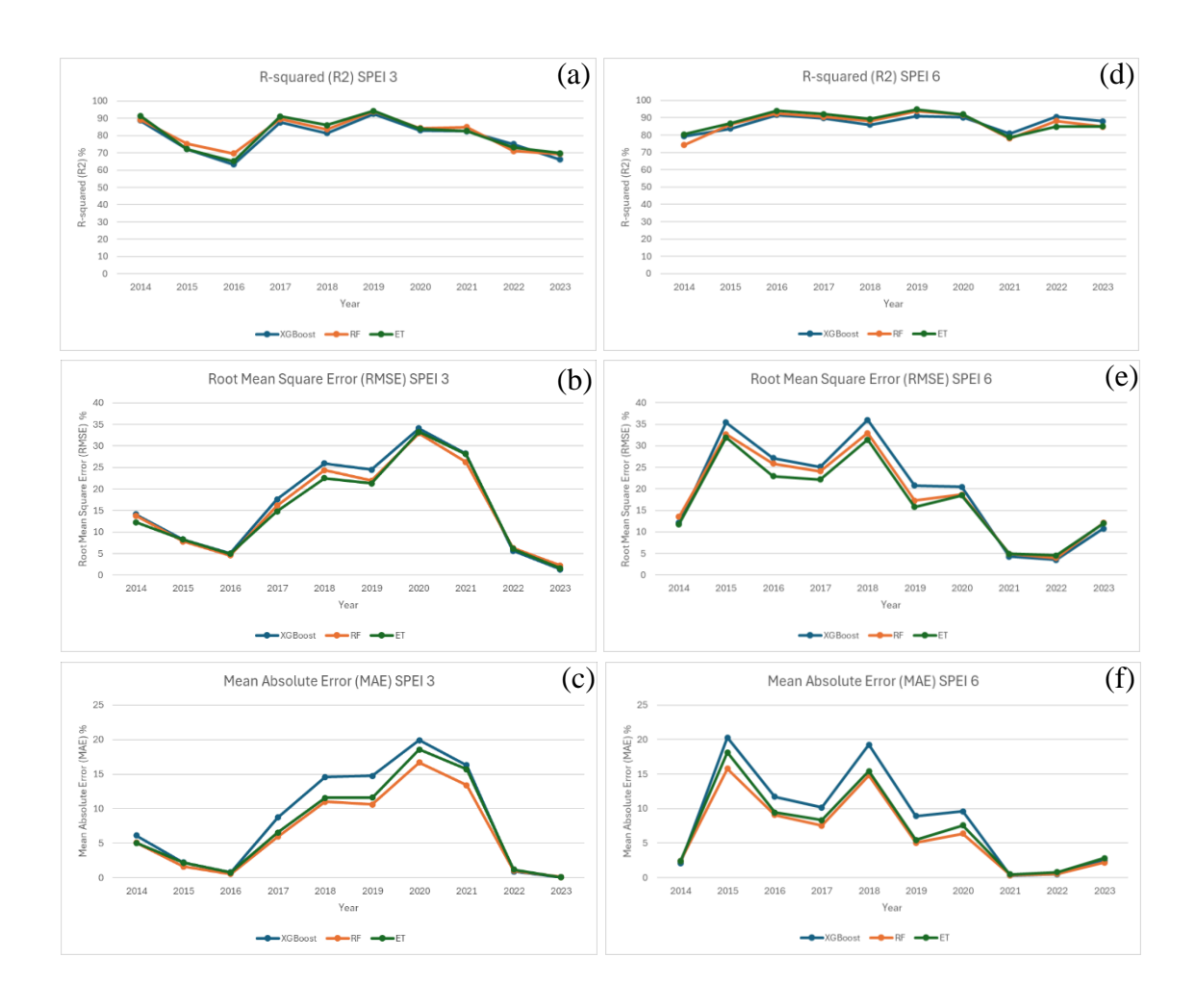


Figure 13 Overall accuracy: (a) R^2 , (b) RMSE, (c) MAE from SPEI 3 and (d) R^2 , (e) RMSE, (f) MAE from SPEI 6

4.2.2 The Importance of Variables

This study investigates the influence of remote sensing and ground observation variables on the estimation of SPEI 3 and SPEI 6 scales spanning from 2014 to 2023. The variables impact was assessed through model influence and permutation importance calculation, enhancing the comparability of these variables, and revealing correlations among all selected parameters. The prioritization factor of three models is illustrated in Figure 14 indicating the significance of these variables across different modeling approaches.

SPEI 3 importance values from 2014 to 2023 reveals notable patterns across the three models. In the XGB model, CHIRPS emerges as the most critical variable, constituting 35.13% to 61.85% of the total importance, followed by DEM (20.09% to 29.74%), TCI (1.94% to 18.88%), EVI (2.50% to 12.15%), and VCI (3.36% to 11.64%). Similarly, in the RF model, CHIRPS remains paramount, ranging from 34.88% to 66.85%, followed by DEM (21.36% to 29.21%), TCI (4.55% to 19.26%), EVI (2.30% to 14.32%), and VCI (2.57% to 7.48%). The ETR model also emphasizes CHIRPS (27.52% to 62.79%), DEM (19.65% to 30.33%), TCI (7.05% to 21.39%), VCI (3.87% to 13.09%), and EVI (3.28% to 12.85%).

SPEI 6 importance values for the same period unveils consistent trends across the models. In the XGB model, CHIRPS dominates (36.81% to 67.77%), followed by DEM (13.83% to 33.83%), TCI (5.5% to 18.88%), EVI (3.01% to 13.58%), and VCI (1.90% to 9.56%). Likewise, in the RF model, CHIRPS remains crucial (40.87% to 72.64%), followed by DEM (14.18% to 35.63%), TCI (5.22% to 15.86%), EVI (2.42% to 13.20%), and VCI (1.87% to 6.49%). The ETR model highlights CHIRPS (28.86% to 67.08%), DEM (18.86% to 37.32%), TCI (6.29% to 21.67%), EVI (3.83% to 14.24%), and VCI (3.92% to 11.45%). Showed in Figure 14.

In conclusion, the study investigated the significance of remote sensing and topography variables in accurately estimating the Standardized Precipitation Evapotranspiration Index (SPEI) at both 3 and 6-month scales from 2014 to 2023. Through permutation importance calculations, it enhanced the comparability of variables and unveiled correlations among them. Across three models (XGB, RF, and ETR), CHIRPS (precipitation data), elevation (DEM), and TCI (Temperature

Condition Index) emerged as the most critical variables for both SPEI 3 and SPEI 6 estimations. While other variables like EVI (Enhanced Vegetation Index) and VCI (Vegetation Condition Index) also held importance, they played secondary roles compared to CHIRPS, elevation, and TCI. These studies examine the role of certain variables in estimating SPEI, thus aiding water resource management and drought monitoring.

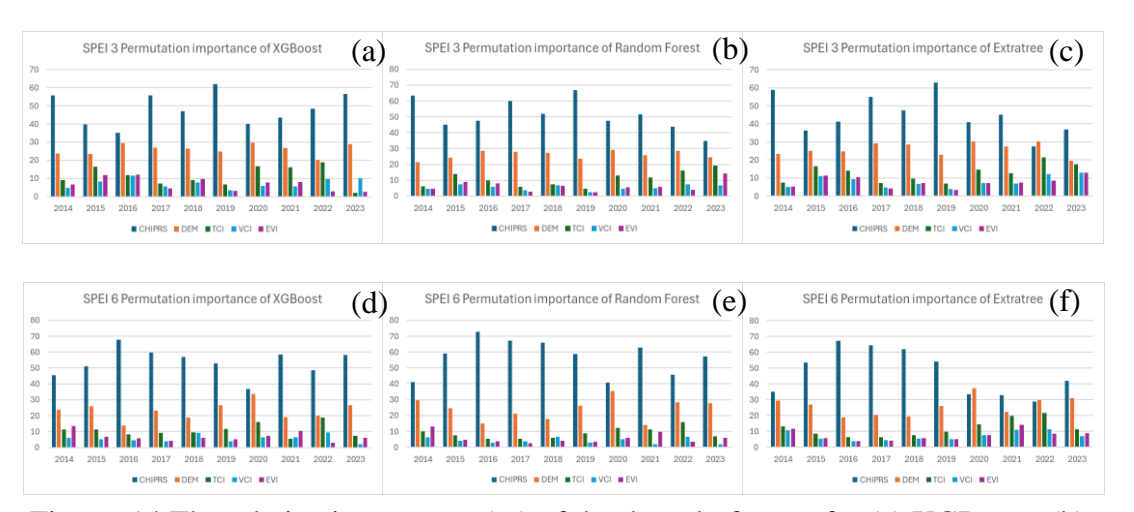


Figure 14 The relative importance (%) of the drought factors for (a) XGBoost, (b) Random Forest, (c) Extra Trees from SPEI 3 and (d) XGBoost, (e) Random Forest, (f) Extra Threes from SPEI 6

4.3 Mapping The Spatial Distribution Drought

The spatial distribution maps the definitive results of this study conducted Leveraging the ETR model the creation of drought distribution maps in northeastern Thailand over a period from 2014 to 2023. The region's topography predominantly consists of the Korat plateau, characterized by extensive flat terrain. The terrain gradually slopes from west to east, culminating in high mountains along the periphery of the area. Predominantly rocky, the terrain also features vast plains, forming expansive basin lands. The average annual precipitation stands at approximately 1,400 mm, with temperatures ranging between 19.5°C and 36.1°C, delineating the climatic profile of the region.

Trend long-term drought indicators SPEI 6 consistently exhibited a higher frequency of area drought category compared to short-term indicators SPEI 3 This suggests the cumulative impact of prolonged precipitation deficits on drought occurrences.

4.3.1 Short-Term Drought Occurrences

In this study, conducted an analysis of drought occurrences in northeastern Thailand, the occurrences of short-term light droughts in 2014, predominantly impacting Ubon Ratchathani (UBN), which reappeared in 2017, followed by a more extensive influence across the study area in 2018. Additionally, moderate drought conditions were discerned in Buriram (BRM) during this timeframe, persisting through 2019. Extreme drought affected 0.47% of the total area, severe drought impacted 0.56%, moderate drought affected 24%, and light drought was observed in 45% of the entire area, as illustrated in Figure 16. Noteworthy is the identification of light drought conditions in Sisaket (SSK) in 2019, alongside sporadic occurrences of moderate drought in Buriram (BRM). Meanwhile, Ubon Ratchathani (UBN) experienced notable instances of moderate drought, with Nakhon Ratchasima (NMA) notably afflicted by extreme drought conditions. consistent with the data that the drought situation in Nakhon Ratchasima (NMA) Province is still ongoing. The water volume in 4 large water storage reservoirs in the province continues to decrease. (Office of Natural Resources and Environmental Policy and Planning). This trend persisted into 2020 with a moderate drought in Nakhon Ratchasima (NMA) and a light drought in Buriram (BRM) and Surin (SRN). Furthermore, similar conditions were observed in 2021 in these areas. Showed in Figure 15.

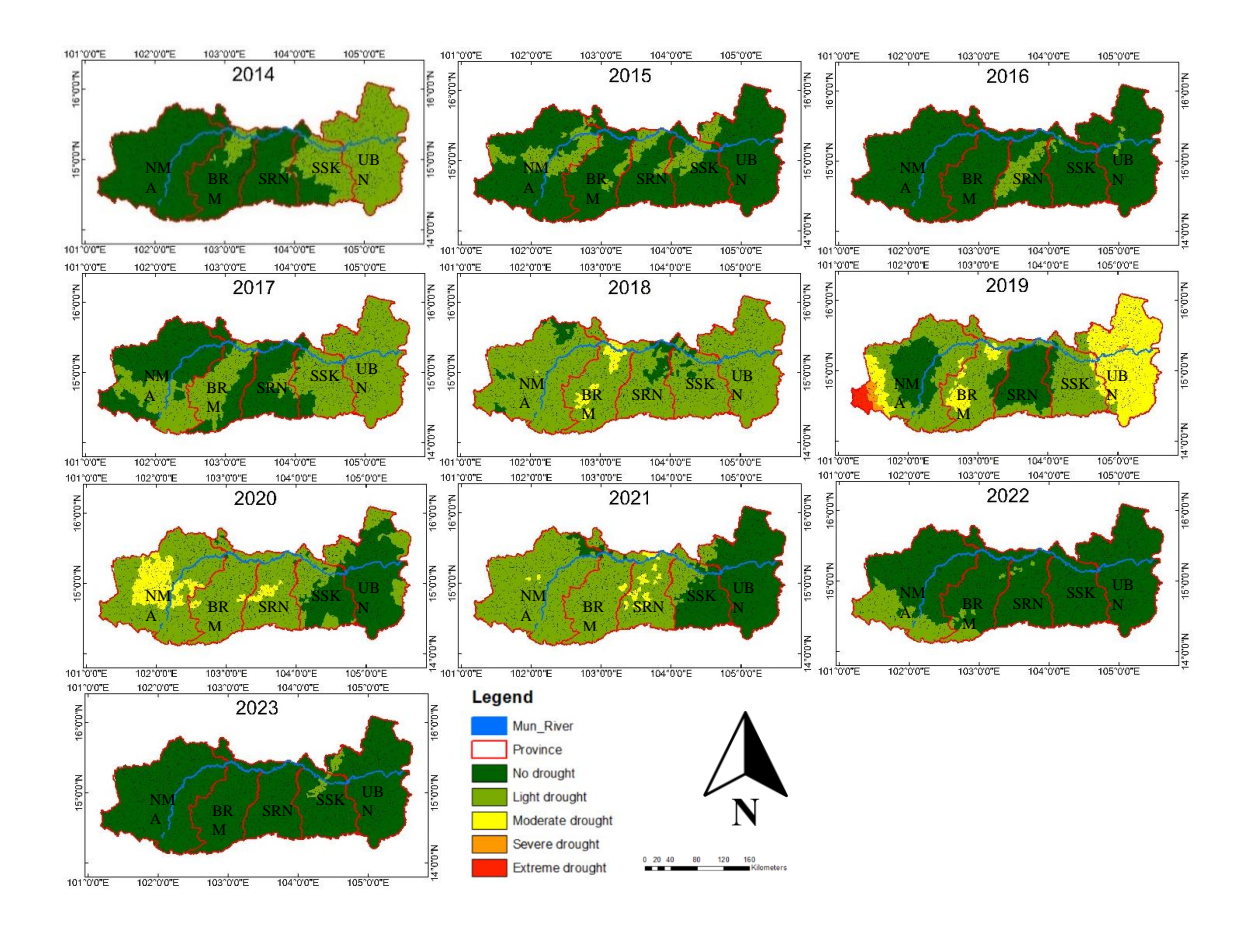


Figure 15 Short-term drought distribution map in the northeast Thailand from 2014-2023

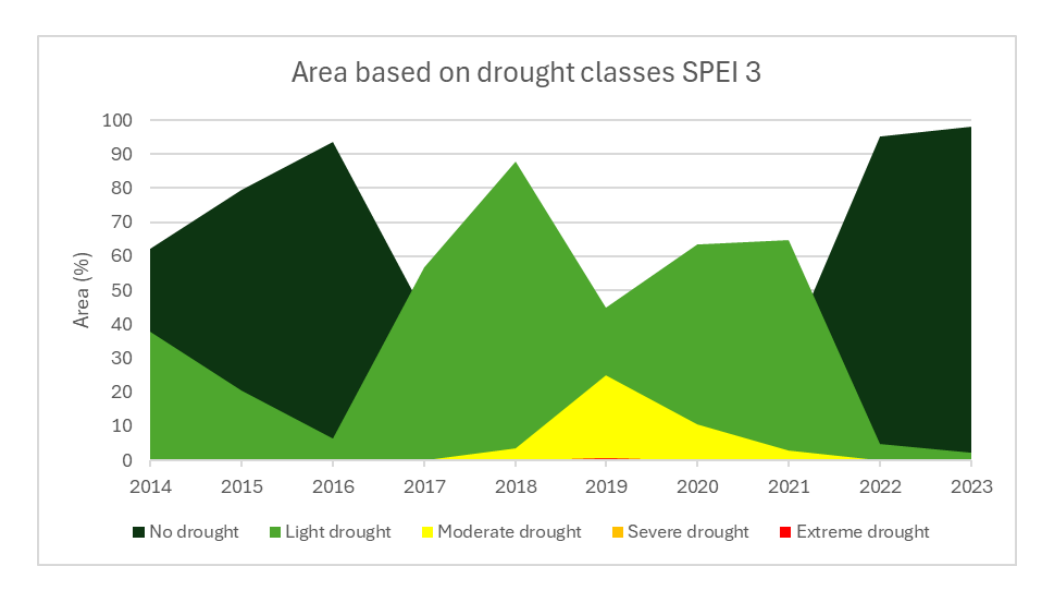


Figure 16 Area based on drought classes SPEI 3

4.3.2 Long-Term Drought Trends

Trend long-term drought indicators (SPEI 6) consistently exhibited a higher frequency in the area drought category. there was a slight occurrence of a long-term drought in 2014, whereas 2015 witnessed a severe drought in Ubon Ratchathani (UBN). This trend of moderate drought persisted through 2016 and 2017, In 2018, severe drought affected 0.47% of the total area, while moderate drought encompassed 27% and light drought covered 51% of the entire region. Notably, as illustrated in Figure 18. severe drought exhibited a pronounced occurrence in the north of Buriram (BRM) during 2018, coinciding with instances of moderate drought in Nakhon Ratchasima (NMA) and various areas within Surin (SRN). In 2019, the study area experienced a prevalence of light drought affecting 83% of the total area, accompanied by a moderate drought affecting 12%. Notably, a distinct area comprising 1.4% encountered severe drought conditions, predominantly observed in Surin (SRN).

Additionally, in 2020, drought conditions were observed in Nakhon Ratchasima (NMA). as shown in figure 17. Significant insights were garnered through the analysis of area percentages extracted from the drought maps, indicating a notable increase in the affected areas across different drought classes over extended time periods, specifically for SPEI 3 and SPEI 6-month scales, as shown in figure 18. This observation implies that prolonged periods of deficient precipitation contribute to the heightened frequency of drought occurrences. Such a thorough examination underscores the different distribution of drought events across various districts of northeast Thailand throughout the period spanning 2014 to 2023. Showed in Figure 17.

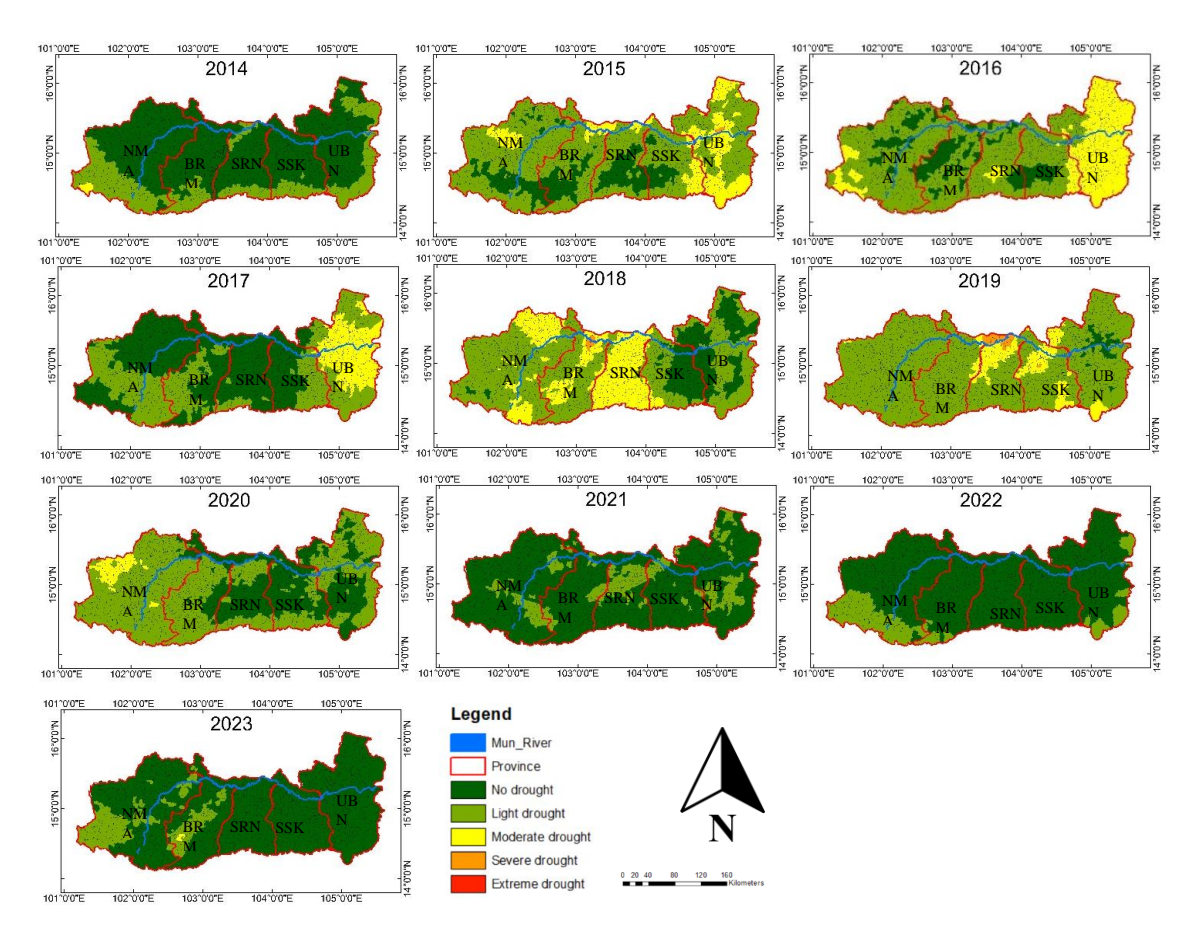


Figure 17 Long-term drought trends distribution map in the northeast of Thailand from 2014-2023

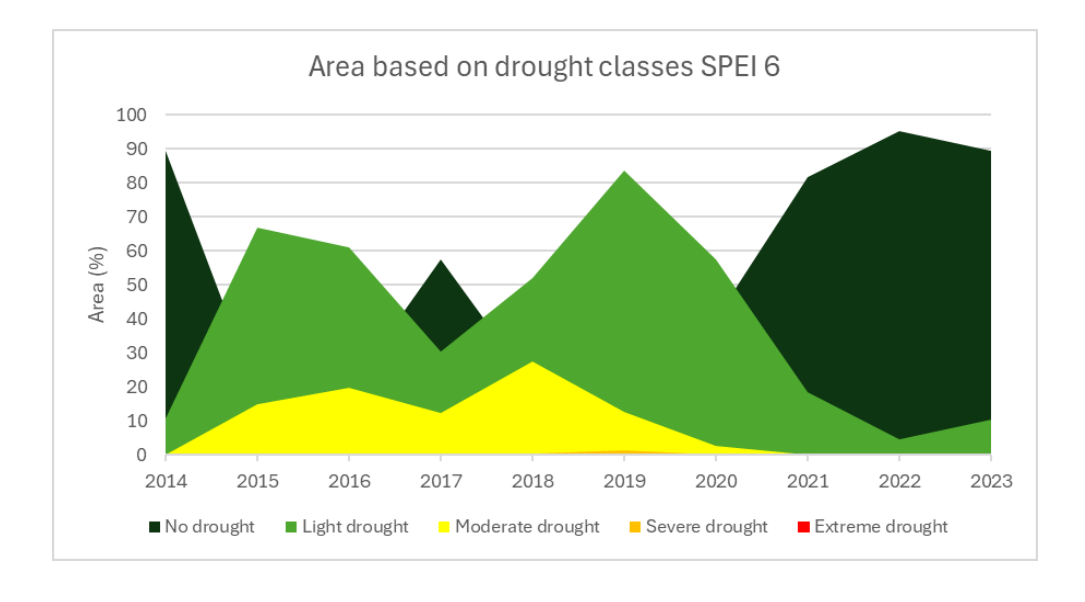


Figure 18 Area based on drought classes SPEI 6

4.4 Summary of Experiment and Result

In conclusion, the assessment of drought and analyzed using remote sensing and ground observation data at a resolution of 30 meters using three machine learning algorithms XGBoost, Random Forest, and Extra Threes. The purpose of this study is to analyze and investigate various droughts and generate a drought map in the northeast of Thailand for the period 2014–2023. The conclusions from this study are summarized as follows.

1) This study analysis the vital role of remote sensing and ground observation variables spanning from 2014 to 2023. Utilizing permutation importance calculations, the study not only enhanced the comparability of variables but also revealed intricate correlations among them. Across three predictive models (XGBoost, Random Forest, and Extra Trees), the Extra Trees model emerges as the most promising candidate for drought index prediction in the Northeast region of Thailand, demonstrating competitive performance across various metrics and datasets. precipitation data (CHIRPS), elevation (Digital Elevation Model), and temperature (Temperature Condition Index) emerged as the most influential variables for estimating both SPEI 3 and SPEI 6. Although variables such as the Enhanced Vegetation Index (EVI) and Vegetation Condition Index (VCI) also contributed significantly, their roles were secondary compared to CHIRPS, elevation, and TCI. These findings on the nuanced interplay of variables in SPEI estimation, offer valuable insights for water resource management and drought monitoring in the northeast of Thailand.

2) This study analysis both short-term and long-term precipitation patterns, utilizing the Standardized Precipitation Evapotranspiration Index (SPEI) as a metric to gauge drought conditions. Short-term observations revealed instances of drought, particularly notable in June 2015 and April 2016, with recurring drought conditions evident towards the end of 2018 and 2019, as well as at the onset of 2020 and 2021. These findings underscore the cyclical nature of reduced precipitation and the consequential threat of water scarcity within shorter time frames.

Furthermore, this study investigation into long-term precipitation trends, evaluated over a SPEI, revealed sustained negative SPEI values from mid-year 2015 to 2016, indicative of emerging drought conditions. Notably, from mid-year 2018 to 2020, the persistent negativity of SPEI values highlighted a protracted period of drought across multiple months, the severity and duration of the drought.

CHAPTER 5 CONCLUSION AND FUTURE WORK

5.1 Conclusion

RS technology has significantly advanced the field of mapping the spatio-temporal dynamics of drought in Northeast Thailand. This area is situated within the tropical zone, characterized by predominantly sandy soil that has a limited capacity to retain water. The frequency and severity of droughts have increased, causing significant damage to the agricultural and economic sectors, resulting in reduced crop yields and hardships for farmers. The terrain is on the Korat plateau because most of it is a plateau. This study the challenge of integrating remote sensing with ground observation data to improve drought monitoring. Ground-based indicators offer precision but limited spatial coverage, while RS indices cover larger areas with lower accuracy. To solve this problem, machine learning algorithms were utilized to combine sources of remote sensing data and ground observation. This approach enhances spatial resolution and accuracy in drought monitoring in Northeast Thailand.

This study found patterns of drought occurrences, attributing them predominantly to insufficient rainfall. Noteworthy drought events are observed in 2018, 2019, and 2020 for short-term droughts, and in 2015, 2016, 2018, 2019, and 2020 for long-term droughts. These findings align with the recurring El Niño phenomenon, which typically induces diminished rainfall across the study area. Data from the Hydro-Informatics Institute of the Ministry of Higher Education substantiate these observations, accentuating the sustained presence of El Niño-induced drought conditions from late 2014 through 2016 and a resurgence in 2019. The consistent association between El Niño occurrences and reduced rainfall highlights its pivotal role in precipitating drought phenomena within the region.

This study analyzes the vital role of RS and ground observation variables spanning the years 2014 to 2023, employing permutation importance calculations. Using three machine learning models (XGBoost, Random Forest, and Extra Trees), it is revealed that precipitation data (CHIRPS), elevation (Digital Elevation Model), and temperature (Temperature Condition Index) are the most influential variables for estimating both short-term (SPEI 3) and long-term (SPEI 6) drought indices. While variables like the Enhanced Vegetation Index (EVI) and Vegetation Condition Index

(VCI) also contribute significantly, their impacts are found to be secondary when compared to CHIRPS, elevation, and TCI. These insights have implications for water resource management and drought surveillance in northeast Thailand.

The spatial mapping of drought distribution in northeast Thailand from 2014 to 2023 was conducted using the Extra Trees model. Long-term drought indicators, particularly SPEI 6, consistently demonstrate a higher frequency of area drought categories compared to short-term indicators like SPEI 3. Analysis of short-term drought events reveals temporal patterns, including predominant short-term light droughts in 2014, with a resurgence in 2017 and expanded influence in 2018. Moderate drought conditions persisted in Buriram (BRM) through 2019, while significant instances of drought, ranging from light to extreme severity, were observed across different areas, notably impacting Sisaket (SSK) in 2019 and sporadic moderate droughts in Buriram (BRM). Substantial instances of moderate to extreme drought were reported in Ubon Ratchathani (UBN) and Nakhon Ratchasima (NMA) based on data from the Office of Natural Resources and Environmental Policy and Planning. Long-term drought indicators (SPEI 6) consistently exhibited higher frequencies, particularly notable in 2015 and 2018, affecting various parts of northeast Thailand.

The main initiatives of the thesis are as follows:

- (1) Applying fusion of drought index from the Landsat 8 satellite and ground observations for the study area. It provides insights into environmental parameters and precise meteorological measurements.
- (2) Compared the performance of various ML models to identify the most effective approach for drought monitoring in the study area.
- (3) Explored spatiotemporal trends in drought distribution to inform water management and mitigation strategies.

5.2 Future work and Suggestions

In summary, the results of the research can be used as a guideline in planning drought and water management. Future research could benefit from integrating additional data sources. Incorporating data from sources such as soil moisture measurements, groundwater levels, and land use and land cover data could provide a more understanding of drought dynamics and improve the accuracy of drought prediction models.

However, in reflecting on the findings presented in this study, it is to certain inherent limitations. The study focused on the northeast Thailand, which warrants caution when extrapolating the results to other geographical contexts. Variations in environmental conditions, other factors, and land use practices across different regions may influence the applicability and generalizability of the findings.

Furthermore, the choice of machine learning models, including XGBoost, Random Forest, and Extra Trees, along with their associated parameters, introduces variability in the outcomes observed. It is important to acknowledge that the performance and efficacy of these models may differ in distinct geographic settings, owing to disparities in data availability, topography characteristics, and climatic pattern.

Future research should extend the geographic scope, encompassing diverse regions beyond northeast Thailand, to gain a more comprehensive of drought dynamics and management strategies. Exploring alternative modeling approaches and incorporating additional environmental variables could further insights into the complexities of drought occurrence and mitigation efforts. Therefore, future research should be conducted to extract the information with deep learning methods or neural network and monitor the drought. remote sensing data and evaluating the impact of these data changes on the regional environment.

REFERENCES

- Abdulraheem, M. I., Zhang, W., Li, S., Moshayedi, A. J., Farooque, A. A., & Hu, J. (2023). Advancement of Remote Sensing for Soil Measurements and Applications: A Comprehensive Review. *Sustainability*, 15(21), 15444. Retrieved from https://www.mdpi.com/2071-1050/15/21/15444
- Adnan, M. N. (2022). On Reducing the Bias of Random Forest. In (pp. 187-195).
- Ali, Z., Abduljabbar, Z., Tahir, H., Sallow, A., & Almufti, S. (2023). Exploring the Power of eXtreme Gradient Boosting Algorithm in Machine Learning: a Review. 12, 320-334. doi:10.25007/ajnu.v12n2a1612
- Arpakorn, W., & Chen, N. (2021). Analysis and investigation on spatio-temporal dynamic pattern of drought in Thailand. *Burapha University*(15). doi:http://ir.buu.ac.th/dspace/handle/1513/380
- Ashour, I., El-Tokhey, M., Mogahed, Y., & Ragheb, A. (2022). Performance of global navigation satellite systems (GNSS) in absence of GPS observations. *Ain Shams Engineering Journal*, 13. doi:10.1016/j.asej.2021.09.016
- Aziz, T., Camana, M. R., Garcia, C. E., Hwang, T., & Koo, I. (2023). REM-Based Indoor Localization with an Extra-Trees Regressor. *Electronics*, 12(20), 4350. Retrieved from https://www.mdpi.com/2079-9292/12/20/4350
- Bahta, Y. T., & Myeki, V. A. (2022). The Impact of Agricultural Drought on Smallholder Livestock Farmers: Empirical Evidence Insights from Northern Cape, South Africa. *Agriculture*, 12(4), 442. Retrieved from https://www.mdpi.com/2077-0472/12/4/442
- Bandoc, G., & Prăvălie, R. (2015). Climatic water balance dynamics over the last five decades in Romania's most arid region, Dobrogea. *Journal of Geographical Sciences*, 25. doi:10.1007/s11442-015-1236-1
- Baykal, T., Terzi, Ö., Yıldırım, G., & Taylan, D. (2023). *Meteorological Drought Modelling by Explainable Artificial Intelligence*.
- Breiman, L. (2001). Random forests. *Machine learning*, 45, 5-32.
- Carrillo, J., Hernández-Barrera, S., Expósito, F. J., Díaz, J. P., González, A., & Pérez, J. C. (2023). The uneven impact of climate change on drought with elevation in the Canary Islands. *npj Climate and Atmospheric Science*, *6*(1), 31. doi:10.1038/s41612-023-00358-7
- Cartwright, J., Littlefield, C., Michalak, J., Lawler, J., & Dobrowski, S. (2020). Topographic, soil, and climate drivers of drought sensitivity in forests and shrublands of the Pacific Northwest, USA. *Scientific Reports*, 10. doi:10.1038/s41598-020-75273-5
- Caruso, G., Palai, G., Tozzini, L., D'Onofrio, C., & Gucci, R. (2023). The role of LAI and leaf chlorophyll on NDVI estimated by UAV in grapevine canopies. *Scientia Horticulturae*, 322, 112398. doi:https://doi.org/10.1016/j.scienta.2023.112398
- Chander, G., Markham, B. L., & Helder, D. L. (2009). Summary of current radiometric calibration coefficients for Landsat MSS, TM, ETM+, and EO-1 ALI sensors. *Remote Sensing of Environment*, 113(5), 893-903. doi:https://doi.org/10.1016/j.rse.2009.01.007
- Chen, T., & Guestrin, C. (2016). *Xgboost: A scalable tree boosting system*. Paper presented at the Proceedings of the 22nd acm sigkdd international conference on knowledge discovery and data mining.

- Diodato, N., & Bellocchi, G. (2008). Modelling vegetation greenness responses to climate variability in a Mediterranean terrestrial ecosystem. *Environmental Monitoring and Assessment*, 143(1), 147-159. doi:10.1007/s10661-007-9964-z
- Du, H., Tan, M. L., Zhang, F., Chun, K., Li, L., & Kabir, M. (2023). Evaluating the effectiveness of CHIRPS data for hydroclimatic studies. *Theoretical and Applied Climatology*, 155, 1-21. doi:10.1007/s00704-023-04721-9
- Ejaz, N., Bahrawi, J., Alghamdi, K. M., Rahman, K. U., & Shang, S. (2023). Drought Monitoring Using Landsat Derived Indices and Google Earth Engine Platform: A Case Study from Al-Lith Watershed, Kingdom of Saudi Arabia. *Remote Sensing*, 15(4), 984. Retrieved from https://www.mdpi.com/2072-4292/15/4/984
- Ekmekcioğlu, Ö. (2023). Drought Forecasting Using Integrated Variational Mode Decomposition and Extreme Gradient Boosting. *Water, 15*(19), 3413. Retrieved from https://www.mdpi.com/2073-4441/15/19/3413
- Ershad, M., & Ali, E. (2020). Geographic Information System (GIS): Definition, Development, Applications & Components.
- Fu, R., Chen, R., Wang, C., Chen, X., Gu, H., Wang, C., . . . Yin, G. (2022). Generating High-Resolution and Long-Term SPEI Dataset over Southwest China through Downscaling EEAD Product by Machine Learning. *Remote Sensing*, 14(7), 1662. Retrieved from https://www.mdpi.com/2072-4292/14/7/1662
- Fujii, K., Hayakawa, C., Panitkasate, T., Maskhao, I., Funakawa, S., Kosaki, T., & Nawata, E. (2017). Acidification and buffering mechanisms of tropical sandy soil in northeast Thailand. *Soil and Tillage Research*, *165*, 80-87. doi:https://doi.org/10.1016/j.still.2016.07.008
- Gessner, U., Reinermann, S., Asam, S., & Kuenzer, C. (2023). Vegetation Stress Monitor—Assessment of Drought and Temperature-Related Effects on Vegetation in Germany Analyzing MODIS Time Series over 23 Years. *Remote Sensing*, 15(22), 5428. Retrieved from https://www.mdpi.com/2072-4292/15/22/5428
- Geurts, P., Ernst, D., & Wehenkel, L. (2006). Extremely randomized trees. *Machine learning*, 63(1), 3-42. doi:10.1007/s10994-006-6226-1
- Gond, S., Gupta, N., Patel, J., & Dikshit, P. K. S. (2023). Spatiotemporal evaluation of drought characteristics based on standard drought indices at various timescales over Uttar Pradesh, India. *Environmental Monitoring and Assessment*, 195(3), 439. doi:10.1007/s10661-023-10988-2
- Gul, E., Staiou, E., Safari, M. J. S., & Vaheddoost, B. (2023). Enhancing Meteorological Drought Modeling Accuracy Using Hybrid Boost Regression Models: A Case Study from the Aegean Region, Türkiye. *Sustainability*, 15(15), 11568. Retrieved from https://www.mdpi.com/2071-1050/15/15/11568
- Guth, P. L., Van Niekerk, A., Grohmann, C. H., Muller, J.-P., Hawker, L., Florinsky, I. V., . . . Strobl, P. (2021). Digital Elevation Models: Terminology and Definitions. *Remote Sensing*, 13(18), 3581. Retrieved from https://www.mdpi.com/2072-4292/13/18/3581
- Gwatida, T., Kusangaya, S., Gwenzi, J., Mushore, T., Shekede, M. D., & Viriri, N. (2023). Is climate really changing? Insights from analysis of 30-year daily CHIRPS and station rainfall data in Zimbabwe. *Scientific African*, 19, e01581. doi:https://doi.org/10.1016/j.sciaf.2023.e01581
- Holden, C., & Woodcock, C. (2016). An analysis of Landsat 7 and Landsat 8 underflight

- data and the implications for time series investigations. Remote Sensing of Environment, 185. doi:10.1016/j.rse.2016.02.052
- Holzman, M. E., Rivas, R., & Piccolo, M. C. (2014). Estimating soil moisture and the relationship with crop yield using surface temperature and vegetation index. *International Journal of Applied Earth Observation and Geoinformation*, 28, 181-192. doi:https://doi.org/10.1016/j.jag.2013.12.006
- Im, S. (2023). Spatial analysis of vegetation cover response to climate trends in Khakassia (South Siberia). *Journal of Mountain Science*, 20(10), 2869-2884. doi:10.1007/s11629-023-8096-4
- John, V., Liu, Z., Guo, C., Mita, S., & Kidono, K. (2016, 2016//). *Real-Time Lane Estimation Using Deep Features and Extra Trees Regression*. Paper presented at the Image and Video Technology, Cham.
- Karnieli, A., Agam, N., Pinker, R., Anderson, M., Imhoff, M., Gutman, G., . . . Goldberg, A. (2010). Use of NDVI and Land Surface Temperature for Drought Assessment: Merits and Limitations. *Journal of Climate J CLIMATE, 23*, 618-633. doi:10.1175/2009JCLI2900.1
- Kocaaslan, S., Musaoglu, N., Türkeş, M., & Tanik, A. (2017). Using Satellite-Based Indices For Monitoring Drought Effects On The Buyuk Menderes River Basin.
- Kogan, F. N. (1995). Application of vegetation index and brightness temperature for drought detection. *Advances in Space Research*, 15(11), 91-100. doi:https://doi.org/10.1016/0273-1177(95)00079-T
- Li, B., Tang, H., & Chen, D. (2009). Drought Monitoring Using the Modified Temperature/Vegetation Dryness Index.
- Li, J., Wang, Z., Wu, X., Xu, C.-Y., Guo, S., Chen, X., & Zhang, Z. (2021). Robust Meteorological Drought Prediction Using Antecedent SST Fluctuations and Machine Learning. *Water Resources Research*, 57. doi:10.1029/2020WR029413
- Li, T., Hu, Y., Liu, B., Jiang, L., Wang, H., & Shen, X. (2023). Co-registration and residual correction of digital elevation models: a comparative study. *The Cryosphere*, 17, 5299-5316. doi:10.5194/tc-17-5299-2023
- Li, X., Jia, H., & Wang, L. (2023). Remote Sensing Monitoring of Drought in Southwest China Using Random Forest and eXtreme Gradient Boosting Methods. *Remote Sensing*, 15(19), 4840. Retrieved from https://www.mdpi.com/2072-4292/15/19/4840
- Lin, Z., & Shelton, S. (2020). Interdecadal Change of Drought Characteristics in Mahaweli River Basin of Sri Lanka and the Associated Atmospheric Circulation Difference. *Frontiers in Earth Science*, 8. doi:10.3389/feart.2020.00306
- Liu, C., Yang, C., Yang, Q., & Wang, J. (2021). Spatiotemporal drought analysis by the standardized precipitation index (SPI) and standardized precipitation evapotranspiration index (SPEI) in Sichuan Province, China. *Scientific Reports*, 11(1), 1280. doi:10.1038/s41598-020-80527-3
- Lou, Y., Ye, Y., Yang, Y., Zuo, W., Wang, G., Strong, M., . . . Payne, C. (2022). Individualized empirical baselines for evaluating the energy performance of existing buildings. *Science and Technology for the Built Environment*, 29, 1-15. doi:10.1080/23744731.2022.2134680
- Marks, D. (2011). Climate Change and Thailand: Impact and Response. *Contemporary Southeast Asia: A Journal of International and Strategic Affairs*, 33, 229-258. doi:10.1353/csa.2011.0132

- Mehraein, M., Mohanavelu, A., Naganna, S. R., Kulls, C., & Kisi, O. (2022). Monthly Streamflow Prediction by Metaheuristic Regression Approaches Considering Satellite Precipitation Data. Water, 14(22), 3636. Retrieved https://www.mdpi.com/2073-4441/14/22/3636
- Mongkolsawat, C., Thirangoon, P., Suwanwerakamtorn, R., Karladee, N., Paiboonsak, S., & Champathet, P. (2001). An evaluation of drought risk area in Northeast Thailand using remotely sensed data and GIS. Asian Journal of Geoinformatics, 1, 33-44.
- Montes-Vega, M. J., Guardiola-Albert, C., & Rodríguez-Rodríguez, M. (2023). Calculation of the SPI, SPEI, and GRDI Indices for Historical Climatic Data from Doñana National Park: Forecasting Climatic Series (2030–2059) Using Two Climatic Scenarios RCP 4.5 and RCP 8.5 by IPCC. Water, 15(13), 2369. Retrieved from https://www.mdpi.com/2073-4441/15/13/2369
- Narimane, Z., Niculescu, S., & Mihoubi, M. (2021). Assessment Of Combining Convolutional Neural Networks And Object Based Image Analysis To Land Cover Classification Using Sentinel 2 Satellite Imagery (Tenes Region, Algeria). The International Archives of the Photogrammetry, Remote Sensing and Spatial Information Sciences, XLIII-B3-2021, 383-389. doi:10.5194/isprs-archives-XLIII-B3-2021-383-2021
- Niazkar, M., Menapace, A., Brentan, B., Piraei, R., Jimenez, D., Dhawan, P., & Righetti, M. (2024). Applications of XGBoost in water resources engineering: A systematic literature review (Dec 2018–May 2023). Environmental Modelling & Software, 174, 105971. doi:https://doi.org/10.1016/j.envsoft.2024.105971
- Nwayor, I. J., & Robeson, S. M. (2024). Exploring the relationship between SPI and SPEI in a warming world. Theoretical and Applied Climatology, 155(4), 2559-2569. doi:10.1007/s00704-023-04764-y
- Orusa, T., Viani, A., Cammareri, D., & Borgogno Mondino, E. (2023). A Google Earth Engine Algorithm to Map Phenological Metrics in Mountain Areas Worldwide with Landsat Collection and Sentinel-2. Geomatics, 3(1), 221-238. Retrieved from https://www.mdpi.com/2673-7418/3/1/12
- Pan, Z., Huang, J., Zhou, Q., Wang, L., Cheng, Y., Zhang, H., . . . Liu, J. (2015). Mapping crop phenology using NDVI time-series derived from HJ-1 A/B data. International Journal of Applied Earth Observation and Geoinformation, 34, 188-197. doi:https://doi.org/10.1016/j.jag.2014.08.011
- Páscoa, P., Gouveia, C., Russo, A., & Trigo, R. (2017). Drought Trends in the Iberian Peninsula over the Last 112 Years. Advances in Meteorology, 2017, 1-13. doi:10.1155/2017/4653126
- Perez, M., & Vitale, M. (2023). Landsat-7 ETM+, Landsat-8 OLI, and Sentinel-2 MSI Surface Reflectance Cross-Comparison and Harmonization Mediterranean Basin Area. Remote Sensing, 15(16), 4008. Retrieved from https://www.mdpi.com/2072-4292/15/16/4008
- Periasamy, T., Palanisamy, M., Ravichandran, V., & Jothiramalingam, K. (2021). Google Earth Engine Based Agricultural Drought Monitoring In Kodavanar Watershed, Part Of Amaravathi Basin, Tamil Nadu, India. The International Archives of the Photogrammetry, Remote Sensing and Spatial Information Sciences, XLIII-B5-2021, 43-49. doi:10.5194/isprs-archives-XLIII-B5-2021-43-2021

- Potopová, V., Stepanek, P., Zahradníček, P., Farda, A., Türkott, L., & Soukup, J. (2018).

 Projected changes in the evolution of drought on various timescales over the Czech Republic according to Euro-CORDEX models: Projected changes in the evolution of drought. *International Journal of Climatology*, 38. doi:10.1002/joc.5421

 Prodham F. Zhang, I. H., Von F., Shi, L., Pangeli, Sharma, T. R., Zhang, D.
- Prodhan, F., Zhang, J.-H., Yao, F., Shi, L., Pangali Sharma, T. P., Zhang, D., . . . Mohana, H. (2021). Deep Learning for Monitoring Agricultural Drought in South Asia Using Remote Sensing Data. *Remote Sensing*, 13. doi:10.3390/rs13091715
- Qin, Q., Wu, Z., Zhang, T., Sagan, V., Zhang, Z., Zhang, Y., . . . Zhao, C. (2021). Optical and Thermal Remote Sensing for Monitoring Agricultural Drought. *Remote Sensing*, 13(24), 5092. Retrieved from https://www.mdpi.com/2072-4292/13/24/5092
- Rousta, I., Olafsson, H., Moniruzzaman, M., Zhang, H., Liou, Y.-A., Mushore, T. D., & Gupta, A. (2020). Impacts of Drought on Vegetation Assessed by Vegetation Indices and Meteorological Factors in Afghanistan. *Remote Sensing*, 12(15), 2433. Retrieved from https://www.mdpi.com/2072-4292/12/15/2433
- SalİK, A. W., & Karacabey, E. (2019). Application of Landsat 8 Satellite Image NDVI Time Series for Crop Phenology Mapping: Case Study Balkh and Jawzjan Regions of Afghanistan. [Landsat 8 Uydu Görüntü Uygulaması Ürün Fenolojisinin Haritalanması İçin NDVI Zaman Serisi: Afganistan'ın Balkh ve Jawzjan Bölgeleri Örneği]. Çanakkale Onsekiz Mart Üniversitesi Fen Bilimleri Enstitüsü Dergisi, 5(1), 49-62. doi:10.28979/comufbed.557792
- Santos, M. S., Soares, J. P., Abreu, P. H., Araujo, H., & Santos, J. (2018). Cross-Validation for Imbalanced Datasets: Avoiding Overoptimistic and Overfitting Approaches [Research Frontier]. *IEEE Computational Intelligence Magazine*, 13(4), 59-76. doi:10.1109/MCI.2018.2866730
- Saruda, S., Jinda, k., & Apiwat, B. (2021). Water with Drought in the Northeast.
- Sedtha, S., Pramanik, M., Szabo, S., Wilson, K., & Park, K. S. (2023). Climate change perception and adaptation strategies to multiple climatic hazards: Evidence from the northeast of Thailand. *Environmental Development*, 48, 100906. doi:https://doi.org/10.1016/j.envdev.2023.100906
- Shrestha, R. P., Chaweewan, N., & Arunyawat, S. (2017). Adaptation to Climate Change by Rural Ethnic Communities of Northern Thailand. *Climate*, *5*(3), 57. Retrieved from https://www.mdpi.com/2225-1154/5/3/57
- Singh, R., Roy, S., & Kogan, F. (2003). Vegetation and Temperature Condition Indices from NOAA AVHRR Data for Drought Monitoring Over India. *International Journal of Remote Sensing*, 24, 4393-4402. doi:10.1080/0143116031000084323
- Slavková, J., Gera, M., Nikolova, N., & Siman, C. (2023). Standardized Precipitation and Evapotranspiration Index Approach for Drought Assessment in Slovakia—Statistical Evaluation of Different Calculations. *Atmosphere*, 14(9), 1464. Retrieved from https://www.mdpi.com/2073-4433/14/9/1464
- Sobrino, J., Jimenez, J.-C., & Paolini, L. (2004). Land surface temperature retrieval from LANDSAT TM 5. *Remote Sensing of Environment*, 90, 434-440. doi:10.1016/j.rse.2004.02.003
- Spadoni, G. L., Cavalli, A., Congedo, L., & Munafò, M. (2020). Analysis of Normalized Difference Vegetation Index (NDVI) multi-temporal series for the production of

- forest cartography. Remote Sensing Applications: Society and Environment, 20, 100419. doi:10.1016/j.rsase.2020.100419
- Sultana, M. S., Gazi, M. Y., & Mia, M. B. (2021). Multiple indices based agricultural drought assessment in the northwestern part of Bangladesh using geospatial techniques. *Environmental Challenges*, 4, 100120. doi:https://doi.org/10.1016/j.envc.2021.100120
- Suwanlee, S. R., Homtong, N., & Som-ard, J. (2023). Drought Monitoring From 2001–2019 In Northeast Thailand Using Modis Ndvi Image Time Series And Savitzky-Golay Approach. *Int. Arch. Photogramm. Remote Sens. Spatial Inf. Sci., XLVIII-M-1-2023*, 367-373. doi:10.5194/isprs-archives-XLVIII-M-1-2023-367-2023
- Suzuki, S., Noble, A., Ruaysoongnern, S., & Chinabut, N. (2007). Improvement in Water-Holding Capacity and Structural Stability of a Sandy Soil in Northeast Thailand. *Arid Land Research and Management ARID LAND RES MANAG*, 21, 37-49. doi:10.1080/15324980601087430
- Tomas-Burguera, M., Vicente-Serrano, S. M., Peña-Angulo, D., Domínguez-Castro, F., Noguera, I., & El Kenawy, A. (2020). Global Characterization of the Varying Responses of the Standardized Precipitation Evapotranspiration Index to Atmospheric Evaporative Demand. *Journal of Geophysical Research: Atmospheres,* 125(17), e2020JD033017. doi:https://doi.org/10.1029/2020JD033017
- Vicente-Serrano, S., & Beguería, S. (2015). Comment on 'Candidate distributions for climatological drought indices (SPI and SPEI)' by James H. Stagge et al. *International Journal of Climatology*, 36. doi:10.1002/joc.4474
- Wilson, J. P. (2012). Digital terrain modeling. *Geomorphology*, 137(1), 107-121. doi:https://doi.org/10.1016/j.geomorph.2011.03.012
- Xiao, X., Braswell, B., Zhang, Q., Boles, S., Frolking, S., & Moore, B. (2003). Sensitivity of vegetation indices to atmospheric aerosols: Continental-scale observations in Northern Asia. *Remote Sensing of Environment, 84*, 385-392. doi:10.1016/S0034-4257(02)00129-3
- Xu, Z., Sun, H., Zhang, T., Xu, H., Wu, D., & Gao, J. (2023). Evaluating established deep learning methods in constructing integrated remote sensing drought index: A case study in China. *Agricultural Water Management*, 286, 108405. doi:https://doi.org/10.1016/j.agwat.2023.108405
- Yang, X., Xu, X., Stovall, A., Chen, M., & Lee, J. E. (2021). Recovery: Fast and Slow—Vegetation Response During the 2012–2016 California Drought. *Journal of Geophysical Research: Biogeosciences*, 126. doi:10.1029/2020JG005976
- Yuzugullu, O., Fajraoui, N., Don, A., & Liebisch, F. (2024). Satellite-based soil organic carbon mapping on European soils using available datasets and support sampling. *Science of Remote Sensing*, 9, 100118. doi:https://doi.org/10.1016/j.srs.2024.100118
- Zafari, A., Zurita-Milla, R., & Izquierdo-Verdiguier, E. (2019). Land Cover Classification Using Extremely Randomized Trees: A Kernel Perspective. *IEEE Geoscience and Remote Sensing Letters, PP*, 1-5. doi:10.1109/LGRS.2019.2953778
- Zarei, A. R., Mahmoudi, M. R., & Moghimi, M. M. (2023). Determining the most appropriate drought index using the random forest algorithm with an emphasis on agricultural drought. *Natural Hazards*, 115(1), 923-946. doi:10.1007/s11069-

- Zhang, Wang, Chen, & Bai, L. (2020). Drought Risk Assessment in Central Asia Using a Probabilistic Copula Function Approach. *Water*, 12, 421. doi:10.3390/w12020421
- Zhang, B., Abu Salem, F. K., Hayes, M. J., Smith, K. H., Tadesse, T., & Wardlow, B. D. (2023). Explainable machine learning for the prediction and assessment of complex drought impacts. *Science of The Total Environment*, 898, 165509. doi:https://doi.org/10.1016/j.scitotenv.2023.165509
- Zhang, J., Ding, J., Wang, J., Lin, H., Han, L., Li, X., & Liu, J. (2023). Remote sensing drought factor integration based on machine learning can improve the estimation of drought in arid and semi-arid regions. *Theoretical and Applied Climatology*, 151(3), 1753-1770. doi:10.1007/s00704-022-04305-z
- Zhang, R., Chen, Z.-Y., Xu, L.-J., & Ou, C.-Q. (2019). Meteorological drought forecasting based on a statistical model with machine learning techniques in Shaanxi province, China. *Science of The Total Environment*, 665, 338-346. doi:https://doi.org/10.1016/j.scitotenv.2019.01.431
- Zhao, Y., Zhang, J., Bai, Y., Zhang, S., Yang, S., Henchiri, M., . . . Nanzad, L. (2022). Drought Monitoring and Performance Evaluation Based on Machine Learning Fusion of Multi-Source Remote Sensing Drought Factors. *Remote Sensing*, 14(24), 6398. Retrieved from https://www.mdpi.com/2072-4292/14/24/6398

APPENDIX

APPENDIX A The information of Ground Observation data from Northeast of Thailand

NO	STATION	NAME	LATITUDE	LONGITUDE
1	407301	Ubonratchathani	15.2455	104.8711
2	407501	Ubonratchathani (Center)	15.2408	105.0195
3	409301	Srisaket	15.0869	104.3269
4	431201	Nakonratchasima	14.9699	102.0803
5	431301	Nakonratchasima (Pakchong)	14.6437	101.3159
6	431401	Nakonratchasima (Chokchai)	14.7396	102.1623
7	432201	Surin	14.8758	103.4939
8	432301	Surin (Agriculture)	14.8926	103.4466
9	432401	Surin (Tatoom)	15.3178	103.6767
10	436201	Buriram	15.2273	103.2422
11	436401	Buriram (Nangrong)	14.6326	102.7156



 $\label{eq:APPENDIXB} \textbf{APPENDIX B}$ The average monthly rainfall data from Northeast of Thailand

		MONTH (MM)												
NO	STATION	YEAR	JAN	FEB	MAR	APR	MAY	JUN	JUL	AUG	SEP	OCT	NOV	DEC
1	407301	2013	1.1	0	41.7	95.3	199.7	142.1	396.2	115.7	502.1	80.4	4.6	66.3
2	407301	2014	0	8.4	0.1	123	54.1	715.8	664.8	162.6	442.6	114.2	0	5
3	407301	2015	0	18.6	0.2	7.4	94.4	157.2	314.1	180.6	271.5	197.5	17.6	0
4	407301	2016	4.8	0	0	60.7	216.1	494.7	185.1	155	347.9	105.3	4.8	14
5	407301	2017	0.4	0	63.9	69.4	343.2	285.2	488.9	233	153.8	79.7	7	0.4
6	407301	2018	0	1.5	72.4	51.4	166.3	352.8	398.2	377.4	387.7	96.4	14.9	12
7	407301	2019	0	9.5	12.6	9.5	249.8	77.5	252.6	350.1	508.7	53.4	17.4	0
8	407301	2020	0	0	1.2	29.1	124.2	201.5	237.2	202.2	347.4	182.8	1.4	0.1
9	407301	2021	0	2.5	3.9	46.1	139.4	257.9	263.1	241.1	347	186.7	0	6.1
10	407301	2022	3.1	29.5	60.8	160.3	386.2	61.7	292.7	388.5	666.7	165.5	34.2	0
11	407301	2023	7.7	48	0	37.1	231.6	218.1	335	189.2	197.9	37.6	10.5	1.5
12	407501	2013	0.7	0	37.2	45.2	322.3	75.8	461.2	164.8	488.1	86.9	5.4	111
13	407501	2014	0	0	0.9	84.6	102.6	563.9	630.7	196.5	218	80.1	0	3.6
14	407501	2015	0	42.1	5	28.9	98.6	227.5	288	186.9	210.7	206.4	35.8	0
15	407501	2016	25.5	0	1.2	40.4	243.2	523.9	265.2	173	520.4	93	13.4	6.6
16	407501	2017	0.6	0.2	43.9	109.8	362.2	258.6	437.1	316.3	152.9	101.3	10.5	1.5
17	407501	2018	0	0	140	98.8	170.5	291.1	309.5	315.4	317	77.3	11.1	0.9
18	407501	2019	0	0	19.5	91.4	236.3	102	318.5	341.9	554.5	26.6	7	0
19	407501	2020	0.9	0	1.4	55	214.8	163.2	242	283.1	439.4	194.7	0.4	0.2
20	407501	2021	0	7.3	8.2	87.1	127.7	261	360.8	295.2	375	231.3	0	4.7
21	407501	2022	2	42.2	70.3	134.8	347.9	46	429.1	557.2	653.9	141.5	25.6	0
22	407501	2023	35.7	0	0	29.3	105.4	342.6	475.1	300.6	205.7	135.3	14.8	12
23	409301	2013	0.3	0	9.8	116.6	188.7	197.1	268.7	89	546.8	73.4	55	46.3
24	409301	2014	0	0.3	0.5	10.9	33.3	288.2	262.6	190.2	279.4	76.6	0	5.3
25	409301	2015	0	53.5	7.3	23.1	66.7	188.9	490.9	188.2	256.1	84.8	23	0
26	409301	2016	0	0	0	12.5	133.8	367.4	183.6	147.4	307.1	135.7	22	1.1
27	409301	2017	0.5	8.9	59.8	33	434.5	66.9	410	342.6	165	131.8	10.1	0.3
28	409301	2018	1.5	8.5	66.1	44.5	154	96.1	358.2	294.3	338	60.7	13.6	0.1
29	409301	2019	0	0	1.8	78.7	245.3	119.6	156.9	187.2	364.4	41.3	7.3	0
30	409301	2020	1.8	0	2.8	66.3	143	146.8	269.8	268.3	396.8	276.7	0.1	0
31	409301	2021	0	1	1	37.6	155.4	140.2	197.3	150.7	445.5	249	0.1	4.1
32	409301	2022	0.3	10.3	60.6	81.3	237.3	102.7	310.9	234.2	510.2	119	21.8	0
33	409301	2023	38.4	0.9	1	75.7	165.7	303.7	441.8	441.5	292.8	180.8	4.6	1.2
34	431201	2013	4.1	0	33.6	19.7	51.6	61.4	260.9	167.8	355.6	321.7	29.3	0.3
35	431201	2014	0	2.7	27	83.8	194.3	53.9	98.7	226	219.9	56.1	13.9	0.4
36	431201	2015	0.9	17.2	47.1	26.6	74.1	92.1	242.7	278.6	284.2	87	17.3	3.3
37	431201	2016	38	0	0	16.1	87.8	77	231.2	154.2	329.2	118.8	37.8	0
38	431201	2017	6	0.1	245.6	13.4	220.9	280.4	102.9	296.4	350.6	97.8	28.2	10.5
39												1010		
	431201	2018	2.6	78.5	28.5	140.9	122.1	95.8	149	87	139.1	106.8	7.9	4.1

								MONT	H (MM)					
NO	STATION	YEAR	JAN	FEB	MAR	APR	MAY	JUN	JUL	AUG	SEP	OCT	NOV	DEC
41	431201	2020	0	0	34.5	36.9	211.3	239.5	147.9	236.1	265.9	282.2	2.7	0
42	431201	2021	0	13.2	19.6	229.9	75.2	37.2	201.9	79.2	267.5	242.2	0	38.1
43	431201	2022	1.9	8.1	67.4	94.3	242.7	83.7	243.3	125.2	307.8	109.2	63.8	0
44	431201	2023	36.8	2.7	0.9	0.7	107.6	279.9	198.9	172.9	195.9	169.4	5.6	1.2
45	431301	2013	46.3	29.5	13.8	91.5	80.8	150.8	59.7	196.3	379.6	266.3	6.7	0.7
46	431301	2014	0	0.5	62.4	107.7	139.4	43.7	52.8	205.1	97.4	76.9	78.8	13.6
47	431301	2015	11	20.6	132.4	56.6	54.1	78.5	64	85	261.9	115.5	44.2	68.1
48	431301	2016	35.7	0	23.9	24.9	47.2	132.1	104.1	74.9	158	105.6	56.7	0
49	431301	2017	3.2	9.3	196.9	71.8	232.4	110.1	175.1	149.7	162.2	268.1	15.5	5.7
50	431301	2018	55.1	41.2	22.7	112.8	343.7	121.6	78.3	276.6	150.2	108	0	120.4
51	431301	2019	0	6.6	23.7	146.4	126.1	129.8	120.4	165.7	233.1	11.1	8.4	0
52	431301	2020	0	0	58.4	95.5	132.8	102.8	107.9	66.9	366.4	212.6	5.5	0
53	431301	2021	0	6.9	96	168.7	100.3	43.6	140.9	109.4	291.1	138.4	23	0
54	431301	2022	3.6	104.1	139.3	28.9	155.3	106.5	260.9	173.1	348.3	36.8	96.7	0
55	431301	2023	4	14.1	0.9	12.3	55.3	76	54.4	72.2	149.6	380.2	57.5	15.6
56	431401	2013	9.3	7.5	22.7	117.6	93.2	92.3	229.2	119	387.4	301.4	25.2	4.8
57	431401	2014	0	0.2	36.5	27.9	51	29.7	111.3	171.7	231.7	203.6	78.1	3.5
58	431401	2015	27.6	11	44.1	70.2	72.5	105.6	138.7	100.9	274.8	170.8	31.3	0.7
59	431401	2016	33.7	0	0	45.6	102.3	207.2	175.3	74	170.6	165.2	29.7	0
60	431401	2017	9.1	0.3	111.8	41.8	234.4	198.5	67.7	182.4	48.2	156.9	42.9	10.9
61	431401	2018	1.1	42.9	1.3	141.4	165.6	76.6	93.3	110.1	148.5	67.6	34.7	7.9
62	431401	2019	0	1	2	57.1	25.9	57.6	60.3	113.5	147.2	107	2.3	0
63	431401	2020	0	0	32.1	50.1	170.2	126.5	115.2	198.1	167.1	315.3	3.3	0
64	431401	2021	0	19.3	4.4	133.6	88.2	68.3	137.2	193.6	390.1	244.3	5.8	68.7
65	431401	2022	0.1	37.9	91.5	120.3	98.4	55.2	225.7	200.2	222.8	131.4	171.7	0.1
66	431401	2023	0	56.8	11.6	129.4	181.8	30.9	66	62	25.6	149.5	0	0
67	432201	2013	3.5	13.4	6.6	30.6	172.5	234.5	246.6	172.1	591.9	99.7	9.6	27.3
68	432201	2014	0	0	0.6	48.2	171.3	137.2	257.2	351.7	162.7	163.5	94	2.1
69	432201	2015	0.1	21.4	34.6	122.8	125.6	112	322.4	210.2	258.5	41.2	9.8	0
70	432201	2016	16	0	0	27.5	146.4	193.1	261.2	323	254.8	135.8	48.4	0
71	432201	2017	3.9	2.4	94.4	19.5	341.9	151.4	342.3	258.6	152.8	119.6	23.7	1.5
72	432201	2018	17.3	0	64.5	48.9	206.3	172.1	109.6	183.7	245.2	55.3	17.9	4.3
73	432201	2019	0	7.5	26.6	49.8	147.2	101.9	227.1	326.5	285.4	19.1	3.1	0
74	432201	2020	0.1	0	1.9	90	118.9	242	158.3	209.3	394	172.3	4.4	0
75	432201	2021	0	46.7	32.9	114.1	240.6	202.4	140.9	143.8	253.9	318.4	33.4	0
76	432201	2022	1	71.5	187.2	142.6	270.7	200.6	239.7	328.1	676.3	94.9	43.6	0
77	432201	2023	16.4	32.3	3.2	74.7	127.5	88.8	22.5	152.1	95.6	253.4	9.4	1.6
78	432301	2013	7.3	28.2	2.6	27.8	208	173	231	134.1	355.7	85.8	4.4	2.5
79	432301	2014	0	2	5	76.2	115.7	121.9	286.5	240	220.1	201.9	90.1	0
80	432301	2015	1.8	7.4	53	30.5	178.6	50.1	262.7	216.8	289.7	119.9	30.9	0.1
81	432301	2016	10.4	0	0	4.5	201	180.6	309.6	185.8	287.1	94.5	48	0
82	432301	2017	2.8	1.6	108.4	17.8	299.9	195.7	334.2	241.2	153.9	152.9	15	1.4
83	432301	2018	13.5	0	24.4	87.1	176.7	118	169.2	168.6	240.7	20.9	37	7.1

		MONTH (MM)												
NO	STATION	YEAR	JAN	FEB	MAR	APR	MAY	JUN	JUL	AUG	SEP	OCT	NOV	DEC
84	432301	2019	0	15.6	17.4	147.3	162.9	102.5	213.2	356.1	348.7	65.6	1.9	0
85	432301	2020	0.6	0	6.3	50.6	53.2	238.7	146.5	150.5	281.3	161	4.8	0
86	432301	2021	0	22.9	11.8	66	214.5	212.6	162.6	166.8	268.7	261.7	16.8	0
87	432301	2022	0	77.9	121.6	184.8	214.1	144	245.3	305.4	651.5	86.6	44.5	0
88	432301	2023	0.8	4.7	9.4	95.9	172	241.7	169.4	279	94.3	131.9	0	0
89	432401	2013	0	0	13.3	113.1	119.3	144.6	170.8	292.1	355.6	63.9	1.6	20.4
90	432401	2014	0	0.1	27	60.1	67.5	238.2	271	213.1	151.8	51	1.4	1.5
91	432401	2015	0	9.5	68.8	30.6	80.7	75.1	222	204.2	217.3	133.4	20.5	0
92	432401	2016	27.2	4.2	0	93.7	156.3	266.4	265.4	108.4	256.8	141.1	41.7	0
93	432401	2017	0	4.5	53.7	81.2	194.7	110.3	358.1	164.6	189.8	74.9	12.2	0.2
94	432401	2018	1.5	0.1	46.1	56.8	232	154.9	232.6	127.7	185.5	0	7	0
95	432401	2019	0	2.1	22.2	113.1	172.6	37.4	130.7	371.3	304.5	32.3	1.8	0
96	432401	2020	0.1	0	19.2	38.3	49.9	83.7	156.6	262	252	179.1	0	0
97	432401	2021	0	30.6	0	96.7	189.7	165.5	132	96.9	372.7	124.1	0	0
98	432401	2022	4.6	23.5	48.9	75.4	76.5	91.4	199.9	144.2	351.1	138.6	37.1	0
99	432401	2023	1.1	7.4	11.9	67	169	299.6	102.7	202.3	129.7	107.6	17.6	1.4
100	436201	2013	35.8	0	16.2	76.2	242.9	123.4	175.5	260	302.5	111.2	3.1	0.9
101	436201	2014	0	0.2	17.1	61.5	95.2	212.3	335.4	252.7	140.5	85.1	6.2	0
102	436201	2015	0	21.3	5.1	41.5	121.1	43.3	312.3	161.7	208.6	100.2	14.2	0
103	436201	2016	14.4	0.7	0	62.7	197.4	151.8	177.2	195.4	382	105.6	83.5	0
104	436201	2017	37	26.3	89.9	34.6	373.5	254.2	338.5	357.9	266.3	76.3	17	2.3
105	436201	2018	0	0	39.8	65.8	156.7	47.8	136.9	111.6	214	35	21.8	2.2
106	436201	2019	0	0	30.1	115.1	293.3	170.2	126.9	217.3	218.8	87.2	2.8	0
107	436201	2020	5.2	0	34.9	46	50.3	212.8	157.9	164.1	307.8	282.8	4.2	0
108	436201	2021	0	7.8	5.2	69.7	145.5	130.9	185	167.5	283.6	216.5	3.7	0
109	436201	2022	7.5	25	84.5	202.7	234.1	142.6	475.6	349.4	417.8	128.5	41.3	0
110	436201	2023	5.4	0	3.2	21.6	56.2	114.8	233.4	152	148	100.9	0	0.9
111	436401	2013	0	3.2	11.1	104.2	136.7	72	225.1	142.7	253.8	290.7	19.3	0.2
112	436401	2014	0	3.4	20	181	174.8	70.4	130.4	315.9	209.4	209.5	6	9.7
113	436401	2015	2.9	10.6	45.7	102.5	58.6	82.3	151.8	206.6	324.6	177.8	23.2	0.8
114	436401	2016	15.2	0	8.4	74	149.8	184.9	311.1	196.2	199.3	122	38.1	0.2
115	436401	2017	1.8	1.7	104.6	67.4	218.5	98.9	238.3	268.6	141.4	80.1	23.9	7.9
116	436401	2018	4.1	6.5	70.3	92	159.2	64.7	44.8	89.8	180.1	27.8	12.8	0.8
117	436401	2019	0	3.8	0.9	75.9	162.9	50	65.4	157.2	222.6	86.3	4.3	0
118	436401	2020	0	2.4	72.8	96.5	165	100.3	337	224.6	308.1	295.6	21.2	0.2
119	436401	2021	0	22.8	18.4	334.4	130	69.4	234.4	105	359.6	282.8	7.4	0
120	436401	2022	0.8	71.6	13.6	180	384.4	141.8	419.2	212.8	392.1	141.4	94.4	0
121	436401	2023	8.7	1	10.4	62.6	133.8	250.6	132.6	156.2	215.9	103	11.6	0.5

 $\label{eq:appendix} \textbf{APPENDIX} \ \textbf{C}$ The monthly maximum temperature data from Northeast of Thailand

							M	ONTH (CELSIU	S)				
NO	STATION	YEAR	JAN	FEB	MAR	APR	MAY	JUN	JUL	AUG	SEP	OCT	NOV	DEC
1	407301	2013	35	39.3	39.5	41	37.5	37.2	35.5	35	35	34.4	35	34
2	407301	2014	33.9	35.8	39.8	39.5	39.8	38.2	35	35.8	35.4	35	35.9	35.2
3	407301	2015	34.9	37.6	38.4	42.4	39.8	40	38.5	36.5	35.5	35	35.6	36.5
4	407301	2016	35.8	37.5	40.1	42.3	40.5	37	35.5	35.2	34.8	35.5	36	35
5 6	407301 407301	2017 2018	34.4 36	38.2 37.4	39.5 39	40.3 40.5	38 37.5	36 35.1	33.8 35	36.3 34	35.9 35.5	34.1 35.8	36.5 35.2	34.4 36
7	407301	2019	35.5	38	40.3	40.7	40.9	38	36.2	34.6	34.2	36	34.5	35.3
8	407301	2020	36.8	38	40.7	40.7	40.3	37	36	35.6	35	33.7	35.4	34.8
9	407301	2021	35.7	38.6	40.4	40.3	39.1	38.7	36.8	35.6	35.1	34.7	35.5	34
10	407301	2022	36	36.7	39	38.2	35.6	37.2	35.8	35.4	35.5	34	36.7	34.5
11	407301	2023	33.9	36.9	40.2	40.8	41.5	36.6	35.6	36	34.4	35.7	33.8	34
12	407501	2013	34.6	38.3	39.4	40.6	38.3	37.4	35.8	36.5	34.3	34.1	34.9	33.8
13	407501	2014	34.2	35.9	39.8	39.4	39	38.6	35.2	35.8	35.6	34.5	35.2	35.2
14	407501	2015	35.3	36.7	37.5	41.5	41.7	39.8	38	36.3	35.7	35.3	35.4	35.7
15	407501	2016	35.3	37.6	40.2	42.6	40.5	37	35.7	35.5	34.3	35.2	35.3	36.7
16	407501	2017	34.9	38.1	39.2	39.7	38	36	34.5	36.1	35.7	34.3	35.8	34.4
17	407501	2018	36.7	37.4	38.8	39.1	37.4	35.4	35.7	34.1	35.1	35.9	35.1	36.2
18	407501	2019	35.5	38.4	39.8	40.6	40.1	37.7	36.4	35	33.8	35.6	34.8	34.8
19	407501	2020	36.7	37.1	40.4	40.4	39.4	37.7	36.3	35.5	34.7	33.7	35.2	34.4
20	407501	2021	35.1	38.2	39.8	38.9	39.1	39	36.6	36.2	34.8	33.9	35.3	33.1
21	407501	2022	35.7	36.1	38.5	38.4	36.3	37	35.6	35.1	35	34.4	35.5	34.2
22	407501	2023	34.5	37.1	40.2	41.2	40.7	36.5	36.5	35.3	33.9	34.5	34	34
23	409301	2013	34.5	37.8	39.6	39.7	38.4	36.5	35.5	33.5	34.3	33.2	34.9	32.3
24	409301	2014	33.5	35.5	39.3	39.5	40.2	38	34.8	35.1	34.5	34	35.4	34
25	409301	2015	34.5	36.6	37.8	42.1	39.2	40.5	38.5	35.5	35.4	34.6	35.2	35.2
26	409301	2016	35.1	37	40.5	42.3	40	37.5	35.3	34.8	33.6	34.4	34.5	34.4
27	409301	2017	34	37.5	39	39.8	37.9	35	33.6	35.5	35	33.1	35.8	33.6
28	409301	2018	35.6	37	37.5	40.3	37.6	35.5	34.8	33.1	35.4	35.3	34	35
29	409301	2019	34.5	38	39.3	40.5	39.9	38.1	37.6	34.8	34.6	36	34.6	35
30	409301	2020	36.3	37.3	40.5	40.1	40.5	37.6	36.4	35.3	34.8	33.8	35	34
31	409301	2021	34.6	38.4	39.8	40	38.3	38.5	38	36.4	33.9	34.2	34.6	32.5
32	409301	2022	35.3	36.2	39.3	38.2	36	36.5	35	34.5	34	33	34.9	33.8
33	409301	2023	34.2	37.9	40.1	40.1	41	37	35.5	35.8	35	34.1	32.9	33
34	431201	2013	34.5	37.9	40.6	41	39.8	37.2	37	35.2	31	34.6	34.3	31.7
35	431201	2014	33.6	36.4	39.6	39.5	38.2	38.3	38.4	37.7	35.8	34.6	35.7	35.9
36	431201	2015	35.3	37.5	38.4	41.5	39.3	40.3	38.2	37.2	35.5	34.8	36.3	35.8
37	431201	2016	36.4	37.3	41.5	43.2	41.8	38.2	37.3	36.5	35	34.8	33.8	33.6
38	431201	2017	34	38.4	39.6	39.1	38.5	36.2	35	35.9	35.4	35.3	35.5	34.9
39	431201	2018	36.6	37.6	38.2	39.4	37.1	36.1	35.9	35.1	36.2	36.1	33.2	35.9
40	431201	2019	34.2	38.8	40.3	41.9	41	39.7	38.5	36.7	34.6	35.8	35.1	35.6
41	431201	2020	37	38.4	41.2	41.1	40.1	38.8	37.7	36.8	35.7	33.8	34.6	35

		MONTH (CELSIUS)												
NO	STATION	YEAR	JAN	FEB	MAR	APR	MAY	JUN	JUL	AUG	SEP	OCT	NOV	DEC
42	431201	2021	34.8	38.7	40.1	39.2	38.2	38.7	39.7	38.3	34.9	35.1	35	32.3
43	431201	2022	36.6	35.8	38.8	38.8	36	36.5	36.4	35.5	35	33.5	34.7	31.3
44	431201	2023	35.1	36.8	40	41.2	41.6	38.7	37.4	39.1	34.8	34.5	30.7	30
45	431301	2013	34	35.9	37.2	38.5	36.7	33.2	32.9	32.1	33	32	32	30.4
46	431301	2014	33	34.1	36	36.4	35.6	35	35	33	33.1	32.6	33	32.1
47	431301	2015	33.8	35.5	36.3	38.1	36	37.7	35.3	34.6	32.9	32.7	33	34.5
48	431301	2016	32.9	35.2	37.9	38.9	39	36.5	33.5	33	32.4	32.1	32.6	32.6
49	431301	2017	33.1	35.2	36.6	36.7	35.6	33.4	32.2	34	33.1	32	32.8	33.1
50	431301	2018	33	35.6	35.2	35.6	34.2	32.8	32.1	31.2	33.1	33.3	32.9	33.1
51	431301	2019	33.3	35.9	37.8	38	36.7	35.1	34	31.7	32.5	34.9	33.9	34
52	431301	2020	35.5	35.1	38.8	38	36.1	35.8	34.5	34.4	33.4	31.5	32.9	32.9
53	431301	2021	32.9	36.1	36.4	37.1	34.9	35.9	36	33.2	33.1	32	32.4	31.6
54	431301	2022	33.9	34.2	36	36.2	33.7	33.6	33.1	33	32.5	31.3	32.3	30
55	431301	2023	32.8	34.6	36.7	38.6	36	35.4	35.6	34.5	32.7	32.1	31	31
56	431401	2014	34.5	36.2	39	39.2	38.5	38.5	37.7	36.2	34.8	34.6	34.7	33.4
57	431401	2013	35.6	37.6	40	40	38.5	36.8	36.2	35.2	34.7	33.6	35.3	32
58	431401	2015	34.7	37.8	39	40.7	39	39	37.9	36.9	35.6	34.6	35.1	35.9
59	431401	2016	36.1	37	41.2	42.5	40.7	37.6	37	36.9	35.5	35	34.9	34.4
60	431401	2017	34.5	38	39.6	39	39	35.8	35.6	36	36.2	34.2	35.1	34.5
61	431401	2018	35.7	37.7	38.1	39	37	36	35.7	35.2	36	36.5	33.5	35.9
62	431401	2019	34.5	38.7	40.1	40.6	40.3	38	37.5	36	35.2	35.7	35.2	35.7
63	431401	2020	37.2	37.9	40.6	40.8	39	38.8	37	36	35.7	34.3	35.7	34.7
64	431401	2021	34.6	38	39.5	39.7	38.2	38.8	38	36.8	35	35.3	35.3	33.2
65	431401	2022	35.7	35.3	38.2	38.8	35.7	37.5	36	35.2	34.8	33.4	34.3	32.2
66	431401	2023	34.8	36.6	39.7	40.2	40.2	37.4	37.2	37.2	35.4	34.5	32.5	31
67	432201	2014	33.9	35.5	39.2	38.7	37.8	37.4	35.7	35.4	34	33.6	34.6	33.2
68	432201	2015	34.6	36.6	37.5	41.3	38.4	39.2	37.9	35.7	34.8	34	35.3	35.9
69	432201	2016	35.4	37	40	42	40.8	37.8	35.8	35.5	34	35.1	34.3	33.8
70	432201	2017	34.4	37.9	39.1	38.8	39	35.6	34.5	35.4	35.5	33.8	36.2	34
71	432201	2018	35.4	37.3	38.8	39.2	38.8	35.7	35.1	34.2	35.9	35.7	34	35.6
72	432201	2019	34.5	38.2	39.7	40.8	40.7	38	37.4	35.9	34.1	34.8	35.5	35.1
73	432201	2020	36.4	37.4	40.1	40.5	41.5	37.5	36.5	35.6	35.5	33.5	34.8	34.3
74	432201	2021	34.9	37.6	39.5	39.2	37.8	37.5	37.4	36	34.5	35.5	34.8	32.3
75	432201	2022	35.8	35.7	38.4	38.5	35.3	36.2	35.7	34.8	34.3	33.1	35	33.7
76	432201	2023	34.1	37.2	40	40.6	41	37	36	35.7	35	34.8	33	32
77	432201	2013	35	37.5	39.7	40	38.6	36.7	35.4	33.8	33.9	33.3	34	33.3
78	432301	2014	33	36.2	38.5	38.5	38.5	37.8	35.5	35.5	35	33.8	34.2	33.2
79	432301	2015	34.6	36.2	37.6	41.6	38.5	38.8	38.6	35.7	35.5	34.7	35.3	35.7
80	432301	2016	35.3	37.4	41.3	43.3	41.2	37.8	36.2	36.2	34.7	34.8	34.5	34.1
81	432301	2017	34.2	37.8	38.8	39.7	39.1	36.2	33.9	35.2	36.3	33.6	35.6	34.1
82	432301	2018	35.5	37.3	39.4	40.7	37.7	35.8	35.3	34.5	35.7	35.8	34.7	35.8
83	432301	2019	35.3	38.6	41	39.9	40.7	38.5	37.7	36	34	35.6	35	34.9
84	432301	2020	36.5	38	40.8	41	42	39	37.6	36.4	36.5	34	35.2	35

		MONTH (CELSIUS)												
NO	STATION	YEAR	JAN	FEB	MAR	APR	MAY	JUN	JUL	AUG	SEP	OCT	NOV	DEC
85	432301	2021	35.2	38.5	40.2	40.3	39.1	38	37.2	36.7	34.5	36.2	35	33
86	432301	2022	36.3	36.2	38.7	39.2	36.7	36.5	36	35	34.5	33.5	35	33.6
87	432301	2023	34.5	37	40	40.5	41.4	37.5	36.1	36.3	36	34.8	33.2	33
88	432301	2013	35.2	37.7	40.8	41.5	39.5	36.7	35.8	34.2	34.1	33.8	34.5	33
89	432401	2014	33.5	36.7	38.9	38.7	38.7	38	35.8	35.1	35	34	34.5	33.8
90	432401	2015	34.5	37.3	37.6	41.5	39	39.1	39.2	37.2	35.5	33.5	35.2	35.8
91	432401	2016	35	36.3	40.3	42	39.8	37	35.8	34.8	34.5	33.8	34.2	33.9
92	432401	2017	34	36.4	37.2	38.6	37.3	35.1	33.9	35.4	34.5	33.8	34.2	33.2
93	432401	2018	34.5	36.4	38.4	38.6	37	35.6	35	34.3	35.6	35.6	33.5	35.2
94	432401	2019	34.3	37.8	39.5	40.3	40.2	38	38	36	34	34.6	34.6	34
95	432401	2020	36	37.2	40	40.2	41.5	37.2	36.1	36.2	35.6	34.1	34.8	34
96	432401	2021	34.8	37	39.2	39.5	38	37	37	36.3	35	33.8	34	32
97	432401	2022	35.1	35	37.7	37.8	34.5	36	35.2	34	34.2	32.5	34.4	32.5
98	432401	2023	34	37	39.8	40	40.5	37	36	35.5	34.5	34.5	31.8	33
99	432401	2013	34.9	37.9	40.6	41.8	39.4	36.2	36.3	38.3	34.4	33.4	33.8	31.5
100	436201	2014	33.5	37.3	40	40.3	39.9	39	36	36	34.2	33.8	35	33.3
101	436201	2015	35	37	39	42.5	39.7	40.3	40.2	35.5	35	33.5	35.5	36
102	436201	2016	35.8	37	41.5	43.2	41	37.5	36	36.3	34	34	35.5	33.5
103	436201	2017	32.7	37	39.5	39.5	38	35.5	33.7	34.5	34.5	33	35	34
104	436201	2018	35	36.8	39	39.3	37	35.8	35.8	33.7	35.1	35	33.8	35.9
105	436201	2019	34.5	38.7	39.8	40.2	39.7	38.1	38.5	35.8	32.9	36.9	35	34.2
106	436201	2020	36	37	39.5	39.6	40.5	37.4	36.4	35	35.1	32.5	33.9	33.9
107	436201	2021	34.4	38.3	39.6	39.6	37.5	38	37.3	35.9	34.6	34.2	34.3	31.7
108	436201	2022	35.7	35.7	38.7	38.2	35.4	36	34.9	33.5	34	33.3	33.5	32.7
109	436201	2023	32.6	36.8	39.8	40.2	41.4	37.6	35.5	36.3	34.3	34.7	32.1	32
110	436201	2013	34.7	38.2	41.2	41.3	40.2	36.7	36	35	34.8	35.5	34	31.9
111	436401	2014	34.5	37	39.4	40.1	38.1	38	37	36	34.9	34.1	34.1	33.5
112	436401	2015	35	37.1	39.2	41.8	39.3	39.8	39.3	36.6	35.5	33.5	34.6	35.4
113	436401	2016	36.2	37.2	41.2	43	40.4	37.8	36.4	36.4	34.6	34.4	34.6	33.8
114	436401	2017	33.8	37.5	39.2	39	38.2	36	35.1	35.9	35.5	34	35.3	33.8
115	436401	2018	35.6	37.5	38.3	39.2	37.5	36.7	36.2	35.5	36.1	35.9	34.7	36.4
116	436401	2019	34.7	38.6	39.7	40.8	40.7	38.5	38.8	36.9	34.8	35.8	35.5	35.6
117	436401	2020	37.6	38	41	41.6	40.5	37.5	36.6	35.6	35.5	33.8	35.2	34.9
118	436401	2021	35.1	38.6	39.6	40	37.5	37.9	37.7	36.5	34.9	35.1	34.8	32.5
119	436401	2022	35	35.4	38.5	39	36.1	36.4	35.6	34.6	34.5	32.8	35	32.6
120	436401	2023	33.7	37	39.7	40.2	40.2	37.9	37.4	37	35.4	34.7	32.3	31
121	436401	2013	35.4	38	41.3	41.6	39.1	37.2	36.5	34.7	34.6	33.2	33.8	31.6

 $\label{eq:APPENDIXD} \textbf{APPENDIX D}$ The monthly minimum temperature data from Northeast of Thailand

			MONTH (CELSIUS)												
NO	STATION	YEAR	JAN	FEB	MAR	APR	MAY	JUN	JUL	AUG	SEP	OCT	NOV	DEC	
1	407301	2013	14.6	19	18.2	22.4	22.5	21.8	22.8	23.4	22.5	20	17.3	12.2	
2	407301	2014	11.5	14.4	19	21.2	23	22.5	22.5	23.1	21.7	21.1	19	13.6	
3	407301	2015	11.5	14	22.1	18.8	23.2	23	22.7	23.5	21.4	20.6	20.5	15.5	
4	407301	2016	13.4	11.5	15.8	23.6	23.4	23.3	22	23.8	22.8	22.5	18.4	17	
5	407301	2017	15.5	13.2	17	19.3	22.8	23.3	23.3	23	23.2	21.3	17.5	13.1	
6	407301	2018	13.5	11.6	16	17	22.2	22.5	23.4	23.2	22	19.5	17.8	16.7	
7	407301	2019	14.8	18.3	20.5	24.5	22.7	24	22.5	22.2	22	20.5	17.7	13.7	
8	407301	2020	14.5	16	19	20.7	23	22.7	22.2	22.6	23	19	17.9	14	
9	407301	2021	9.5	13.8	18.9	22.6	22.5	22.9	21.7	22	23	20	18.2	15.5	
10	407301	2022	16.5	14.7	19.8	17.6	18.7	22.4	22.7	22.3	22.4	18.5	15.8	13.8	
11	407301	2023	13	15.2	17.5	23.4	23.2	22.8	23.1	22.7	22.7	22.2	22.2	22	
12	407501	2013	14.4	19.5	19	23.5	23	22.7	22.9	23.4	22.8	20	17.6	12.4	
13	407501	2014	12.1	15.5	19.8	21.9	23.6	22.8	23.2	23.5	22.6	21.9	19.4	14.2	
14	407501	2015	12.6	15.1	22.8	20	24.2	23.7	22.8	23.5	21.4	21.5	20.6	15.1	
15	407501	2016	13	11.5	16.3	23.8	23.8	23	22.8	23.5	22.9	23.2	18.6	16.9	
16	407501	2017	17.3	14.8	17.7	19.5	23	23.5	23.5	23	23.6	20.1	17.7	12.2	
17	407501	2018	14.1	11.8	16.4	17.2	23	22.4	23.6	23.5	22.4	19.6	18.6	16.9	
18	407501	2019	16.4	19.5	22.6	23.4	22.9	24.6	22.7	22.8	22.8	21	18.8	13.7	
19	407501	2020	14.7	16.5	21.9	20.8	23.5	23.8	23	23.2	23.3	19.5	18	14.2	
20	407501	2021	10.5	14.6	19.3	23.4	22.7	22.9	22	23	23	20.1	18.4	15.6	
21	407501	2022	17.2	14.5	20.5	18	18.8	23	23.2	22.6	22.8	18	16.8	14.2	
22	407501	2023	13.6	15.8	18.2	23.9	23.8	23.7	23.5	23.3	23.1	22.9	23	22	
23	409301	2013	14.9	19	18.9	22.9	23.5	23	22.9	23.7	23	21	17.7	12.6	
24	409301	2014	11.9	14	20.2	22.8	24	23	23.2	23.2	23.4	22.3	19.4	14.3	
25	409301	2015	12.2	15.2	22.5	20.1	24.5	24	23.2	22.9	22	21.7	21.1	15.9	
26	409301	2016	12	11.4	16.6	24.6	23.1	23.6	22.6	23.8	23	22.8	18.7	16.9	
27	409301	2017	15.2	15.2	17.5	19.1	23.5	23.8	23.6	22.5	23	20.2	17.5	12.5	
28	409301	2018	13.8	12.1	16.5	17.2	23.8	22.6	23.4	22.9	22.5	21.9	18.6	16.6	
29	409301	2019	15.8	19.2	21.5	21.7	22.9	23.8	22.7	22	22.5	20	16.7	12.8	
30	409301	2020	14.7	16	19.5	21.4	22.8	23.2	22.8	22.8	23	19.5	19.1	14	
31	409301	2021	11.2	15	19.2	23.8	24.2	23.8	23	23.5	23.1	20.8	19.2	16.1	
32	409301	2022	17.7	14.8	21.1	17.5	19.3	23	23.1	23	22.5	19.1	18.1	14.8	
33	409301	2023	13.8	16	18.6	23.5	23.5	23.3	24	23	24	23.5	23.2	23	
34	431201	2013	16.5	20	20.3	23.5	23.3	24.4	23	22.8	24.6	21.5	18.6	12.2	
35	431201	2014	11.2	16.9	21.7	22.8	23.5	24.3	24	23.7	23.7	22.7	20.1	15.3	
36	431201	2015	13.6	16.7	22.7	21.7	24.8	24.5	22.6	23.6	23.3	21.4	21.4	17.1	
37	431201	2016	12	12.6	18.2	24.3	22.8	22.8	23.7	23.6	23	23.7	20	16.6	
38	431201	2017	16.8	16.3	19.3	20.8	23.9	23.4	23.2	23.2	22.7	20.5	18.5	12.8	
39	431201	2018	14.9	13.5	19.7	17.8	23.7	24	23.6	23.4	23	20.3	18.1	17.8	
40	431201	2019	17.2	20.1	20.2	23.4	23.6	23.8	22.5	23.3	22.2	20.7	18.4	13.5	

	MONTH (CELSIUS)													
NO	STATION	YEAR	JAN	FEB	MAR	APR	MAY	JUN	JUL	AUG	SEP	OCT	NOV	DEC
41	431201	2020	17.4	17.5	22.9	23.1	23.2	23.1	24	23.4	23.3	19.2	19	14.4
42	431201	2021	12	16.7	20.6	23.1	22.3	24.6	23.5	23.2	22.6	20.5	19.3	16.3
43	431201	2022	17.7	16.2	21.9	16	18.9	22.8	23.7	22.7	22.8	18.4	17.5	15.5
44	431201	2023	14.1	16.2	19.6	23.8	23.5	24.2	24.2	24.5	24.3	23	23.9	22.8
45	431301	2013	14.4	18.5	19.2	20.5	22.7	21.4	22.4	21.6	21	19.4	18.1	11.5
46	431301	2014	10	15.7	18.4	21.7	21.9	23	23.4	21.6	21.5	19.9	18.4	15
47	431301	2015	13.6	16	20.4	20.5	22.3	22.7	21.5	22.4	21.5	19.5	20.6	16.3
48	431301	2016	10.6	10.6	17.5	21.7	22.2	22.7	22.4	21.9	22.1	21.2	19	15.6
49	431301	2017	16.9	15.5	18	20.5	22.3	21.3	22	22.1	21.5	21	17.5	12
50	431301	2018	14	13.5	17.8	19.1	21.6	21.8	22.6	21.8	20.7	21.1	17	17.5
51	431301	2019	15.5	18.4	0	21.5	22.4	22.6	21	0	20.3	19.3	15.9	12.7
52	431301	2020	17.4	17	20.2	21.7	21.6	22.5	21.4	22	21.4	17.5	18.7	14.8
53	431301	2021	10.5	16	19	21.5	21.8	21.6	21.5	21.5	21.3	19.9	19	13.4
54	431301	2022	16.4	16.8	20	14.8	18	21.4	21.6	21.1	21.5	17.5	15.7	14.1
55	431301	2023	12.6	14.5	16.6	21	22.1	22.6	22.3	22.2	23.1	21	22.6	21
56	431401	2013	15.4	19.4	19.6	22.2	23.5	23.3	23.5	22.9	22.5	21	17.5	11.5
57	431401	2014	10.6	15.4	21.5	22.2	24.3	24.5	24	23.2	23.3	22	18.7	13.9
58	431401	2015	13	15.5	22.5	20.1	24.5	23.5	23	23.5	22.9	20.7	20.6	16
59	431401	2016	11.8	11.3	16.5	23.5	22.7	22.1	23.5	24.3	23.2	22.5	19.3	15.7
60	431401	2017	15.7	15.4	18.3	20.5	23.1	23.5	23	23.7	23.4	20	17.6	10.9
61	431401	2018	13.7	12.7	19.7	17.7	23.5	23.7	23.5	23.4	22.7	22	17.5	17.2
62	431401	2019	15.4	18.9	19.7	23.4	23.6	23.4	22.5	24	22	19.6	17	12.3
63	431401	2020	16.5	16.5	22.6	23	22.8	23.5	23.5	23	23.1	19.5	17.7	13.5
64	431401	2021	10.8	16.7	19.7	22.9	22.7	23.9	23.4	23.5	22.2	20	18.1	14.8
65	431401	2022	16.9	15.7	21.7	15.5	18.2	22.6	23.3	23	22.4	18.5	16.2	14.2
66	431401	2023	13.5	16.1	17	23.7	23.5	24	24	24	23.5	22.7	22.7	21
67	432201	2013	15	18.7	20.3	23	24	22.6	23.4	22.9	22.8	20.2	17.1	12
68	432201	2014	11.7	15.6	20.7	21.9	23.5	23	23.5	23	23	21.7	18.7	14
69	432201	2015	12.8	15.5	22.3	19.8	21.5	22.6	21.9	21.2	20.6	19	19	13.6
70	432201	2016	9.7	8	16.5	24.2	23.5	23.5	23.6	23.5	23.4	23.1	18.6	15.5
71	432201	2017	15.9	14.8	18.7	20	21.7	23.3	22.5	23	22.3	19.9	17	11.5
72	432201	2018	13	11.8	16.9	17.1	23.5	24	23.6	23.6	22.9	19.6	18.3	15.9
73	432201	2019	14.5	19	22	22.7	22.6	22.8	22.2	22.8	22	19.3	17.9	11.6
74	432201	2020	14.5	16	21.4	20	21.6	21.3	21.3	21.5	21	17.1	16.3	11.1
75	432201	2021	10.9	16.5	18.8	23	23.1	23	23.2	23.3	22.8	19.9	17.6	14.7
76	432201	2022	17	14.6	21.9	15.6	18.3	23	23	22.3	22.2	17.7	16.4	13.8
77	432201	2023	12.7	15.8	18	22.8	23.4	23.4	23.8	22.3	22.8	22.3	22	21
78	432301	2013	14	18.5	18.7	23.2	23.8	22.7	23.7	23.2	23	19.8	16.8	10.9
79	432301	2014	10	12.8	20.2	21.5	23.2	23.5	23.2	23.2	22.8	21.3	18.2	13.7
80	432301	2015	11.5	15	22	20	23.2	23	22.5	22.5	21.9	18.4	18.5	13
81	432301	2016	9.9	9.5	15	23.2	23.4	23	23	23	23	22.9	18	14.5
82	432301	2017	14.6	14.1	17.3	19.5	22	23.5	22.5	21.6	23	19.2	16	10.3
83	432301	2018	12.5	11.2	16.4	17	23	23.5	23.4	23.2	22.5	20.5	16	15.7

	MONTH (CELSIUS)													
NO	STATION	YEAR	JAN	FEB	MAR	APR	MAY	JUN	JUL	AUG	SEP	OCT	NOV	DEC
84	432301	2019	14.2	17.5	15	22	23.5	23.5	22.3	23	21.5	18.8	16.5	10.7
85	432301	2020	14	15	19.5	20.4	21.5	22.5	21.6	21.8	21.4	16.5	15	10.8
86	432301	2021	9.5	14	18.4	22.9	22.5	22	22.2	22	21.4	18.3	16.2	13.5
87	432301	2022	15.6	14.5	20.6	15.5	18.5	23.2	22.7	22.9	22.2	19.1	16	13.5
88	432301	2023	12.5	15.2	17.2	23	23	23.6	23.8	23	23.4	22.5	22.1	21.5
89	432401	2013	15	18.9	20	22.9	23.4	23.2	22.9	22.4	22.5	20	17.2	12.2
90	432401	2014	10.7	14.8	20	22	23.7	23	22.1	23.1	23.6	21.5	18.3	13.3
91	432401	2015	12	15.1	22.2	17.7	23	23.7	22.7	22.2	22.3	20	19.2	15
92	432401	2016	11	10.8	16.2	21.6	22	23	23.4	24	24	24	18.5	16.1
93	432401	2017	16.5	14.1	17.2	20	23	24.2	23	23.8	23.8	22.2	17.9	10.7
94	432401	2018	13.2	11.7	16.8	17.6	23.8	24.5	23.8	24	23.4	21	18.3	17.9
95	432401	2019	15.5	19	23.2	23.4	23.8	24.5	23.5	22.5	22	22.1	18.5	12.6
96	432401	2020	14.8	16.2	21	20.3	23.5	23.2	23.2	22.3	23.5	18.1	17.8	13
97	432401	2021	10.5	16	20	23.5	22	23.2	22	22	22	18.5	18.5	14.5
98	432401	2022	17	14.3	19.8	15	18.5	24	24	24	23	18.5	18	13
99	432401	2023	12.7	15.5	18.4	23.5	24	24.4	23	23	23.6	22.8	23.9	22.5
100	436201	2013	13	17.7	20	22.4	23.5	23.1	22.9	22.4	16.7	18.7	17	10.1
101	436201	2014	9	13	18	22	22.5	23	23	23	22	20.4	17	12.9
102	436201	2015	11.4	14	21.3	17.2	22	21.8	18.6	19.6	21	20	18.5	14.4
103	436201	2016	9.4	8.5	13.7	21	21.7	21	20	22	21	22	17.8	13.5
104	436201	2017	15	13	16.8	19	22.5	23.2	22	23	21.7	18.5	16	9.3
105	436201	2018	12	11.3	16.4	16	22.5	23.3	23.3	23	21.7	20.9	17.2	15.7
106	436201	2019	14.6	18.1	16.6	22	22.3	22.7	23.1	22.6	21.2	18.9	17.5	10.8
107	436201	2020	13.4	15.8	21.8	20.7	22.3	23.3	23.4	23.1	23.1	19.2	17.1	12.6
108	436201	2021	9.4	15.1	18.5	22.7	20.6	22.9	23	22.8	22.9	20.1	17.4	14
109	436201	2022	16.2	14.2	21	15.4	18	23.6	22.2	22.2	22.5	18.2	17.7	13
110	436201	2023	11.9	15.2	17.6	23	22.3	22.8	23.5	23	23.3	22.1	21.8	22
111	436401	2013	14.2	18.7	19.5	22.8	22.7	22.6	23	22.4	22.3	20.9	17.5	11.4
112	436401	2014	10.7	14.8	21.4	21.7	22.5	22.8	23	23.5	23.2	22.3	18.7	13.7
113	436401	2015	12.2	14.7	22.7	19.9	24.3	23.2	22.3	23	21	20.4	19.7	15.3
114	436401	2016	11.5	11	15.8	21.5	22.3	22.3	22.1	23.5	23.3	22.8	18	15
115	436401	2017	15	14.5	16.3	19.8	22.4	23.5	22.6	23	22.2	18.8	16.7	11.2
116	436401	2018	13.7	11.9	18.3	17.8	22.1	23.8	23.8	23.4	22.3	19.4	17.2	16.5
117	436401	2019	15.5	18.7	23.5	23	22.2	24.4	22.1	23.8	22.3	20.6	17.6	12.3
118	436401	2020	16	16.2	22.3	22.3	22.8	23.8	22.3	22.8	22.9	19	17.5	13.5
119	436401	2021	10.6	15.2	19.6	22.3	22.5	23.7	23.6	22.2	23.3	20.3	18.1	15.1
120	436401	2022	16.1	15.6	20.5	15.5	18.2	23.5	23.7	22.7	22.1	18	15.9	13.2
121	436401	2023	13.3	16	18.4	23.5	23.5	23.7	23.7	23.4	23.5	22.9	22.8	21.4